MODELING AND SIMULATION OF COMBUSTION CHAMBER AND PROPELLANT DYNAMICS AND ISSUES IN ACTIVE CONTROL OF COMBUSTION INSTABILITIES

Thesis by

Giorgio C. Isella

In Partial Fulfillment of the Requirements

for the Degree of

Doctor of Philosophy

California Institute of Technology

Pasadena, California

2001

(Defended February 26, 2001)

Acknowledgements

I would like to thank Professor Fred E. C. Culick for giving me the opportunity to study at Caltech and for his advice, help and encouragement over the years. Thanks also to Dr. Gharib, Dr. Leonard and Dr. Murray for serving as committee members, and to the whole GALCIT community.

A special thanks goes to Professor Ed Zukoski, the first GALCIT member I met when coming here, and an assiduous visitor of the lab when I was involved in experimental work.

I would like to acknowledge the financial support provided over these years by the MURI Research Program, the Air Force Office of Scientific Research, the Advanced Gas Turbines System Research program of the Department of Energy, the Italian power company ENEL and the California Institute of Technology.

Many thanks also are due to my friends here at Caltech; in particular Claude Seywert: he collaborated in all the experimental work, shared relaxing breaks at the Red Door, and kept me grounded with his constant irony. Also I want to mention my group mates for their help, collaboration and friendship: Winston Pun, Sanjeev Malhotra, Steve Palm, Grant Swenson, Konstantin Matveev, Olivier Duchemin. Thank you, guys; it has been fun!

A very special thank goes to Ying Huang, for her love, help and support, and to my family, especially my father, Franco, who repeatedly traveled the 6500 miles that separate us with the sole purpose of seeing me. Thanks!

Abstract

A method for a comprehensive approach to analysis of the dynamics of an actively controlled combustion chamber, with detailed analysis of the combustion models for the case of a solid rocket propellant, is presented here. The objective is to model the system as interconnected blocks describing the dynamics of the chamber, combustion and control (including sensors and actuators).

The analytical framework for the analysis of the dynamics of a combustion chamber is based on spatial averaging, as introduced by Culick. This method results in the determination of a set of coupled oscillator equations that are then integrated with the appropriate forcing terms deriving from combustion and control.

Combustion dynamics are analyzed for the case of a solid propellant. Considerable data exists suggesting that the response functions for many solid propellants tend to have higher values, in some ranges of frequencies, than predicted by the conventional quasi-steady theory. Hence, quasi-steady theory is extended to include the dynamics of the gas-phase and also of a surface layer interposed between the gaseous flame zone and the heated solid phase of the propellant. The models are constructed so that they produce a combustion response function for the solid propellant that can be immediately introduced in the our analytical framework. The principal objective of this analysis is to determine which characteristics of the solid propellant are responsible for the large sensitivity, observed experimentally, of propellant burning response to small variations in the conditions. We show that velocity coupling, and not pressure coupling, has the potential to be the mechanism responsible for that high sensitivity. Some issues related to the

modeling of solid propellant are also discussed, namely the importance of particulate modeling and its effect on the global dynamics of the chamber and a revisited interpretation of the intrinsic stability limit for burning of solid propellants.

Active control is also considered in the analysis. A critical discussion about the most commonly used control strategies used in combustion allows us to define which are the most promising algorithms to use on future experiments. Particular attention is devoted to the effect of time delay (between sensing and actuation) on the control strategy; several methods to compensate for it are presented and discussed, with numerical examples based on the approximate analysis produced by our framework.

Experimental results are presented for the case of a Dump Combustor. The combustor exhibits an unstable burning mode, defined through the measurement of the pressure trace and shadowgraph imaging. The transition between stable and unstable modes of operation is characterized by the presence of hysteresis, also observed in other experimental works, and hence not a special characteristic of this combustor. Control is introduced in the form of pulsed secondary fuel. We show the capability of forcing the transition from unstable to stable burning, hence extending the stable operating regime of the combustor. The transition, characterized by the use of a shadowgraph movie sequence, is attributed to a combined fluid-mechanic and combustion mechanism.

Table of Contents

List of Figures

List of Tables

1 Introduction

Propulsion systems, especially rocket engines, are prone to developing large undesired pressure oscillations in the combustion chamber. These oscillations are referred to as 'combustion instabilities'. When dealing with combustor dynamics we will refer to a combustor with very small pressure oscillations as 'stable' versus 'unstable' for a combustor exhibiting large pressure oscillations. The term 'unstable' refers to the fact that the combustor is linearly unstable and does not imply an infinite growth of the oscillations, which in general exhibit a limit cycle determined by the nonlinearities present in the system.

The problem of combustion instabilities was observed since early development of liquid and solid rocket engines and afterburners and ramjets since the early 1940's. The consequence of these large oscillations was often the loss of the engine due to mechanical failure, degradation of performance or simply intolerable mechanical vibrations induced into the vehicle. The first approach, based mainly on laboratory tests, led to the use of passive devices to prevent instability (for example baffles placed in appropriate locations in the chamber) and to redesign of the injectors, in the case of liquid propellants, in order to obtain a favorable distribution of energy release. The Rayleigh's criterion might be invoked to justify this approach, even though there was no accurate measurement of the energy release distribution to perform a quantitative analysis.

In general, pressure oscillations appear as spontaneous or pulsed. A spontaneous oscillation is due to intrinsic instability of the system: the combustor is (or becomes, due to a change of operation conditions) linearly unstable and hence perturbations grow exponentially. Linear theory, the main subject of research during the years 1950-60, deals with this situation. Pulsed oscillations (or

triggering) are a purely non-linear effect: in this case the system is linearly stable to 'small' perturbations, while it grows exponentially, possibly reaching a large amplitude limit cycle, if subjected to a sufficiently large perturbation. An example of triggering is presented in Figure 1.1, taken from Blomshield 2000. The figure shows the experimental results for two motors, characterized by different chamber pressure. In both cases, a *large enough* perturbation causes the motors to exhibit instability.

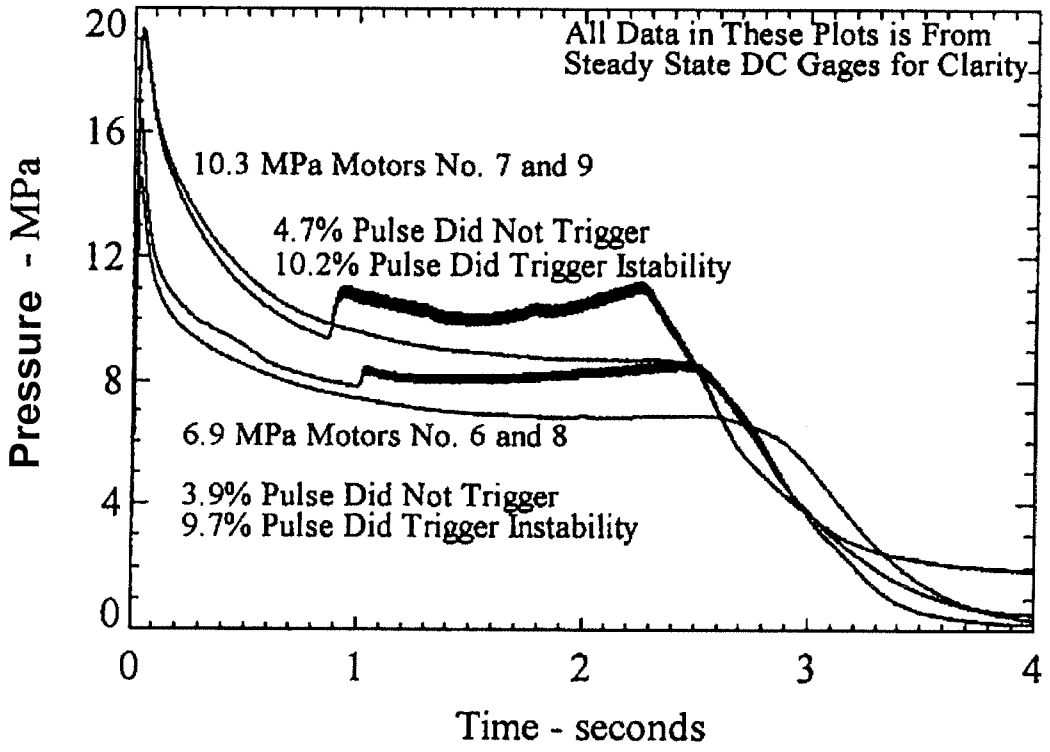

Figure 1.1. Triggering instability (from Blomshield 2000).

Recently, triggering was addressed by Burnley 1996, using the approximate theory developed by Culick to define some of the characteristics of a combustor exhibiting this dynamic behavior. More recently, combustion instabilities have been observed in gas-turbine combustors dedicated to power generation. The necessity of reducing emissions (particularly NO_x) has pushed industry to using existing 'stable' combustors in very lean conditions; as a consequence, many combustors exhibit pressure oscillations of the two kinds described above.

Active control of instabilities, first investigated in the early 1980's, initially on small laboratory scale combustors, now is being considered as a viable option for full scale plants.

First applications of control were limited to a simple proportional feedback of the pressure signal, and based on purely experimental trials. A problem in using more 'sophisticated' control algorithms lies in the fact that a reasonably accurate and simple model of the combustor is needed.

A very promising approach is to look at the combustor itself as a feedback system between the combustion chamber and 'combustion' (Figure 1.2): this separation allows the use of fairly well developed and tested analytical tools used to represent and simplify the dynamics of the combustor (including geometry and gasdynamics), coupled with appropriate models for the 'combustion' block.

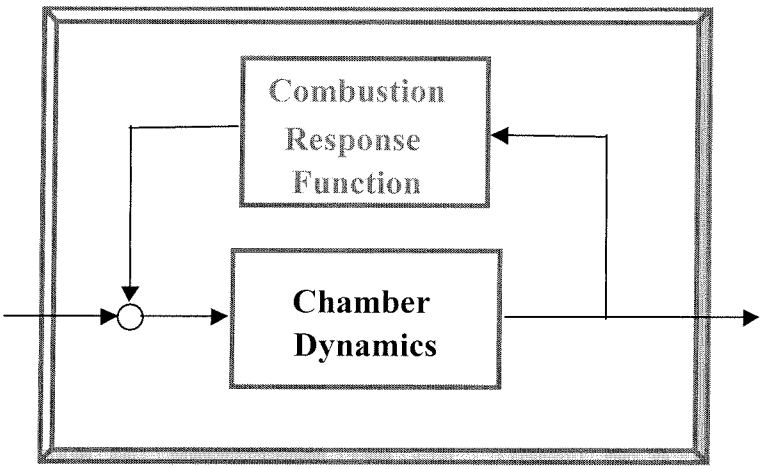

Figure 1.2. Combustor system.

In the case of solid propellants, for example, experiments show a large sensitivity of the global dynamics on small changes in the propellant composition. One example is presented in Figure 1.3, from Blomshield 2000. In this case, the addition of 1% stabilizer in the propellant mixture prevents the insurgence of a catastrophic instability that would otherwise lead to the loss of the motor. An objective of this work is to develop tools that would allow the analytical study and the prediction of this sensitivity, and also of instabilities like triggering.

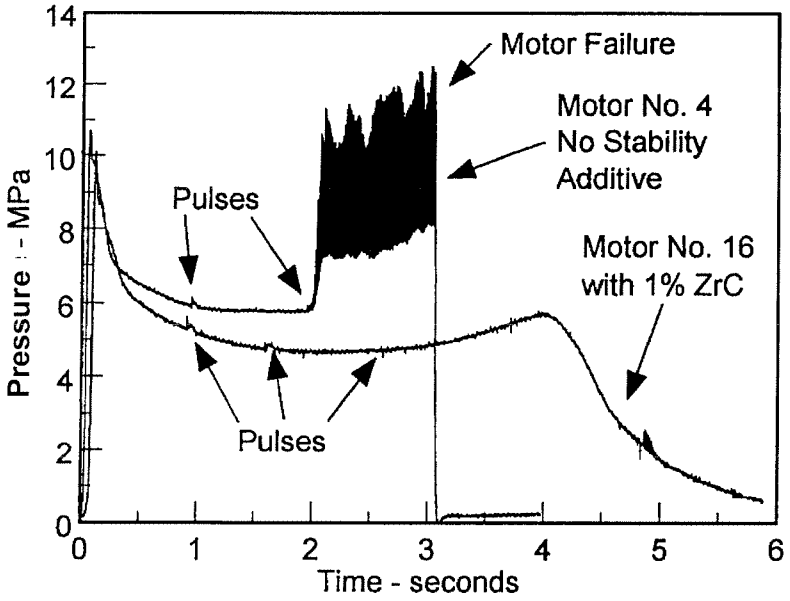

Figure 1.3. Sensitivity of combustor on propellant changes (from Blomshield 2000).

Two main issues are the modeling of the combustion block (Figure 1.2) and the modeling of the coupling mechanism between the combustion and chamber dynamics.

Notice that, if active control is added, another feedback loop is closed between the controller and the plant represented by the shaded box in Figure 1.2.

The models of the coupling mechanism between combustion and combustion chamber can be grouped in three general categories: pressure coupling, velocity coupling and vortex shedding-acoustics interactions. Pressure coupling, especially in the case of solid propellants, is a widely used approach: this model gives a fairly good agreement with experimental results at low frequencies, but it fails to provide an analytical explanation for the observed sensitivity of solid propellant burning behavior to small minor changes in the composition or in the physical state, and also it seems unable to predict triggering (a typical nonlinear instability found in rocket motor and gas combustors burning away from stoichiometric conditions).

The idea of velocity coupling comes from the observation that combustion of a burning surface is sensitive to the magnitude of the velocity and fluctuations parallel to the surface itself: this gives

a nonlinear mechanism that could be able to explain triggering. A problem with velocity coupling is that there is no satisfactory theory and no effective means of measuring it in the laboratory.

Large vortices, developing from unstable shear layers in flow past edges may couple directly to the acoustic field or produce local acoustic sources when impinging on surfaces, and hence be the energy source for unstable motions.

In the case of liquid and gas combustors, oscillations in the acoustic field can give rise to oscillations in the fuel-oxidizer ratio, and hence introduce a further source of instability. This phenomenon is also responsible for an increase in NOx emission, and hence poses severe limitation on the use of these combustors for power generation, due to the current very strict emission regulations.

In this context, control can be seen as a means to act on the feedback mechanism between combustion and combustion chamber in order to prevent or reduce the instability. In this sense, a good understating of the complete mechanisms would allow the design of very efficient controllers, able to act directly on the source of the instability. Historically, passive control was first introduced and it developed mainly from experimental trial and error. The introduction of baffles, acoustic liners, Helmholtz resonators and an accurate design of the injection system was often able to eliminate or reduce observed instability by "breaking" the feedback link between the combustion and the dynamics of the chamber.

Active control was successively introduced to overcome some of the limitations of passive methods: larger operating range, reduction of experimental testing (see Culick 1999 for a historical overview of the passive and active control approaches). The control problem is particularly complicated by the typical characteristics of a combustion system: internal instabilities, significant time lags, intrinsic non linearities, large internal noise and disturbances. Regarding the design of controllers, the major problems come from the fact that the controller changes the system (typically with the introduction of acoustic sources, secondary fuel, etc.),

modeling of combustion/combustors is not completely understood (large uncertainties), sensors and actuators are not well defined and the effect of scaling from laboratory combustors to full-scale items is not at all clear.

The work presented here covers several of the issues described above. The purpose of this work is to present a comprehensive approach to the analysis of the dynamics of an actively controlled combustion chamber, with detailed analysis of the combustion models for the case of a solid rocket propellant.

The principal contributions of this work can be summarized in three categories: propellant and combustor dynamics, experimental control of hysteresis, and control of systems with time delay.

Regarding propellant and combustor dynamics, we construct a framework, based on transfer function representations, that allows analysis of sensitivities of the combustor to small changes in the propellant. To this purpose, we extend the traditional quasi-steady approach with novel consideration of unsteady dynamics of the propellant surface. We then use global combustor simulations as a tool to identify sensitivities. This method allows us to identify the surface as partly responsible for some experimental measurements regarding the combustion response at relatively high frequency. We also assess that velocity coupling in the combustion response function is an important mechanism that allows to explain sensitivity and triggering.

By using a Dump Combustor, we show that secondary fuel injection can extend the stable operating region of the combustor; we then use high speed shadowgraph as a diagnostic method to identify the mechanism responsible for the effectiveness of the control.

By using an analytical approach, we investigate the possibility of using time delay compensation networks to control combustors affected by large time delays between sensing and control action.

In Chapter 2, we will outline the analytical framework for the analysis of the dynamics of a combustion chamber, based on spatial averaging, as introduced by Culick. This method results in the determination of a set of coupled oscillator equations that are then integrated with the appropriate forcing terms deriving from combustion and control. The procedure used to integrate the system and determine the results presented in all the subsequent chapters is also described. Some issues regarding the modeling of actuators (used to introduce the control action into the system) are also illustrated in the last part of the chapter.

Chapter 3 deals with the modeling of the combustion dynamics of a solid propellant. The traditional approach, based on quasi-steady theory, is extended to include the dynamics of the gas-phase and also of a surface layer interposed between the gaseous flame zone and the heated solid phase of the propellant. The models are constructed so that they produce a combustion response function for the solid propellant that can be immediately introduced in the formulation presented in Chapter 2 and hence close the feedback loop depicted in Figure 1.2. The principal objective of this analysis is to determine which characteristics of the solid propellant are responsible for the large sensitivity, observed experimentally, of propellant burning response to small variations in the conditions. We will analyze a response based on pressure coupling and also velocity coupling, showing that velocity coupling, and not pressure coupling, has the potential to be the mechanism responsible for the mentioned high sensitivity. Some issues related to the modeling of solid propellant are also discussed here, namely the importance of particulate modeling and its effect on the global dynamics of the chamber and a revisited interpretation of the intrinsic stability limit for burning of solid propellants.

Chapter 4 closes the 'outer' loop by introducing the active control terms into the system. We will show how the simplified analysis in Chapter 2 lends itself naturally to the convenient State-Space representation used in control theory and hence allows using conventional control analysis and design tools. A critical discussion (a more detailed discussion about the control work at the

Georgia Institute of Technology is presented in Appendix D) about the most commonly used control strategies used in combustion allows us to define which are the most promising algorithms to use on future experiments. Particular attention is devoted to the effect of time delay (between sensing and actuation) on the control strategy; several methods to compensate for it are presented and discussed.

Chapter 5 presents a short overview of some of the experimental work conducted in our facilities. In particular, the case of a dump combustor is analyzed in detail. The combustor exhibits an unstable burning mode, characterized through the measurement of the pressure trace and Shadowgraph imaging. The transition between stable and unstable mode is characterized by the presence of hysteresis (also observed in other experimental works, and hence not a special characteristic of this combustor); control is introduced in the form of pulsed secondary fuel, and we show the capability of forcing the transition from unstable to stable burning, hence extending the stable operating regime of the combustor. The transition is characterized by the use of a shadowgraph movie sequence.

Finally, the most important results are summarized in the concluding Chapter 6.

2 Linear and Nonlinear Modeling of the Combustion Chamber

2.1 Derivation of the Nonlinear Acoustic Equations

The flow in combustion chambers, especially when burning solid propellants, is characterized by the presence of a mixture of different gases and of a substantial amount of condensed matter. Consequently, the changes in the properties of the flow inside the chamber are accounted for by writing conservation equations for the two-phase flow. Following Culick 1976, the problem is greatly simplified by considering average properties for the gas mixture and the condensed species and then combining the two-phase flow equations into expressions having the mass-averaged properties of the two phases. The resulting conservation equations for the mixture are

(2.1)
$$\frac{\partial \rho}{\partial t} + (\mathbf{u} \cdot \nabla)\rho = \mathcal{W}$$

(2.2)
$$\rho\left[\frac{\partial \mathbf{u}}{\partial t} + (\mathbf{u} \cdot \nabla)\mathbf{u}\right] = -\nabla p + \mathcal{F}$$

(2.3)
$$\frac{\partial \rho}{\partial t} + \bar{\gamma} p \nabla \mathbf{u} = -\mathbf{u} \cdot \nabla p + \mathcal{P}$$

where, neglecting terms involving interactions between phases

(2.4)
$$\mathcal{W} = -\rho \nabla \cdot \mathbf{u}$$

(2.5)
$$\rho\left[\frac{\partial \mathbf{u}}{\partial t} + (\mathbf{u} \cdot \nabla)\mathbf{u}\right] = -\nabla p + \mathcal{F} = \nabla \cdot \vec{\tau}$$

(2.6)
$$\mathcal{P} = (\bar{\gamma} - 1)[\nabla \cdot \mathbf{q} + \mathcal{Q} - \mathbf{u} \cdot (\nabla \cdot \vec{\tau})]$$

The conservation equation can then be combined to form a nonlinear wave equation for the pressure. We start by writing all variables as sums of averaged and small-amplitude fluctuating parts (Culick 1976).

$$p(t) = \overline{p} + p'(t)$$

(2.7)

$$\rho(\mathbf{r},t) = \overline{\rho}(\mathbf{r}) + \rho'(\mathbf{r},t)$$

$$\mathbf{u}(\mathbf{r},t) = \overline{\mathbf{u}}(\mathbf{r}) + \mathbf{u}'(\mathbf{r},t)$$

Properly, the equations for the mean flow should be derived by subtraction of the time average of the difference of the general equations and those for the fluctuations. In this case, the resulting equations would contain terms involving the time average product of mean flow and fluctuations; these extra terms would require some additional theory to close the problem. In the case of the present analysis, for simplicity we assume that the mean variables satisfy their own conservation equations, in the form (2.1)-(2.3).

After substitution of (2.7) in the momentum and energy conservation equations, we can write the following equations for the unsteady quantities.

(2.8)
$$\overline{\rho}\frac{\partial \mathbf{u}'}{\partial t} + \nabla p' = -\rho'\frac{\partial \mathbf{u}'}{\partial t} - \overline{\rho}\left(\overline{\mathbf{u}}\cdot\nabla\mathbf{u}' + \mathbf{u}'\cdot\nabla\overline{\mathbf{u}} + \mathbf{u}'\cdot\nabla\mathbf{u}'\right) - \rho'\left(\overline{\mathbf{u}}\cdot\nabla\overline{\mathbf{u}} + \overline{\mathbf{u}}\cdot\nabla\mathbf{u}' + \mathbf{u}'\cdot\nabla\overline{\mathbf{u}}\right) + \mathcal{F}'$$

(2.9)
$$\frac{\partial p'}{\partial t} + \overline{\gamma p}\nabla\mathbf{u}' = -\overline{\gamma}p'\nabla\cdot\overline{\mathbf{u}} - \overline{\gamma}p'\nabla\cdot\mathbf{u}' - \overline{\mathbf{u}}\cdot\nabla p' - \mathbf{u}'\cdot\nabla\overline{p} - \mathbf{u}'\cdot\nabla p' + \mathcal{P}'$$

where we dropped terms of order above the second in the perturbation. Third order gasdynamic terms affect the quantitative values, without affecting the qualitative behavior (Yang, Kim and Culick 1987, 1988, 1990, Paparizos and Culick 1990), and hence have been neglected.

The nonlinear wave equation used for the analysis is derived by first differentiating equation (2.9) with respect to time and then substituting in (2.8). If we introduce the further assumption that entropy waves can be neglected, and we use an isentropic relation to substitute the density in terms of the pressure, the resulting expression is:

(2.10)
$$\nabla^2 p' - \frac{1}{\bar{a}^2}\frac{\partial^2 p'}{\partial t^2} = h$$

where

(2.11)
$$h = -\bar{\rho}\nabla\cdot\left(\bar{\mathbf{u}}\cdot\nabla\mathbf{u}' + \mathbf{u}'\cdot\nabla\bar{\mathbf{u}}\right) + \frac{1}{\bar{a}^2}\bar{\mathbf{u}}\cdot\nabla\frac{\partial p'}{\partial t} + \frac{\bar{\gamma}}{\bar{a}^2}\frac{\partial p'}{\partial t}\nabla\cdot\bar{\mathbf{u}} - \bar{\rho}\nabla\left(\mathbf{u}'\cdot\nabla\mathbf{u}' + \frac{p'}{\bar{\gamma}\bar{p}}\frac{\partial\mathbf{u}'}{\partial t}\right) +$$
$$+ \frac{1}{\bar{a}^2}\frac{\partial}{\partial t}\left(\mathbf{u}'\cdot\nabla p'\right) + \frac{\bar{\gamma}}{\bar{a}^2}\frac{\partial}{\partial t}\left(p'\nabla\cdot\mathbf{u}'\right) + \nabla\cdot\mathcal{F}' - \frac{1}{\bar{a}^2}\frac{\partial\mathcal{P}'}{\partial t}$$

The boundary condition for the pressure oscillations is set by the scalar product of the normal vector (positive outward) with the momentum equation (2.8).

(2.12)
$$\hat{\mathbf{n}}\cdot\nabla p' = -f$$

where

(2.13)
$$f = \bar{\rho}\frac{\partial\mathbf{u}'}{\partial t}\cdot\hat{\mathbf{n}} + \bar{\rho}\left(\bar{\mathbf{u}}\cdot\nabla\mathbf{u}' + \mathbf{u}'\cdot\nabla\bar{\mathbf{u}}\right)\cdot\hat{\mathbf{n}} + \bar{\rho}\left(\mathbf{u}'\cdot\nabla\mathbf{u}'\right)\cdot\hat{\mathbf{n}} + \frac{p'}{\bar{a}^2}\frac{\partial\mathbf{u}'}{\partial t}\cdot\hat{\mathbf{n}} - \mathcal{F}'\cdot\hat{\mathbf{n}}$$

2.2 Approximate Analysis

The partial differential equation describing the problem, equation (2.10), is then transformed into a set of ordinary differential equations obtained by averaging over the combustion chamber's volume using a method similar to Galerkin's (Culick 1971, 1976). The basic idea is to seek the solution to our problem as the perturbation of an eigenvalue problem whose solution is known. In this case, we use the unperturbed waveform predicted by classical acoustics for the same chamber with rigid boundaries and no flow. The mode shapes can be simply obtained by setting $h = f = 0$ in the equations describing the mode shapes for the unperturbed case.

(2.14)
$$\nabla^2\psi_n + k_n^2\psi_n = 0$$

(2.15)
$$\hat{\mathbf{n}}\cdot\nabla\psi_n = 0$$

where k_n denotes the wave number for the n^{th} mode. Now multiply (2.10) by ψ_n, (2.14) by p', subtract the results and integrate over the volume, i.e., spatial average the weighted difference.

(2.16) $$\int\left(p'\nabla^2\psi_n - \psi_n\nabla^2 p'\right)dV + \frac{1}{\bar{a}^2}\int\psi_n\frac{\partial^2 p'}{\partial t}dV + k_n^2\int\psi_n p'dV = -\int\psi_n h dV$$

Now we can use Green's theorem on the left-hand side and substitute the boundary conditions.

(2.17) $$\frac{1}{\bar{a}^2}\int\psi_n\frac{\partial^2 p'}{\partial t}dV + k_n^2\int\psi_n p'dV = -\int\psi_n h dV - \int\psi_n f dS$$

We assume an expansion of the unsteady pressure and velocity in terms of the unperturbed normal acoustic modes.

(2.18) $$p'(\mathbf{r},t) = \bar{p}\sum_{m=1}^{\infty}\eta_m(t)\psi_m(\mathbf{r})$$

(2.19) $$\mathbf{u}'(\mathbf{r},t) = \sum_{m=1}^{\infty}\frac{\dot{\eta}_m(t)}{\bar{\rho}k_m^2}\nabla\psi_m(\mathbf{r})$$

This approach is based on the idea that combustion instabilities are dominated by acoustic waves. In general, small disturbances are composed of three kinds of waves: acoustic, entropy and vorticity waves. In the lowest approximation, they propagate independently and entropy and vorticity components are neglected (Chu and Kovásznay 1956). As a consequence, the expansions above solve the unperturbed acoustic problem term by term and are valid for problems of linear stability up to third order, but are not valid for problems involving mean flow/nonlinear acoustic interactions or problems of higher order. Assuming that the average pressure and speed of sound are uniform throughout the chamber, we can substitute (2.18) and (2.19) into (2.17), apply orthogonality and find a system of second order differential equations describing the evolution of the amplitude of the acoustic modes.

(2.20) $$\frac{d^2\eta_n}{dt^2} + \omega_n^2\eta_n = F_n$$

where $\omega_n = \overline{a} k_n$ and

(2.21) $$F_n = -\frac{\overline{a}^2}{\overline{p} E_n^2}\left(\int \psi_n h dV + \int \psi_n f dS\right)$$

(2.22) $$E_n^2 = \int \psi_n^2 dV$$

The solution of equation (2.20) requires knowledge of the two functionals f and h. These include the gasdynamics effects and all other mechanisms such as like viscous losses, particle damping and combustion response. More details of the derivation of the equations above are given in Culick 1976, Culick and Yang 1992.

2.2.1 Time Averaging

To further simplify the equations, the method of time averaging has been widely used, starting with Culick 1971 and 1976. Burnley 1996 presents a detailed comparison between original oscillator equations and time-averaged equations, and shows that time averaging preserves the dynamical characteristics of the original system. The method is based on the idea that the amplitudes and phases of the oscillations vary slowly with time, when compared to the period of the first acoustic mode of the chamber. In this case, time averaging, based on the method developed by Kryliov and Bogoliubov 1947, allows reducing the system of differential equations from second to first order.

In short (details can be found in Culick 1976), the amplitude is written in the form:

(2.23) $$\eta_n = A_n(t)\sin\omega_n t + B_n(t)\cos\omega_n t$$

where A_n and B_n are slowly varying functions of time (when compared to $\omega_n t$). Substitution equation (2.23) in (2.20) and simplification yields the differential equations for the time averaged evolution of the amplitudes.

(2.24)
$$\frac{dA_n}{dt} = \frac{1}{\omega_n \tau_1} \int^{+\tau_1} F_n \cos \omega_n \tilde{t}\, d\tilde{t}$$

(2.25)
$$\frac{dB_n}{dt} = -\frac{1}{\omega_n \tau_1} \int^{+\tau_1} F_n \sin \omega_n \tilde{t}\, d\tilde{t}$$

The importance of the time averaged equation lies in the possibility of analytical solution for simple cases, especially when truncated to two modes, as in Culick 1994, Wicker, Greene, Kim and Yang 1996, Burnley and Culick 2000.

2.3 The Combustion Chamber as a Dynamical System

Dynamical Systems Theory offers some valuable tools for the analysis of the behavior of combustion systems. One objective of the work relative to the modeling of the response of a solid propellant (chapter 0) is to find a connection between propellant characteristics and global dynamics, i.e., dynamic behavior of the coupled system propellant-combustion chamber. For this purpose, dynamical systems theory provides an approach that draws attention to the global trends; for example, it simplifies the analysis of a parametric variation on the global dynamics, and the identification of some characteristics, such as limit cycles, regions of possible nonlinear instabilities: triggering, hysteresis, switching.

In particular, we will use bifurcation diagrams, a representation of the equilibrium points of the system as a function of one (or more) parameters. For a given value of the parameter, the diagram shows all the possible equilibrium states and their stability characteristics. Note that, for this purpose, a limit cycle, when the system oscillates at a constant amplitude and period, counts as an equilibrium state.

As an example, the bifurcation diagram of Figure 2.1 shows the behavior of a system that presents a pulsed instability. The result refers to a case with 6 modes; the parameter α_1 is the growth rate of the first mode. The system presents a subcritical pitchfork bifurcation followed by

a saddle-node bifurcation; this pattern is typical of pulsed instabilities or triggering and systems presenting hysteresis (Strogatz, 1994). If the pulse is small (point 1 in Figure 2.1) the oscillation decays and the system falls back to the initial state; on the other hand, if the pulse is large enough (point 2), the oscillation grows and eventually reaches a limit cycle. Also note that the system exhibits hysteresis in the parameter α_1. Both triggering and hysteresis have been observed experimentally in rocket motors and laboratory combustors (for example, Isella, Seywert, Culick and Zukoski 1997, Lieuwen and Zinn 2000).

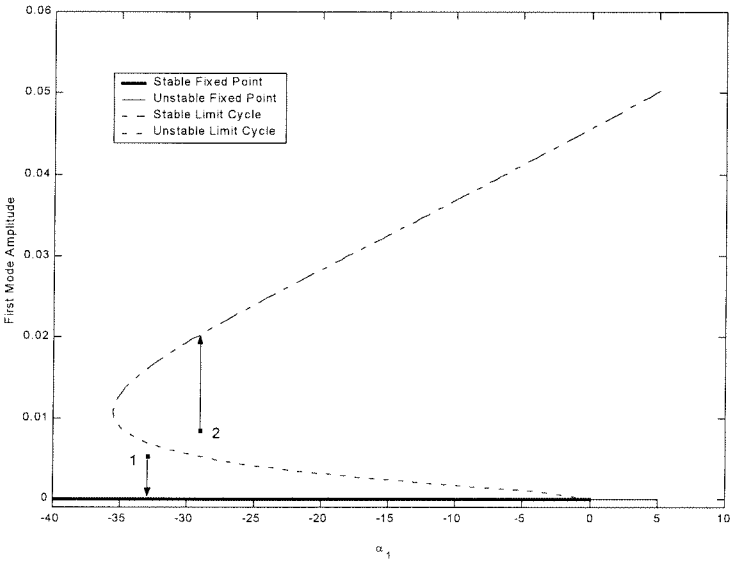

Figure 2.1. Bifurcation diagram obtained from the model of a combustor; it presents a subcritical pitchfork bifurcation followed by a saddle-node bifurcation at the turning point.

2.3.1 Method of Continuation

If we let

(2.26)

$$\mathbf{x} = \begin{pmatrix} \eta_n \\ \dot{\eta}_n \end{pmatrix}$$

then the set of equations (2.20) reduces to first order and can be written in the general form

$$\frac{d\mathbf{x}}{dt} = f(\mathbf{x}, \mu) \tag{2.27}$$

where $\boldsymbol{x}$ is unknown and μ is a parameter of known value. The starting point of the analysis is to find the equilibrium points for the system, i.e., the values of $\boldsymbol{x}$ and μ for which $f(\mathbf{x}, \mu) = 0$. In the case of our equations, describing a combustion chamber, we already know that the trivial solution (i.e., no oscillations) is going to be an equilibrium. The question then becomes the stability characteristics of the point. A theorem from dynamical system theory (Hartman-Grobman, Wiggins 1996) establishes that the flow generated by (2.20) is $\mathbf{C}^0$ conjugate to the flow generated by the linearized system, provided that the Jacobian of the system has no eigenvalues on the imaginary axis (see Appendix A for more details). Hence, as a first result, the stability of the system can be determined from the linearized version. Note that the value of the eigenvalues depends on the parameter μ. Bifurcations occur when, changing μ, there is a change of the stability characteristics of the system. A "Hopf bifurcation," for example, occurs when there is a pair of purely imaginary eigenvalues; a branch of periodic solutions is created. If the periodic solutions are initially stable, the bifurcation is called supercritical; if initially unstable (Figure 2.1), the Hopf bifurcation is called subcritical.

A key tool for tracing diagrams like the one of Figure 2.1 is the use of the local continuation method. For the calculations presented here, we use the software XPPAUT, created by Ermentrout 1998 and based on the continuation package AUTO by Doedel 1997. The method is based on the implicit function theorem, and takes advantage of the fact that, as long as f in (2.27) is sufficiently smooth, the steady states are continuous functions of the parameters. AUTO uses a variation of this method, based on the pseudo-arclength continuation technique developed by Keller, to allow the possibility of following different folds; moreover, eigenvalues of the Jacobian are calculated and displayed at every step during the computation, to allow determination of the

stability characteristics of the equilibria and bifurcations. More details about the program and the methods can be found in Doedel, Keller, Kernevez 1991 and in Keller 1977. Note that AUTO also allows continuation of periodic solutions and determination of bifurcations of periodic orbits, performed by the use of Floquet multipliers (see Appendix A for more details).

2.3.2 Computation of the Global Dynamics of the Combustion Chamber

We refer to global dynamics of the combustion chamber when dealing with the coupled response of the chamber acoustics and the combustion. The previous sections contain a short outline of the theoretical derivation of a set of equations describing the dynamics of the combustion chamber and the reduction to a system of coupled oscillators. Terms arising from combustion modeling (described in the following chapters) appear in these equations as forcing, and depend on the combustor state itself, thus creating a feedback loop between the dynamics of the two systems. Most of the effort in the study of combustion instabilities is devoted to the study of the characteristics of the feedback loop between chamber and combustion dynamics, responsible for the phenomena typically observed in a combustor.

The numerical results and observations presented in the following sections are based on the numerical solution of the set of equations representing the global system. The algorithm proceeds as summarized in Figure 2.2. After setting a geometry for the combustion chamber, the acoustic modes are calculated (with the assumption of no combustion), and then the system is truncated by selection of an appropriate number of modes. A discussion of the effect of truncation on the result of the simulations can be found in Jahnke and Culick 1993, and Burnley 1996. More recently, Ananthkrishnan 2001 has developed a semi-analytical rule to determine the minimum number of modes required to completely capture the dynamics (in a qualitative manner) depending on which mode is unstable. In particular, for a 1^{st} mode instability, 4 modes are required, for a 2^{nd} mode instability, 8 modes are required.

After that spatial (and time, if required) averaging is performed and then the system is coupled with the appropriate combustion model and the equation solved. The result of the simulation is typically the trace of the mode amplitudes and chamber pressure versus time.

We generally use a fourth order Runge-Kutta solver, except for the cases when a particular software is used (for example, Simulink or AUTO). In that case the integrated solver is used. In some cases, the system requires some care in order to obtain an accurate solution. For these cases, details on the solution method and problems encountered are described in the relative section.

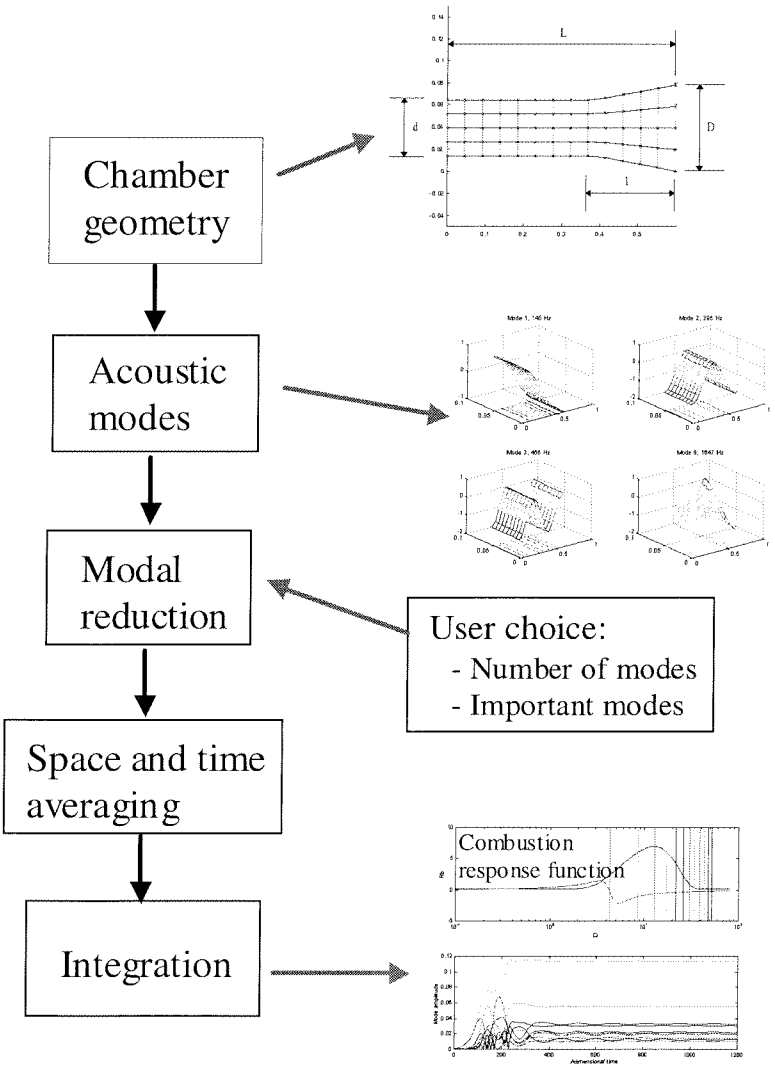

Figure 2.2. Solution Algorithm.

3 Modeling of Solid Propellant Dynamics

As mentioned in Chapter 1, solid rocket motors present some interesting phenomena, like large sensitivity of the global dynamics on very small changes in the propellant and pulsed instabilities (triggering).

The objective of this chapter is to develop a diagnostic tool that would allow the analytical consideration of propellant characteristics on the global dynamics. In order to achieve this goal, we will follow three steps.

1. Construct a model of the propellant dynamics.
2. Simulate the combustor (combustion chamber dynamics and propellant dynamics).
3. Use the results as a diagnostic tool to identify sensitivities and important characteristics in the dynamics (e.g., triggering).

We also want a model based on *transfer functions* that describe each part, so that different models can be easily constructed and tested by simply replacing a new transfer function for a section of the entire system.

To construct a model of the propellant dynamics, we start from the traditional approach, based on the QSHOD (Quasi-Steady Homogeneous One-Dimensional) model (Culick 1968, Beckstead, Mathes, Price and Culick 1969), which includes the dynamics of the thermal wave in the solid phase, while treating the gas phase response in a quasi-steady manner. This leads to a model that gives no consideration to dynamical processes with a characteristic time shorter than that of the

thermal wave in the solid phase, while experimental data suggest that many solid propellants have a combustion response function with values higher than those predicted by the QSHOD model. The natural extension of the QSHOD theory is to include the dynamics of the thermal wave in the gas phase. Two previous works seeking to correct this deficiency (T'ien 1972, Lazmi and Clavin 1992) have focused their attention on this intent. T'ien's analysis is based on direct numerical integration of the equations describing the temperature, species and velocity evolution in the flame zone of the gas phase. The chemistry is described by a one-step forward chemical reaction, with the reaction rate expressed by an Arrhenius-type expression.

Clavin achieves some simplification by applying the ideas of 'activation energy asymptotics' to the reaction zone. While their results differ in detail, both works show influences at frequencies higher than those near the broad peak of the response due to the thermal wave in the solid phase.

It is well known from many observations, both with high speed films and from pictures taken with scanning electron microscopes, that the surface of a burning solid propellant is certainly not smooth and in general contains both liquid and solid particles. For metallized propellants the agglomeration of aluminum drops is an important process affected, for example, by small amounts of impurities or additives. It seems clear that the dynamics of this region may be significant to the response of a burning propellant to external disturbances, but this phenomenon has not previously been studied. Section 3.1.3 contains the governing equations and presents a simple framework in which phenomenological modeling of that surface layer can be introduced in the general model considering the thermal waves in both the gas and solid phases. The modeling of the surface is based on thermal analysis of the layer and matching of the boundary conditions on the solid and gas-phase side. No chemical reactions (except for decomposition, based on the Arrhenius law) are considered in either the solid phase or the surface layer. The response function characterizing the behavior of the system is derived by considering small

harmonic oscillations and linearizing the equations describing the different sections of the propellant.

It has been shown (Isella and Culick 2000) that the representation of the dynamics of the solid propellant by the use of a response function based on pressure coupling only does not justify the experimental observations reporting large variations in the global dynamic response of the chamber to even minimal variation of the propellant composition or physical characteristics (e.g., grain size or distribution).

Previous work (Levine and Baum 1983, Burnley 1996) has been done showing that another mechanism, based on velocity coupling, might be fundamentally important in explaining such behavior. Levine and Baum introduced a model based on nonlinear velocity coupling to explain the observed experimental result of pulsed instabilities, and were able to match experimental results by varying the parameter representing the relative weight of the velocity coupling terms. Burnley used the same model and investigated the global dynamics by using the solution-continuation method briefly described in section 2.3.1.

The result of propellant modeling are then incorporated in the dynamical analysis of a small rocket motor to illustrate the consequences of the combustion dynamics for the stability and nonlinear behavior of unsteady motions in a motor. That allows to study the influences of propellant composition and chemistry on the global dynamical behavior of a solid rocket combustor by connecting the microscopic and macroscopic through the response function.

3.1 Derivation of the Equations

The definition of the coordinate system is shown in Figure 3.1. The problem is reduced to one-dimension, and the x axis has the origin always fixed to the propellant surface, the boundary between solid and surface layer. Hence solid material flows from the left at the rate $r = r(t)$, not

the average burning rate often assumed. This choice has an effect on the momentum equation; typically, the momentum equation is used to eliminate the dependence of the pressure from the longitudinal coordinate x. In this case, the assumption that pressure is only a function of time is still valid, provided that the time derivative of the burning rate is small compared to the inverse of the Mach number based on the gas phase.

Reduction to a one-dimensional formulation implies an averaging in transverse planes not examined here.

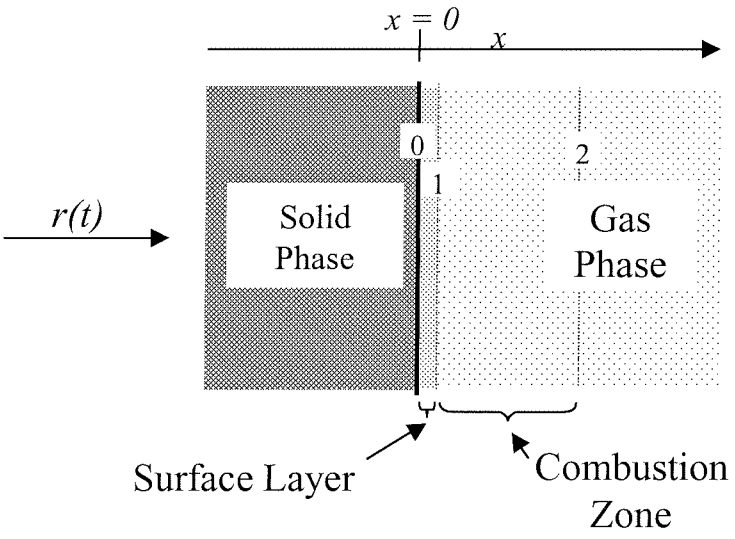

Figure 3.1. Coordinate definition.

For the purpose of the analysis, the system can be divided into four different regions:

Solid phase: $x = (-\infty, 0)$.

Surface layer: $x = (0, x_1)$.

Gas phase, combustion zone: $x = (x_1, x_2)$.

Gas phase, containing products of combustion: . $x = (x_2, \infty)$

A set of conservation equations is written for each region, and the boundary values are suitably matched.

3.1.1 Solid Phase

The propellant in the solid phase (from $x = -\infty$ to $x = 0$) is assumed to be homogeneous with no chemical reactions. The energy equation for the temperature, written in non-dimensional form, is:

(3.1)
$$\rho_c \frac{\partial T}{\partial t} + r(t)\frac{\partial T}{\partial x} - \chi_c \frac{\partial^2 T}{\partial x^2} = 0$$

The non-dimensional quantities are defined with respect to the quantities in the non-reacting gas phase as ($x \to \infty$):

(3.2)
$$\rho_c = \frac{\rho_c^*}{\rho_\infty^*} \quad T = \frac{T^*}{T_\infty^*} \quad r = \frac{r^*}{\overline{r}^*} \quad t = t^* \frac{\rho_\infty^* C_p u_\infty^2}{k_\infty} \quad x = x^* \frac{\rho_\infty^* C_p u_\infty}{k_\infty} \quad \chi_c = \frac{C_p k_c}{C_c k_\infty}$$

where k is the thermal conductivity; the subscript c refers to the condensed phase, while the subscript ∞ refers to the gas phase.

Note that the caloric properties of the propellant have been assumed to be uniform and constant.

For the purpose of linear analysis, in the limit of small amplitude oscillations, the variables can be split into the sums of average values and much smaller fluctuating parts, i.e., for the temperature: $T = \overline{T} + \tilde{T}$. Correspondingly, the equations can be written for the steady and unsteady part of the solution.

The boundary conditions for equation (3.1) are (in non-dimensional form):

For $x \to -\infty$, i.e., at the "cold end" of the propellant: $\overline{T}\big|_{x \to -\infty} = T_0$ and the oscillating temperature $\tilde{T} = 0$.

For $x = 0$ the boundary condition is set by the energy balance at the surface:

(3.3)
$$\left.\frac{\partial T}{\partial x}\right|_{0^-} = \chi_l \left.\frac{\partial T}{\partial x}\right|_{0^+} - \chi_l r L_c$$

where χ_l is the ratio of thermal conductivity of the propellant in the solid phase ($x < 0$) and conductivity of the gas phase; L_c is the non-dimensional latent heat ($\frac{L^*}{C_p T_\infty^*}$) of the phase transformation between solid and the state in the surface layer. Note that no assumption is made so far concerning the state of the surface layer: it can still be a solid state in a different crystalline state, or a liquid film. Whatever chemical transformation takes place between the solid-phase propellant and the surface layer, we assume that it can be described as a chemical change according to the Arrhenius law. In non-dimensional variables, the law can be written as:

(3.4)
$$r = e^{-E_c\left(\frac{1}{T_1}-\frac{1}{\overline{T}_1}\right)}$$

Note that we neglect the direct dependence on pressure and temperature in (3.4); this is justified by the fact that the phase transition from solid state is relatively independent of pressure and temperature. This assumption is also common in the literature (T'ien 1972, Clavin and Lazmi 1992).

The solution to the steady part of equation (3.1) for the average temperature ($\overline{T}$) is:

(3.5)
$$\overline{T} = T_0 + \left(\overline{T}_1 - T_0\right)e^{\frac{x}{\chi_c}}$$

Equation (3.5) can be used in the equation for the fluctuating temperature ($\tilde{T}$) to obtain:

(3.6)
$$\rho_c \frac{\partial \tilde{T}}{\partial t} + r\frac{\partial \tilde{T}}{\partial x} - \chi_c \frac{\partial^2 \tilde{T}}{\partial x^2} + \tilde{r}\frac{\overline{T}_s - T_0}{\chi_c}e^{\frac{x}{\chi_c}} = 0 \qquad (-\infty < x < 0)$$

Substituting the unsteady version of expression (3.4):

(3.7)
$$\tilde{r} = E_s \frac{\tilde{T}_s}{\bar{T}_s^2}$$

into equation (3.6) and assuming oscillatory behavior for the time dependence of the independent variables (i.e. $\tilde{T} = \hat{T}e^{i\Omega t}$, etc.; Ω is the non-dimensional frequency), equation (3.6) becomes:

(3.8)
$$\chi_c \frac{\partial^2 \hat{T}}{\partial x^2} - \frac{\partial \hat{T}}{\partial x} - i\omega\rho_c \hat{T} = \frac{E_s}{\bar{T}_s^2} \frac{\bar{T}_s - T_0}{\chi_c} \hat{T}(0) e^{\frac{x}{\chi_c}}$$

Solving for the oscillatory temperature in the solid phase:

(3.9)
$$\hat{T}(x) = \hat{T}(0)\left(1 + \frac{1}{i\Omega\rho_c} \frac{E_s}{\bar{T}_s^2} \frac{\bar{T}_s - T_0}{\chi_c}\right) e^{\frac{1+\sqrt{1+4\chi_c i\Omega\rho_c}}{2\chi_c}x} - \frac{1}{i\Omega\rho_c} \frac{E_s}{\bar{T}_s^2} \frac{\bar{T}_s - T_0}{\chi_c} \hat{T}(0) e^{\frac{x}{\chi_c}}$$

where we used the boundary conditions specified above to eliminate the exponentially growing terms of the general solution. Note that for $\Omega \to 0$, expression (3.9) reduces to the correct limit:

(3.10)
$$\hat{T}(x) = \hat{T}(0) e^{\frac{x}{\chi_c}}$$

Equation (3.9) is then substituted into the unsteady version of (3.3) to form a relation between the temperature and the temperature gradient at the surface of the solid phase ($x = 0$) in the form:

(3.11)
$$\left.\frac{\partial \hat{T}}{\partial x}\right|_{0^+} = \frac{\hat{T}(0)}{i\Omega\rho_c\chi_l}\left[(i\Omega\rho_c + \Psi)\frac{1+\sqrt{1+4\chi_c i\Omega\rho_c}}{2\chi_c} - \frac{\Psi}{\chi_c} + i\Omega\rho_c \frac{E_s}{\bar{T}_s^2} L_c \chi_l\right] = K(\Omega)\hat{T}(0)$$

$$\Psi = \frac{E_c}{\bar{T}_1^2} \frac{\bar{T}_1 - T_0}{\chi_c} \qquad \left(x = 0^+\right)$$

This expression will be used as a boundary condition on the left side of the surface layer. Note that if we were to use the quasi-steady approach (QSHOD), in which no intrinsic dynamics is associated with the gas phase (and no surface layer is present), (3.11) would contain all the dynamics associated with the combustion of the solid propellant, i.e., the response of the solid phase. In the following section, we use this expression as a reference to analyze the effect of

including the dynamics of the surface layer in the model. In the limit of $\Omega \to 0$, equation (3.11) reduces to the steady state expression written above.

Note that using the non-dimensional variables defined in (3.2), the non-dimensional frequency assumes the following expression:

(3.12) $$\Omega = \omega \frac{k_c \rho_g}{\overline{m}^2 C_p}$$

The convention adopted to express the non-dimensional frequency in the literature of QSHOD theory (Culick 1968, Beckstead et al. 1969) often uses the density in the solid phase instead of the gas phase. With the parameter values used in the examples reported here (Table 3-2), the frequency will be scaled by $\rho_c = 1000$.

Since we assume that there is no active chemical reaction in the surface layer, the species balance is unaltered until the boundary of the surface layer and the gas-phase (boundary *1*, in Figure 3.1). The mass flux balance at the surface states:

(3.13) $$\rho_c^* r^* = \rho^* u^*$$

Writing (3.13) in non-dimensional form and considering that $\frac{r^*}{u_\infty^*} \cong \frac{1}{\rho_c}$ (with $\rho_c = \frac{\rho_c^*}{\rho_\infty^*}$), we obtain:

(3.14) $$r = \rho_{0^+} u \qquad (x = 0)$$

Substitution of equation (3.7) into the unsteady part of (3.14) results in a relation between unsteady mass flux and unsteady temperature:

(3.15) $$\hat{m}\big|_{o^+} - \frac{E_s}{\overline{T}_s^2}\hat{T} = 0$$

This simply states that the oscillations of the temperature and the mass flux are in phase at the interface *0*.

If we were to consider only the dynamics of the solid phase, and assume quasi-steady behavior for the gas phase, we can obtain an expression that falls into the quasi-steady approach. Culick 1967 presents in detail the derivation of the quasi-steady response function that can be written as (Culick 1967)

(3.16)
$$R_b = \frac{nAB}{\lambda + \frac{A}{\lambda} - (1+A) + AB}$$

Furthermore, Culick 1968 shows that every quasi-steady theory leads to a response function that can be cast in the form (3.16). In the literature, this is normally referred to as the "AB form" of the combustion response function. The values of the coefficients A and B are related to the physical characteristics of the propellant, and their expression differs depending on the theory under consideration.

3.1.2 The Intrinsic Stability Limit for Burning of Solid Propellant

Regarding expression (3.16) as a transfer function, it is interesting to locate its poles: their position defines the stability characteristics of the system (in our case, the propellant) associated with the transfer function.

The denominator of (3.16) vanishes if

(3.17)
$$\lambda^2 + (AB - A - 1)\lambda + A = 0$$

or, defining $\kappa = (A + 1 - AB)$

(3.18)
$$\lambda = \frac{\kappa \pm \sqrt{\kappa^2 - 4A}}{2}$$

$$\lambda = \begin{cases} \frac{\kappa}{2} \pm i\sqrt{A - \left(\frac{\kappa}{2}\right)^2} & \left(\frac{\kappa}{2}\right)^2 < A \\ \frac{\kappa}{2} \pm \sqrt{\left(\frac{\kappa}{2}\right)^2 - A} & \left(\frac{\kappa}{2}\right)^2 > A \end{cases}$$

This condition is important in the dynamics of the chamber since an infinitesimally small disturbance in the pressure would cause a large (within the linear limit, infinite) response of the mass flux produced by burning; this in turn strengthens the original pressure disturbance, and hence it provides a mechanism that leads to instability in the chamber.

Now consider the energy equation for the solid phase (3.1). Assuming harmonic motions $\tilde{T} \approx e^{i\omega t}$, the spatial dependence can be determined from (3.1) to be $\exp(\lambda \xi_p)$, where λ satisfies

(3.19) $$\lambda(\lambda - 1) = i\Omega$$

and Ω is the non-dimensional frequency parameter:

(3.20) $$\Omega = \frac{k_c \rho_c}{\overline{m}^2 C_p}\omega$$

Equation(3.19) yields two values for λ

(3.21) $$\lambda = \frac{1 \pm \sqrt{1 + i4\Omega}}{2}$$

in order for $\tilde{T} \to 0$ when $x \to -\infty$ (i.e., the disturbance propagating inside the propellant must vanish, see Figure 3.1) we need to discard the solution with negative real part, hence the condition

(3.22) $$\mathrm{Re}(\lambda) > 0$$

The equation above sets a mathematical condition for the solution to have physical sense in space.

Another condition, based on stability considerations, can be set on Ω, the frequency of harmonic time variations. In order to have stable transient motions, we need

(3.23) $$\mathrm{Im}(\Omega) > 0$$

If we regard equation (3.18) as a relation between λ and A and B, we can combine (3.18) with (3.19) to obtain an expression for Ω in terms of A and B

$$\left(\frac{\kappa}{2}\right)^2 < A$$

(3.24)

$$\Omega_r = \pm(\kappa - 1)\sqrt{A - \left(\frac{\kappa}{2}\right)^2}$$

$$\Omega_i = (1-\kappa)\frac{\kappa}{2} + A$$

$$\left(\frac{\kappa}{2}\right)^2 > A$$

(3.25)

$$\Omega_r = 0$$

$$\Omega_i = (1-\kappa)\left[\frac{\kappa}{2} \pm \sqrt{\left(\frac{\kappa}{2}\right)^2 - A}\right] - A$$

Relative to the time behavior, equation (3.24) represents an exponential decay or growth (depending on the sign of Ω_i) with superimposed oscillations, while equation (3.25) is a pure exponential growth or decay with no oscillation.

If we now combine conditions (3.22) and (3.23), we obtain the following table, which contains all the possible combinations for having a physically significant pole (in λ space) of the response function.

	Decay in space: $\mathrm{Re}(\lambda) > 0$		Decay in time: $\mathrm{Im}(\Omega) > 0$
$\left(\frac{\kappa}{2}\right)^2 < A$	$\kappa > 0$	AND	$(1-\kappa)\frac{\kappa}{2} + A$
		OR	
$\left(\frac{\kappa}{2}\right)^2 > A$	$\frac{\kappa}{2} \pm \sqrt{\left(\frac{\kappa}{2}\right)^2 - A} > 0$ (always true)	AND	$(1-\kappa)\left[\frac{\kappa}{2} \pm \sqrt{\left(\frac{\kappa}{2}\right)^2 - A}\right] - A > 0$

Table 3-1. Conditions for 'intrinsic stability.'

Let's analyze condition

(3.26)
$$\left(\frac{\kappa}{2}\right)^2 = A$$

for the typical values of the parameter space

(3.27)
$$0 < A < 20$$
$$0 < B < 5$$

Solving for B

(3.28)
$$A = \frac{B + 1 \pm 2\sqrt{B}}{(B-1)^2}$$

Figure 3.2 shows the regions defined by equation (3.26), and hence defines the areas where the top or bottom conditions of Table 3-1 are valid.

The conditions in the top row of Table 3-2 can be rewritten as

(3.29)
$$B + 1 > A(B+1)^2$$

(3.30)
$$B < 1 + \frac{1}{A}$$

Figure 3.3 portraits the regions defined by the conditions above. Shaded areas represent regions where either the propellant is 'unstable', i.e., condition (3.29) is violated, or the solution loses physical significance, i.e., condition (3.30) is violated.

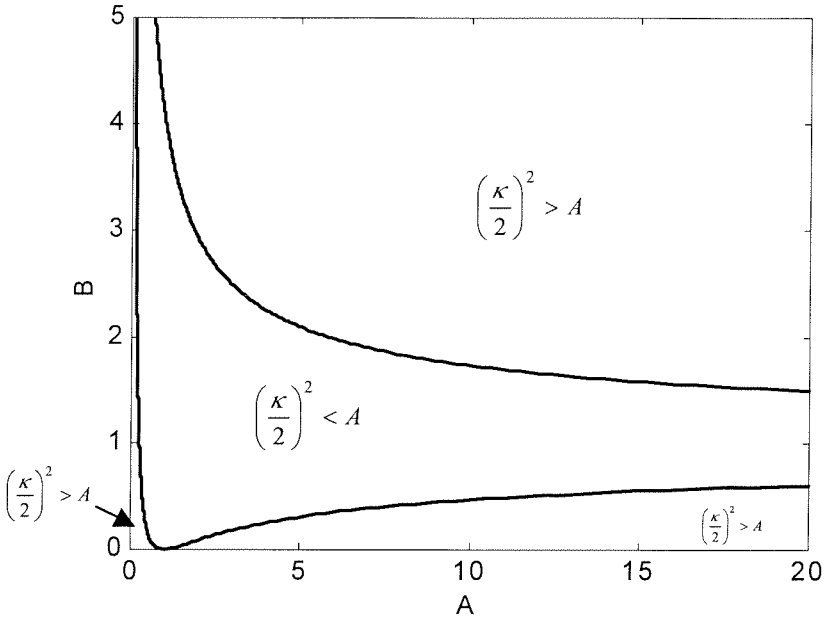

Figure 3.2. Regions defined by equation (3.26).

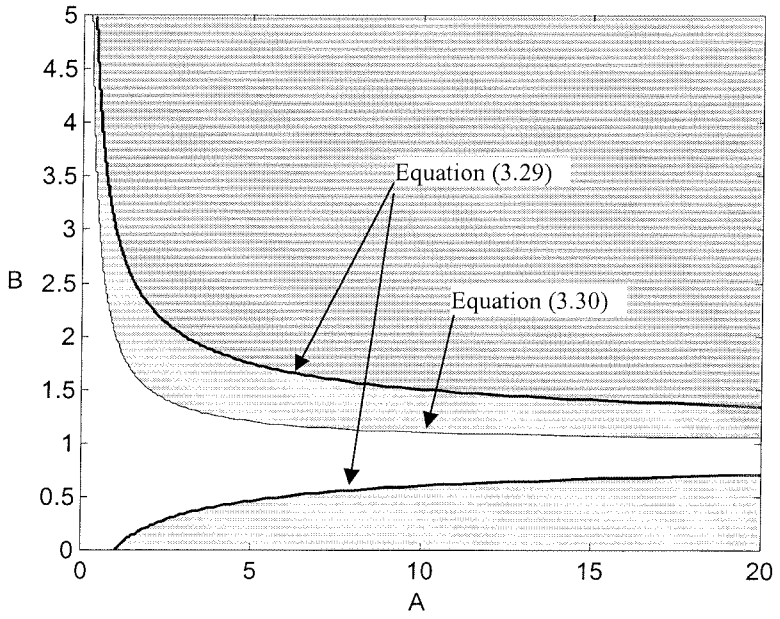

Figure 3.3. Stability limits; shaded areas are "forbidden" regions for propellant characteristics.

Consider the case when $\left(\frac{\kappa}{2}\right)^2 > A$, then, as said before, λ is a real number. Then it is possible to show that equation (3.19) and condition (3.23) lead to the necessary condition

(3.31)
$$B > 1 + \frac{1}{A}$$

Thus the locus defined by the last of the inequalities in Table 3-2 (which covers a very small area at the top left corner of the *AB* plane) lays in a 'forbidden' region for the response function, and hence is not relevant.

Figure 3.4 presents the final results of the present analysis. In the *AB* plane, the only poles of the combustion response function that actually satisfy all the other physical requirements lie on the line separating the shaded region, that becomes a 'forbidden region' for propellant characteristics. For reference, the figure also shows regions in the *AB* plane occupied by real propellants. Global dynamics simulations show that for propellants in those regions, the pressure coupled response derived from the QS theory can not justify the combustor sensitivity observed in the experiments.

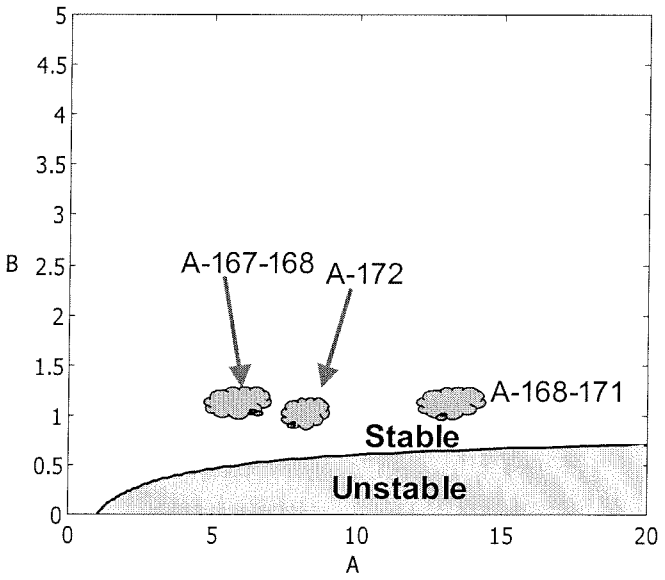

Figure 3.4. 'Forbidden region' of the *AB* plane.

3.1.3 Surface Layer

In general, the dynamics of the surface layer (band *0-1* in Figure 3.1) can be represented by introducing transfer functions connecting fluctuations of mass flux, temperature and heat transfer at the edges of the zone:

$$\hat{m}_1 = M_{surf}(\Omega)\hat{m}_0$$

(3.32)

$$\hat{T}_1 = T_{surf}(\Omega)\hat{T}_0$$

$$\left.\frac{d\hat{T}}{dx}\right|_1 = Q_{surf}(\Omega)\left.\frac{d\hat{T}}{dx}\right|_0$$

The transfer functions appearing in the equations above can be derived directly from experiments or from modeling. Note that by using this representation, the result of the QS formulation can be immediately extended to include the surface layer:

(3.33)

$$\frac{\hat{m}_1}{\overline{m}} = R_b(\Omega)M_{surf}(\Omega)\frac{\hat{p}}{\overline{p}} \quad (x = x_1)$$

where the term $R_b(\Omega)$ represents the result of the QS approach.

Generally, to accommodate true dynamical behavior in the surface layer, the functions M_{surf}, T_{surf}, Q_{surf} are complex functions.

3.1.3.1 Representations of Surface Dynamics with a Time Lag

Within the quasi-steady theory, the generation of a second peak in the response function can also be interpreted as a consequence of a time delay between the heat generation in the gas phase and the feedback into the solid propellant.

In general, a pure time-lag theory produces a combustion response function that does not present any peak (Grad 1949, Cheng 1962) and is hence not suited to describe properly the response of a solid propellant (experimental evidence shows the presence of one or more peaks). On the other

hand, the use of a quasi-steady approach (with no consideration of the surface layer) produces a response function that can be put in the general form (3.16).

Assuming that there is a relaxation time τ (or time delay) between the mass flux and the pressure perturbation, we can write

(3.34)
$$\frac{d}{dt}\left(\frac{\tilde{m}}{\overline{m}}\right)=\frac{1}{\tau}\left(R_b\frac{\tilde{p}}{\overline{p}}-\frac{\tilde{m}}{\overline{m}}\right)$$

For harmonic fluctuations with frequency Ω, equation (3.34) becomes:

(3.35)
$$\frac{\hat{m}_1}{\overline{m}}=\frac{1}{1+i\Omega\tau}\left(R_b\frac{\hat{p}}{\overline{p}}\right)=R_b\frac{e^{-i\Omega\tau}}{\sqrt{1+\Omega^2\tau^2}}\frac{\hat{p}}{\overline{p}}$$

Note that for $\Omega \to 0$, the correction term due to the relaxation time approaches *1* and (3.35) reduces to the correct limit.

Recall that in the case of the quasi-steady theory, the dynamics of the gas phase are neglected ($\frac{\partial p}{\partial t}=0$), so $\frac{\partial m}{\partial x}=0$ and hence $\tilde{m}_1=\tilde{m}\big|_{x\to\infty}$ in the gas phase, so, within this approximation, (3.16) or (3.35) are enough to complete the description of the propellant behavior.

This result differs from other time-lag theories for solid propellants. In Grad 1949, the author obtains an expression similar to (3.35), but without the R_b term. In Cheng 1962, the author presents a result that includes an exponential term in the numerator and the denominator, but it is still missing a proper way to introduce the physical characteristics of the propellant, described by A and B in the quasi-steady theory. In our case, the delay is introduced by an extra layer while the normal quasi-steady response is considered for the solid and gas phases.

Equation (3.35) produces the response shown by the thin line in Figure 3.5, where the real part of the delayed combustion response function is plotted. The thick line presents the traditional QS

response. The values used for the plot are: $A = 14$, $B = 0.85$, unitary n and time delay of 1.5 non-dimensional time units.

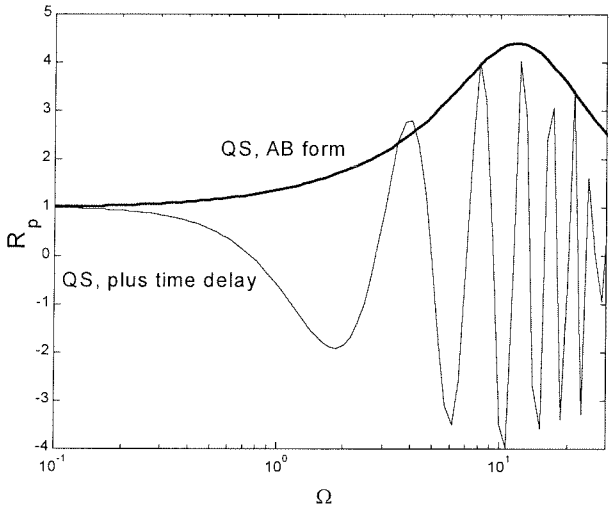

Figure 3.5. *AB* form with time delay (thin line), *AB* form (thick line).

Note that the response shows several peaks at a higher frequency: the expression of the time delay as an exponential brings in a series of successive peaks that may not be justified by the experiments. In this respect, the consideration of the effect of a surface layer, as in section *3.1.3.2*, likely gives a more realistic picture.

3.1.3.2 Representation of the Surface Layer as a Region with Different Properties

The surface layer (band *0-1* in Figure 3.1) is assumed to be homogeneous with no chemical reaction (all the active chemical reactions are assumed to take place in the gas-phase). Substantially the surface layer represents the zone of the propellant where the heat feedback from the reacting gas causes sensible modifications in the physical characteristics of the solid. It can be a mixture of liquid propellant with solid particles, or just the solid in a different physical state.

The dynamics of the surface layer will be represented by the use of transfer functions connecting fluctuations of mass flux, temperature and heat transfer at the edges of the layer and feeding into

the gas-phase. Experimental evidence suggests that the surface layer might exhibit significant response at a frequency higher than the usual peak in the response function derived from quasi-steady theory. The effect of the dynamics of the surface layer will be considered in comparison to the analysis with the solid phase only.

The structure of the analysis for the surface layer is analogous to the analysis of the solid layer. The equations governing the dynamics of the layer are solved with boundary conditions derived from the physical conservation conditions written for small control volumes across the boundary; the problem is considered to be one-dimensional and physical characteristics are assumed to remain constant throughout the zone.

We assume that the dependence of the surface layer density on pressure is negligible when compared to that of the gas phase. This gives an energy equation for the temperature of the surface layer similar to (3.1):

(3.36)

$$\rho_{sl}\frac{\partial T}{\partial t}+r_{sl}\frac{\partial T}{\partial x}-\chi_{sl}\frac{\partial^2 T}{\partial x^2}=0 \qquad \left(0<x\le x_1\right)$$

The non-dimensional quantities are defined in a way analogous to (3.2). The decomposition of the layer is governed by an Arrhenius equation that gives an exponential dependence, through the activation energy, from the temperature. In this case the decomposition from the surface layer phase to the gas phase happens at the interface $x = x_1$.

The boundary conditions are set by the values of the temperature on the right end of the solid phase and expression (3.11), and the value of the average temperature on the downstream side of the surface layer. The analysis is carried out in a similar way as before: equations are linearized and the average and unsteady parts split and solved separately. The average temperature profile is still an exponential function of position because we assume that no energy is released or gained in the surface region.

Particularly important is the general solution for the oscillating temperature at position x within the layer, since it carries a frequency dependence in it. The unsteady part of equation (3.36), solved assuming oscillating solutions, gives an expression for the oscillating temperature in the surface layer:

(3.37)
$$\hat{T}(x)=\hat{T}(x_1)\left\{\left[\Xi+\chi_l\Theta\right]e^{\frac{1+\sqrt{1+4\chi_l\rho i\Omega}}{2\chi_l}x}+\Theta e^{\frac{1-\sqrt{1+4\chi_l\rho i\Omega}}{2\chi_l}x}-\frac{\Psi_l}{i\Omega\rho_l}e^{\frac{x}{\chi_l}}\right\}\quad(0\le x\le x_l)$$

where:

(3.38)
$$\Psi_l=\frac{E_l}{\overline{T}_l^{\,2}}\frac{\overline{T}_l-\overline{T}_s}{\chi_l}$$
$$\Xi=1+\frac{1}{i\Omega\rho_l}\Psi_l$$
$$\Theta=\frac{K(\Omega)+\dfrac{\Psi_l}{i\Omega\rho_l}-\dfrac{1+\sqrt{1+4\chi_l\rho_l i\Omega}}{2\chi_l}(\Xi)}{\sqrt{1+4\chi_l\rho_l i\Omega}}$$

where $K(\Omega)$ is defined in equation (3.11). Expression (3.37), used to write a boundary condition for the gas-phase, carries the frequency dependence characteristic of the surface layer into the solution to the problem.

The principal physical characteristics that influence the dynamics of the surface layer are the activation energy (E_l) that originally appears in the Arrhenius expression and the density (ρ_l), relative to the density of the other zones. Figure 3.7 presents a plot showing the effect of the variation of these two quantities on the shape of the transfer function describing the dynamics of the surface layer. Equation (3.37) can be used to substitute in the unsteady energy balance at boundary *1*:

(3.39)
$$\left.\frac{d\hat{T}}{dx}\right|_{x_1^+}=\frac{1}{\chi_g}\left.\frac{d\hat{T}}{dx}\right|_{x_1^-}+E_l\frac{\hat{T}(x_0)}{\overline{T}_1^{\,2}}L_l$$

This produces an expression relating temperature and temperature gradient at the boundary, similar to expression (3.11).

(3.40)
$$\left.\frac{d\hat{T}}{dx}\right|_{x_1^+} = \hat{T}(x_1)F(\Omega) \quad \left(x = x_1^+\right)$$

The explicit expression for $F(\Omega)$ is quite involved; it can be easily obtained from (3.37) upon substitution and is reported in Appendix B.

It is interesting to compare the position of the maximum values in equations (3.11) and (3.40). For reference, their plot versus non dimensional frequency is reported in Figure 3.6.
Given the form of the equations, an exact analytical expression for the position of the maximum can not be obtained. If we consider the typical values of the coefficients (reported in Appendix C) appearing in those expressions, and we perform an order of magnitude analysis on the derivatives and retain only the terms that contribute the most, we can find the approximate expressions

(3.41)
$$\Omega\rho_c = \Psi$$

(3.42)
$$\Omega\rho_c = \left(\Psi + \Psi_l\right)\left(\frac{\rho_c}{\rho_l}\right)^{\frac{2}{3}} + \frac{L}{L_l}\rho_c$$

valid for the quasi steady and the surface layer case respectively. The constants are defined in equations (3.11) and (3.38). In the case of the boundary condition for the surface layer, equation (3.41) still defines the approximate position of the inflection point of the function (see Figure 3.6 on the right). In both cases we see that the ratio of the activation energy appearing in the Arrhenius exponent for the decomposition law and the thermal conductivity is the one that defines the position of the maximum. In the case of the solid layer, the relative density and the latent heat also play a (minor) role.

As stated before, no active chemical reactions are considered in the solid phase and in the surface layer; the reactions are concentrated in the gas-phase, where we assume a one step chemical reaction from fuel and oxidizer to products (see section 3.1.4.1 for a more detailed explanation). As a consequence, the concentration of fuel and oxidizer remains constant throughout the band $-\infty < x \leq x_1$ and no balance equations are needed for the species within the solid phase and the surface layer. On the other hand in the gas phase, where there are chemical reactions, species equations have to be considered; hence the need for setting boundary conditions on the species at the surface $x = x_1$. Since only *3* species are present (fuel, oxidizer, products), the species equations can be reduced to one only (T'ien 1972, Huang and Micci 1991). If we decide to use the equation for the fuel concentration, the required boundary condition can be expressed by considering the fuel flux balance, written as

(3.43)
$$Y^{x_1^-} = Y^{x_1^+} - \frac{1}{m}\frac{\partial Y}{\partial x}\bigg|_{x_1^-}$$

Equation (3.43) can be rewritten in terms of the oscillating quantities as

(3.44)
$$\hat{Y}(x_1) - \frac{d\hat{Y}}{dx}\bigg|_{x_1^-} + \hat{m}\frac{d\overline{Y}}{dx}\bigg|_{x_1^-} = 0 \qquad (x = x_1)$$

Also, for unitary Lewis number and two species in the analysis, the average species flux is related to the average temperature through the heat of combustion q:

(3.45)
$$\overline{Y} = \frac{1}{q}\left(1 - \overline{T}\right)$$

The last equation we need is provided by the mass flux balance that, as for the solid phase, equation (3.14), yields a mass flux oscillation in phase with the temperature oscillations:

(3.46)
$$\hat{m}\big|_{x_1} - \rho_1 \frac{E_1}{\overline{T}_2^2}\hat{T}_1 = 0$$

It is interesting to analyze what is the effect of the surface layer on the gas-phase. Table 3-2 presents some typical values of the characteristics of a solid propellant (Becksetead et al. 1969, T'ien 1972, Clavin and Lazmi 1992, Culick and Dehority 1969).

E_c	8.0	T_0	0.15
E_l	4.0	T_1	0.35
ρ_c	1000	T_2	0.40
ρ_l	50	χ_c	1.0
γ	1.2	χ_l	1.0
L_c	0.1122	χ_g	1.0
L_{sl}	0.0025	Q_f	12.5

Table 3-2. Non-dimensional values of the physical characteristics of the solid propellant used in the examples.

In the quasi-steady approach (QSHOD) no intrinsic dynamics are associated with the gas phase, so the response of the solid phase to the heat feedback coming from the combustion zone is the one that creates the characteristic response function with a low frequency peak. In our case, (3.11) would represent the dynamics of the solid phase (it was shown that the temperature and mass fluctuation solutions only differ by a scale factor). Using the values presented in Table 3-2, it is possible to plot the solid response, i.e., equation (3.11), and the solid plus surface layer response, represented by equation (3.40). The two plots are presented in Figure 3.6 and Figure 3.7. The axes have been re-scaled so that the convention for the non-dimensional frequency is the common one adopted in the literature (i.e., $\Omega = 1000\ \varpi$), and the value at the origin is *1*.

All the value of the parameters for the curves presented in Figure 3.6 are the same used as the reference T'ien case, and are listed in Table 3-2.

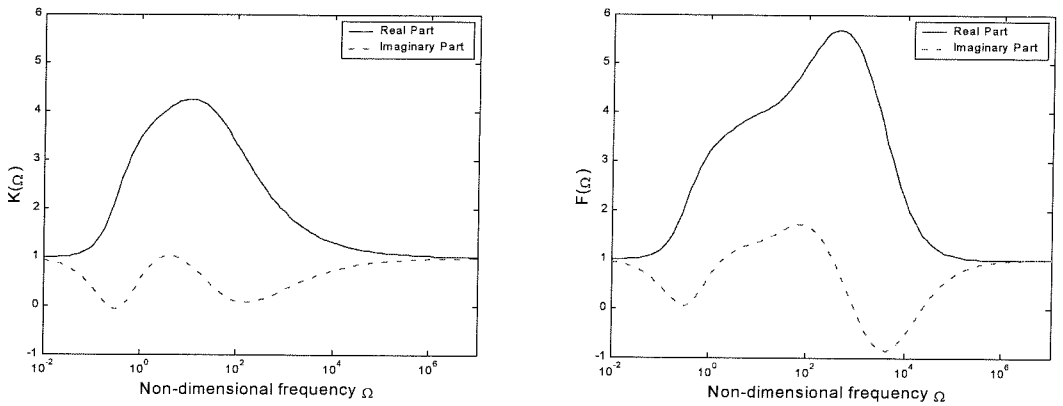

Figure 3.6. Frequency dependence of the temperature boundary condition for a model including the solid phase only (left) and solid plus surface layer (right).

The effect of the surface layer is to generate a second peak in the response function, at a higher frequency than the peak generated by the solid phase alone, and, for the parameters used here, of higher absolute value. Also, as expected, it reduces the influence of the solid phase resonance: the value of the response at the first peak is lower than the case with solid phase only.

Figure 3.7 shows the effect of activation energy and density of the surface layer on the response function.

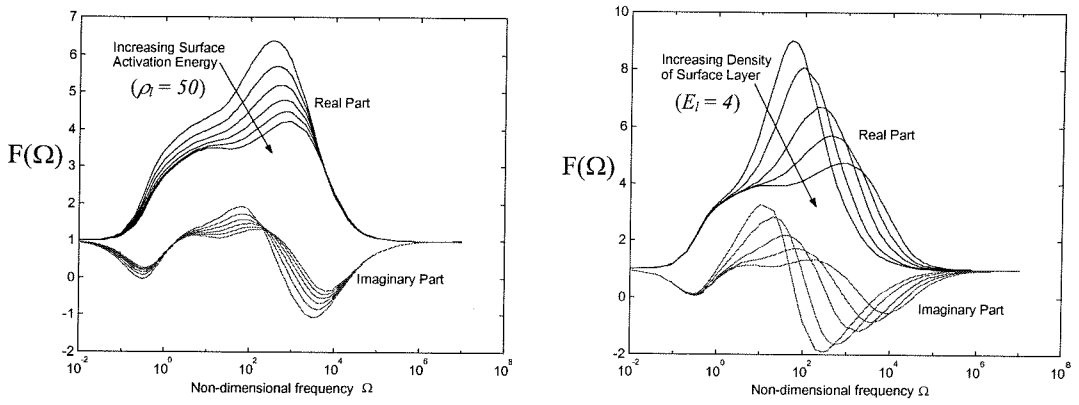

Figure 3.7. Effect of the activation energy and density on the dynamics of the surface layer.

The peak value of the response function decreases with increasing activation energy and with increasing density of the material composing the surface layer.

More complex models of the surface layer can be devised, including chemical reactions, for example; in the limit of the linear analysis presented here, models can be reduced to the form of equations (3.32) and simply introduced in the representation of the whole system as a different transfer function.

3.1.4 Gas Phase

The flame is assumed to be one-dimensional, laminar and premixed. The thermodynamic characteristics of the gas are assumed to be constant, and later we will use the perfect gas relations to simplify the equations.

For a one-step forward chemical reaction (fuel + oxidizer → products), the continuity and species conservation equations, in non-dimensional form, are (Culick 1969):

(3.47)
$$\frac{\partial \rho_g}{\partial t} + \frac{\partial (\rho_g u_g)}{\partial x} = 0$$

(3.48)
$$\rho_g \frac{\partial Y}{\partial t} + \rho_g u_g \frac{\partial Y}{\partial x} - \frac{\partial^2 Y}{\partial x^2} = -w$$

Note that, in the previous expressions, u_g is measured relative to the solid interface.

By using the energy equation and perfect gas properties, the temperature energy equation for a moving gas can be written as (neglecting viscous terms)

(3.49)
$$\tilde{\rho}_g C_p \frac{D\tilde{T}}{D\tilde{t}} = \frac{D\tilde{p}}{D\tilde{t}} - \nabla \cdot \tilde{q} + \tilde{Q}_f \tilde{w}$$

where C_p is the specific heat, assumed constant; w is the reaction rate and Q_f is the heat of combustion. By proper scaling of the momentum equation, it can be shown that the spatial variation of the pressure over the flame zone is negligible, so (3.47) can be re-written (in non-dimensional form) as:

(3.50)

$$\rho_g \frac{\partial T}{\partial t} + \rho_g u_g \frac{\partial T}{\partial x} - \frac{\partial^2 T}{\partial x^2} - \frac{\gamma - 1}{\gamma} \frac{\partial p}{\partial t} = Q_f w$$
$$\left(x_2 < x < \infty\right)$$

where $Q_f = \dfrac{\widetilde{Q}_f}{C_p \widetilde{T}_\infty}$ is the non-dimensional specific heat of combustion.

Again, all the variables can be written as the sum of an average and a (small) fluctuating part; hence equations (3.47), (3.48) and (3.50) can be divided into steady-state and fluctuating equations.

3.1.4.1 Chemistry

In our model we consider active chemical reactions only in the gas phase; solid phase and surface layer are only admitted to have the possibility of change of phase reactions, which will be simply represented by using an Arrhenius-type exponential dependence on the thermodynamic quantities.

For the chemical reaction in the gas phase we assume a one-step forward chemical reaction; such an assumption is common in the literature (T'ien 1927, Huang and Micci 1990, Lazmi and Clavin 1992) and is justified by the enormous complexity of the chemical reactions taking place in the flame zone of a solid propellant and by the relative scarcity of experimental data and chemical flame models.

For a one-step forward reaction:

(3.51)

$$\nu'_f [f] + \nu'_o [o] \rightarrow \nu''_p [p]$$

Defining ν_i ($i = o, f$) as

(3.52)

$$\nu_i = \frac{W_i \left(\nu''_i - \nu'_i\right)}{W_f \nu_f}$$

and considering that fuel, oxidizer and products mass fraction are related by reaction (3.51), only one equation is required for the species evolution, plus the fact that

(3.53)
$$\frac{Y_i}{\nu_i} = \frac{Y_f}{\nu_f} + const$$

where the constant can be determined by observing that at the flam edge both fuel and oxidizer vanish. This allows writing the reaction rate w, appearing in (3.50), as

(3.54)
$$w = BjT^{\delta}\left(\frac{p}{T}\right)^{n} Y_f^{n} e^{-\frac{E}{T}}$$

where j is the oxidizer-fuel ratio. If Le = 1, the steady state equation for the temperature and the one for the species (3.59) can be made similar with the substitution:

(3.55)
$$\overline{Y} = \frac{1}{Q_f}\left(1 - \overline{T}\right)$$

If we consider a second order reaction, the steady state part of the reaction rate yields

(3.56)
$$\overline{w} = \frac{B}{Q_f^2} j \overline{T}_g^{\alpha-2}\left(1 - \overline{T}_g\right)^2 e^{-\frac{E}{\overline{T}_g}}$$

For the non steady part we obtain

(3.57)
$$\hat{w} = \overline{\left(\frac{\partial w}{\partial p}\right)}\hat{p} + \overline{\left(\frac{\partial w}{\partial T}\right)}\hat{T} + \overline{\left(\frac{\partial w}{\partial Y}\right)}\hat{Y}$$

where the coefficients are the value of the partial derivative in the mean state:

(3.58)
$$\overline{\left(\frac{\partial w}{\partial p}\right)} = Bj\overline{T}^{\delta-n} n \frac{e^{-\frac{E}{\overline{T}}}}{q^n}\left(1 - \overline{T}\right)^n$$
$$\overline{\left(\frac{\partial w}{\partial T}\right)} = Bj\overline{T}^{\delta-n-1} \frac{e^{-\frac{E}{\overline{T}}}}{q^n}\left(1 - \overline{T}\right)^n\left(\delta - n + \frac{E}{\overline{T}}\right)$$
$$\overline{\left(\frac{\partial w}{\partial Y}\right)} = Bj\overline{T}^{\delta-n} n \frac{e^{-\frac{E}{\overline{T}}}}{q^{n-1}}\left(1 - \overline{T}\right)^{n-1}$$

3.1.4.2 Steady-State Equations

The pressure, as explained before, is only a function of time, and can be written as $p(t) = 1 + \hat{p}e^{i\Omega t}$, where $\hat{p}$ is a small quantity and Ω is the non-dimensional frequency. Also all the other quantities are split in steady and oscillating part: $f(x,t) = \overline{f}(x) + \hat{f}(x)e^{i\Omega t}$. After the substitution, the steady-state equations are

$$\begin{aligned} &\overline{\rho}_g \overline{T}_g = 1 \\ &\overline{m}_g = \overline{\rho}_g \overline{u}_g = 1 \\ &\frac{d\overline{Y}}{dx} - \frac{d^2\overline{Y}}{dx^2} = -\overline{w} \\ &\frac{d\overline{T}_g}{dx} - \frac{d^2\overline{T}_g}{dx^2} = Q_f \overline{w} \end{aligned} \tag{3.59}$$

Note that the solution to the equation for the species concentration can be derived from the solution of the temperature equation with the transformation: $\overline{Y} = \frac{1}{Q_f}(1 - \overline{T})$.

The solution of the steady state problem corresponds to the solution of the last of (3.59) with (3.56).

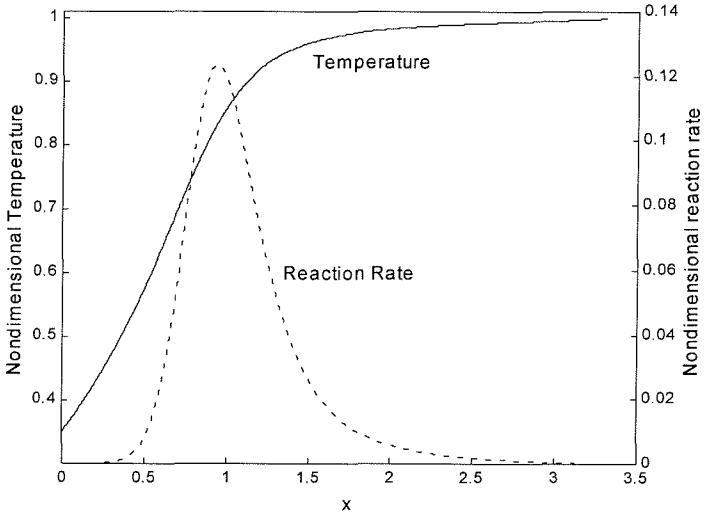

Figure 3.8. Typical steady-state solution for the gas-phase. Temperature (left axis), non-dimensional reaction rate (right axis).

The end of the flame zone (x_2) is defined during the computation as the location where the temperature reaches its final value (within a specified tolerance). The value of B, which appears in (3.56), is obtained by integrating the equations backwards (from the right end of the flame) with a guessed value for B, and then iterating until convergence to the imposed temperature boundary condition on the left end side. A typical solution is presented in Figure 3.8.

3.1.4.3 Unsteady Equations

By using the perturbed equation of state, it is possible to write the mass conservation equation for the mass flow directly, eliminating the explicit dependence on velocity and density:

(3.60)
$$\overline{T}_g \frac{d\hat{m}_g}{dx} - i\frac{\omega}{\overline{T}_g}\hat{T}_g = -i\omega$$

Also, from the steady equation of state and continuity, $\overline{u}_g = \overline{T}_g$. By making use of this fact, equations (3.48) and (3.50), written for the oscillating quantities, become

(3.61)
$$\frac{d^2\hat{Y}}{dx^2} - \frac{d\hat{Y}}{dx} - i\frac{\omega}{\overline{T}_g}\hat{Y} = \frac{d\overline{Y}}{dx}\hat{m}_g + \hat{w}$$

(3.62)
$$\frac{d^2\hat{T}_g}{dx^2} - \frac{d\hat{T}_g}{dx} - i\frac{\omega}{\overline{T}_g}\hat{T}_g = \frac{d\overline{T}_g}{dx}\hat{m}_g - Q_f\hat{w} - i\frac{\gamma-1}{\gamma}\omega$$

where $\hat{w}$ is given by equation (3.57).

Equations (3.60), (3.61) and (3.62) form a fifth order system of differential equations (with variable coefficients, depending on the steady state solution to the temperature, species concentration and reaction rate), that can be integrated numerically, with proper boundary conditions.

3.1.5 Boundary Conditions

As shown in section 3.1.4.2, the steady-state equations for the flame zone in the gas-phase reduce to a single equation for the average temperature distribution. The two boundary conditions for the second order equation are the temperatures at the interface with the surface layer and the temperature at the outer edge of the flame zone:

(3.63) $$\overline{T}(x_2) = \overline{T}_2 \qquad \overline{T}(\infty) = 1$$

The unsteady equations form a fifth order differential system. Two boundary conditions at the flame edge are $\hat{Y} = 0$ and $\frac{\partial \hat{Y}}{\partial x} = 0$. A condition on the temperature can be derived from the energy equation written for the temperature outside the flame zone (where there are no heat sources or reactions), assuming that the average temperature in that zone is constant ($\overline{T} = \overline{T}(\infty) = 1$). This, for oscillating quantities, gives the same expression as in T'ien 1972:

(3.64) $$\frac{d\hat{T}}{dx} = i\omega\left(\frac{\gamma - 1}{\gamma} - T\right) \quad x \to \infty$$

The other conditions are given at the inner boundary of the gas layer. A condition on the mass flux is the given by the phase-change equation at the interface, written as $\hat{m} = E_1\hat{T} + 1$. The last boundary condition relates the temperature oscillations with the temperature gradient at the interface, and is expressed by equation (3.40).

3.1.6 Numerical Solution Method

The numerical method used for the integration is based on linear conversion (Na 1979). The use of this method allows us to reduce the boundary value problem to multiple initial condition problems. The advantage over a shooting method (used in T'ien 1972) is that it does not require

iteration. A Runge-Kutta algorithm is used to perform backward integration of the differential equations from the flame edge ($x = \infty$) to the inner edge ($x = x_2$). Since part of the boundary conditions are specified on the inner edge and part on the outer edge, the first integration assumes some guessed values for the boundary conditions at the outer edge. The objective of linear conversion is to determine the correct boundary values at the outer edge using the information on the inner boundary.

Using linearity of the system of equations, the inner boundary conditions can be written as a function of the outer boundary conditions and a particular solution of the system:

(3.65)

$$\begin{Bmatrix} \hat{m} \\ \hat{T} \\ \frac{d\hat{T}}{dx} \\ \hat{Y} \\ \frac{d\hat{Y}}{dx} \end{Bmatrix}_{x=0} = [J] \begin{Bmatrix} \hat{m} \\ \hat{T} \\ \frac{d\hat{T}}{dx} \\ \hat{Y} \\ \frac{d\hat{Y}}{dx} \end{Bmatrix}_{x\to\infty} + \begin{Bmatrix} \hat{m} \\ \hat{T} \\ \frac{d\hat{T}}{dx} \\ \hat{Y} \\ \frac{d\hat{Y}}{dx} \end{Bmatrix}_{p}$$

Note that *[J]* and $\{...\}_p$ (particular solution) depend on the system of differential equations but not on the initial conditions. The solution can be obtained in four steps:

Determine $\{...\}_p$ by setting $\{...\}_{x\to\infty} = 0$ and integrating the system once.

Determine *[J]* by using unitary values to the guessed boundary conditions

(3.66)

$$\begin{Bmatrix} \hat{m} \\ \hat{T} \\ \frac{d\hat{T}}{dx} \\ \hat{Y} \\ \frac{d\hat{Y}}{dx} \end{Bmatrix}_{x\to\infty} = \begin{Bmatrix} 1 \\ 0 \\ 0 \\ 0 \\ 0 \end{Bmatrix}, \begin{Bmatrix} \hat{m} \\ \hat{T} \\ \frac{d\hat{T}}{dx} \\ \hat{Y} \\ \frac{d\hat{Y}}{dx} \end{Bmatrix}_{x\to\infty} = \begin{Bmatrix} 0 \\ 1 \\ 0 \\ 0 \\ 0 \end{Bmatrix},$$

and subtracting the particular solution obtained before. This gives the columns of *[J]* one at a time. Note that some of the boundary conditions on the right end side of the flame zone are known (see section 3.1.5), hence the system actually requires only three integrations.

Determine the correct values of the boundary conditions at the flame outer edge, using the knowledge of the correct boundary conditions at the inner edge and the coefficients evaluated in the previous step; this simply requires the solution of a third order linear system.

Integrate the system (from the right boundary to the left) with the correct boundary values at the right boundary of the flame edge.

3.2 Particle Damping Modeling

In this study, we are dealing with response functions that, compared to the quasi-steady result, have a more significant an effect at higher frequencies; it is important then to carefully consider the major source of damping: the particles present in the combustion chamber.

The equations representing the dynamics of the chamber, equations (2.20), can be re-written with the linear contribution explicitly marked:

(3.67) $$\ddot{\eta}_n + \omega_n^2 \eta_n = 2\alpha_n \dot{\eta}_n + 2\omega_n \vartheta_n \eta_n + (F_n)^{NL}$$

where α_n and ϑ_n are the (linear) growth rate and frequency shift of mode n. Several factors contribute to these two parameters. In particular: combustion, inert surfaces and condensed material in the flow. In general, combustion drives the response, and its contribution is calculated by using proper response functions. Inert surfaces, particularly the nozzle, have a stabilizing effect, and their effect can be introduced by the use of an appropriate value for the admittance (Culick and Yang 1992). Condensed material in the flow also has a stabilizing effect, and also a very strong dependence on frequency.

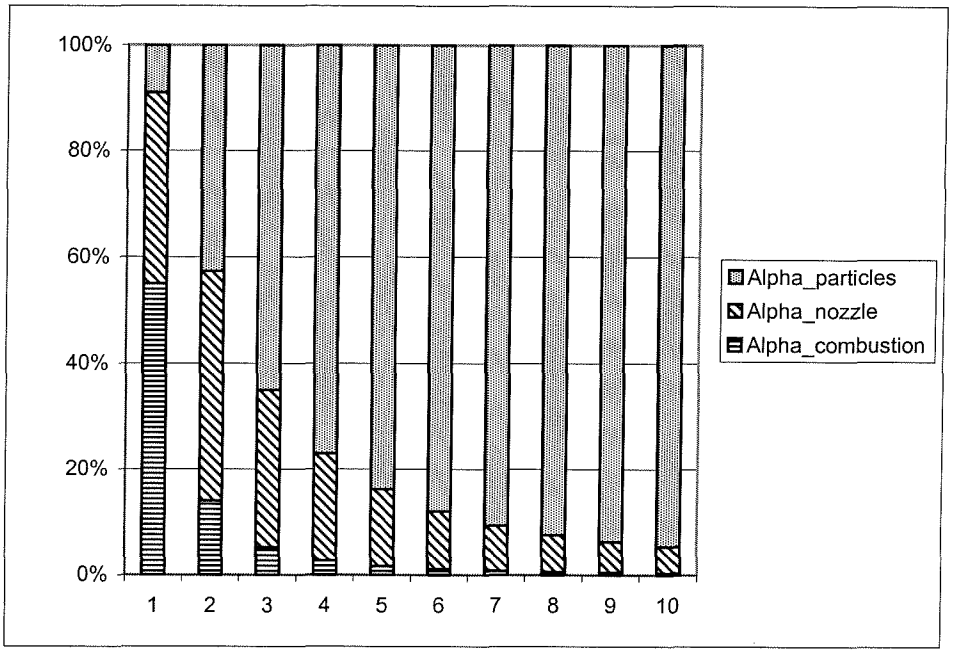

Figure 3.9. Relative values of contribution to α_n, for fixed particle diameter. First 10 modes.

Figure 3.9 presents graphically the relative values of the factors contributing to the value of α_n for the first ten modes of the chamber used in the examples of the following paragraphs. For clarity, the contributions are presented in their absolute value (α_{Nozzle} and $\alpha_{Particles}$ would be negative). It is clear that, after the second mode, the damping due to the condensed material is dominating the dynamics of the system.

The mechanism responsible for the damping due to condensed material is the viscous interaction between the particles and the gas. Particle damping is calculated by using the linearized multi-component fluid mechanics equations (Culick and Yang, 1992). Also the assumption is made that the Reynolds number based on the relative speed between gas and particle is less than unity, and hence Stokes' flow approximation holds.

As it can be expected, the damping is a strong function of the size of the particles and the frequency of oscillation; in particular, the damping at a given frequency presents a maximum at a specific diameter, and, for a given size (within a range, cf. Figure 3.10), the damping increases greatly with frequency. The situation is summarized in Figure 3.10.

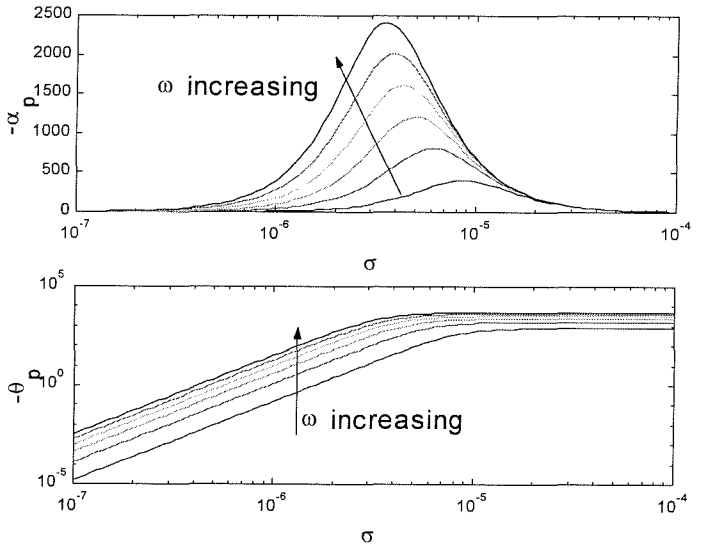

Figure 3.10. Damping due to condensed material.

Some calculations (Culick and Yang 1992, Isella and Culick 2000) assumed a constant value ($\sigma = 2x10^{-6}\ m$) for the particle diameter, resulting, as Figure 3.9 and Figure 3.10 show, in a very large damping in the high frequency modes.

In Isella and Culick 2000, it was noticed that an artificial reduction of the particle damping (10% constant reduction over the entire frequency range) could have a significant effect on the global dynamics of the combustion chamber. To investigate further this possibility, we considered introducing a realistic distribution of particle sizes in the calculation. In Kraeutle 1978, the author finds that, for a typical aluminized propellant, about 65% of the particles has a diameter between 0.2 and 1 μm ($1x10^{-6}m$), 10% is between 1μm and 10 μm, the remaining 25% is almost entirely between 10μm and 30μm, with a few particle (0.02%) falling outside of the categories listed.

Introducing this distribution in the model used to calculate condensed material damping, we obtain the curves presented in Figure 3.11. The dotted line presents the damping in the case of fixed particle diameter (σ = 2 μm) and the continuous line shows the damping corresponding to the particle distribution measured by Kraeutle 1978. Note that the particle diameter distribution is slightly bimodal, and this is reflected by the two peaks in the damping curve. Note also that,

while for the first mode the damping is higher, the particle damping associated with the higher modes is noticeably lower. For reference, in the example presented later, $\omega_1=5.6x10^3$, and $\omega_6=3.4x10^4$.

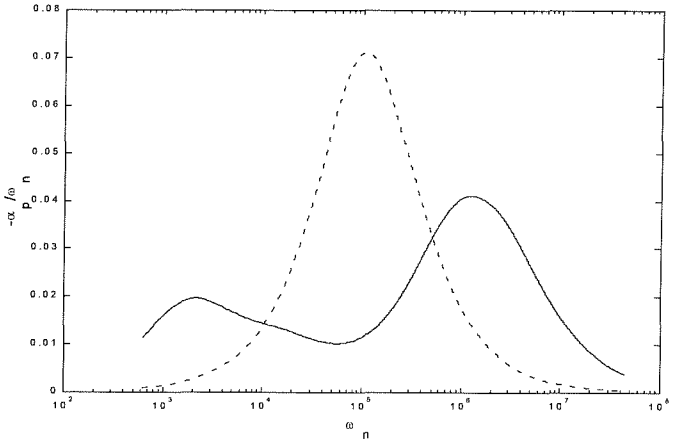

Figure 3.11. Condensed material damping with variable particle size (continuous line) and constant particle diameter (dotted line) $\sigma=2\mu m$.

With this model, the relative influence of the various components of the growth rate of the modes becomes the one presented in Figure 3.12 (to be compared with Figure 3.9).

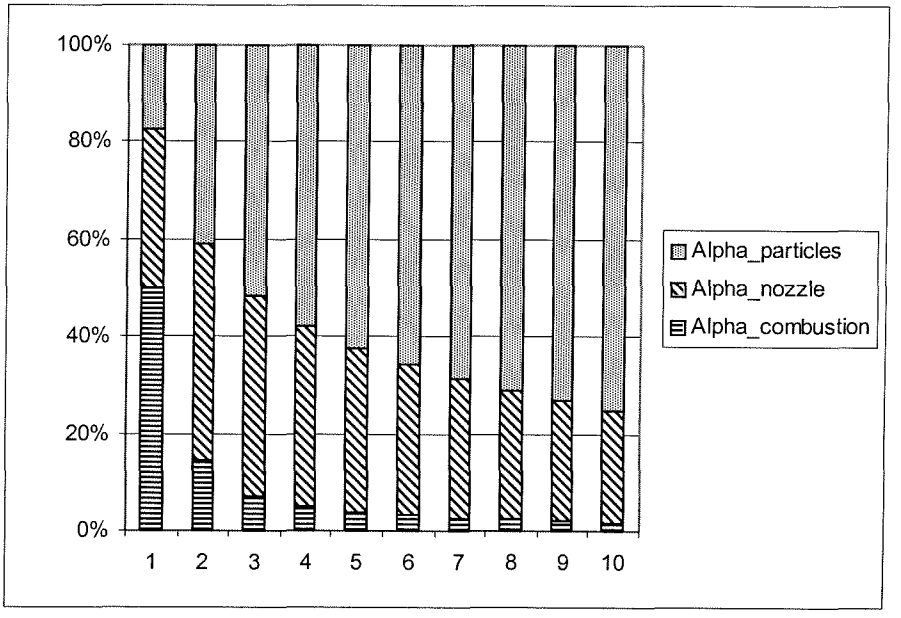

Figure 3.12. Relative values of contribution to α_n, for distributed particle diameter. First 10 modes.

An example of the calculation of the global response using this model is presented later.

3.3 Effect of Surface Layer Dynamics and Gas Phase Dynamics on Propellant Response

Typically, the experimental measurement of the frequency response of a solid propellant is limited to a few data points at relatively low frequency and with considerable scattering. The quasi-steady theory gives a satisfactory representation of the behavior at low frequency, but there is evidence that the response at higher frequency is higher than predicted by QS theory and it might be responsible for the observed sensitivity of propellant burning behavior on small variations in the propellant composition.

In this section we combine the models developed above to analyze the effect of the surface layer and of the gas phase dynamics on the shape of the frequency response curve.

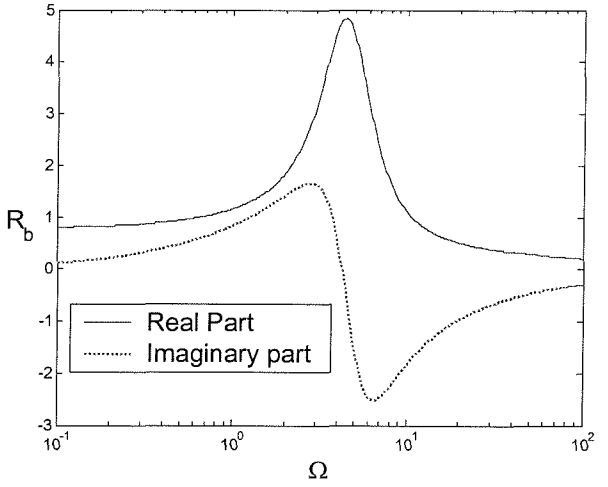

Figure 3.13. Reference case: quasi-steady response.

The reference case is shown in Figure 3.13 and is the quasi-steady case with parameters: $A = 6.0$, $B = 0.60$.

Adding the dynamics of the gas phase, we obtain the response function presented in Figure 3.14, calculated for the parameters in Table 3-2, without the surface layer. As noted by T'ien 1972, this

calculation verifies the quasi steady case for low frequency, but also shows another peak at a higher frequency. An interesting characteristic is that the acoustic admittance and the burning rate have the same trend at low frequency, while they assume opposite behavior at the high frequency peak; for higher frequencies, the acoustic admittance grows again to positive values. The acoustic admittance represents the velocity perturbation at the outer edge of the flame zone, and hence the ability to amplify or damp disturbances. T'ien notes that a decreasing ratio of solid to gas densities, which is inversely related to the ratio of gas residence time to solid characteristic thermal time, produces much higher values of the acoustic admittance at high frequency. This is verified by Clavin and Lazmi 1992 and also in the computations done here. Since very high pressure burning is the typical application for solid propellants, this observation is very important for experimental purposes: low pressure testing of a solid propellant will lead to a misleading result for the high frequency (here "high" refers to the region following the peak in the quasi steady response) region of the response. Effectively, low pressure (i.e., high density ratio) testing results in the observation of a behavior that is opposite to the behavior at high pressure.

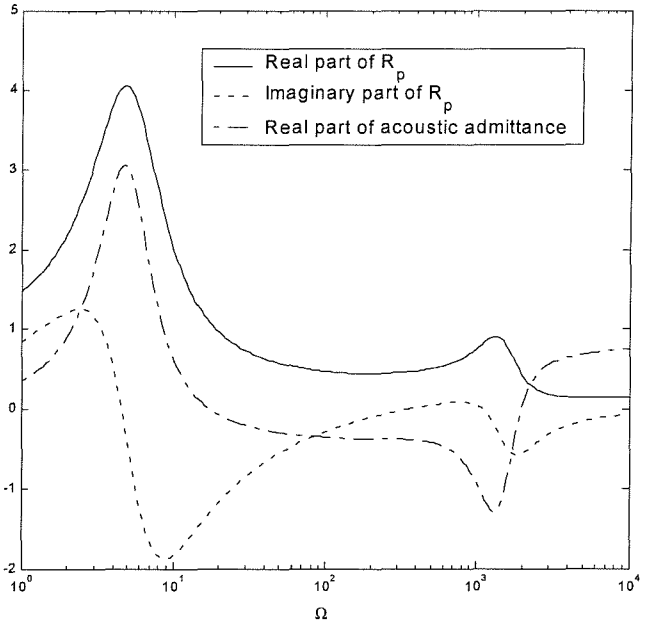

Figure 3.14. Combustion response curve for model with gas phase dynamics.

Figure 3.15 presents a similar case, including the dynamics of the surface layer, where we used the previous values for solid and gas phase, and the values reported in Table 3-2 for the characteristics of the surface layer.

In this case, the amplitude of the response function is lower, but the second peak is more evident. Again, the acoustic admittance becomes positive and large at high frequency.

The principal parameters that characterize the surface layer are relative density (ρ_l), activation energy (E_l), latent heat (L_l), thermal conductivity (χ_l) and thickness of the surface zone (x_l). The effect of the variation of these quantities on the resulting response function is shown in Figure 3.16 to Figure 3.20. In these figures, one parameter is varied, while the others assume the values reported in Table 3-2.

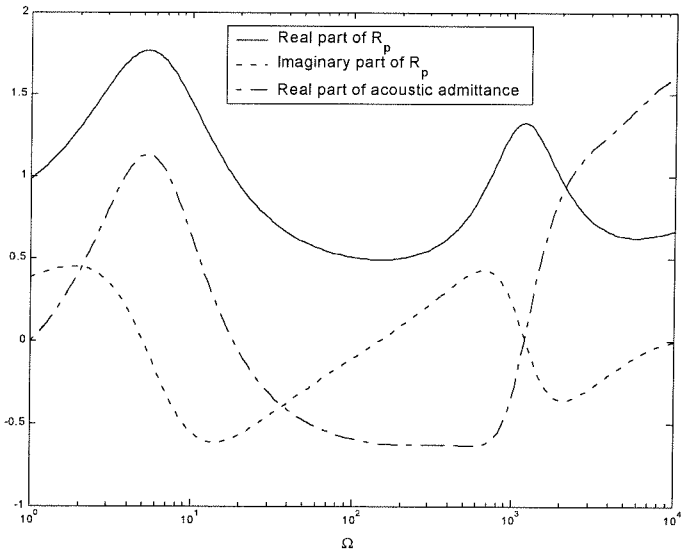

Figure 3.15. Combustion response curve with surface layer and gas phase dynamics.

The relative density of the surface layer (Figure 3.16; some of the imaginary parts are not drawn for clarity) has a strong effect on the response function: both the position of the peaks and the amplitude are influenced. In particular, for increasing ρ_l, we observe a large peak at intermediate

frequency. Burnley 1996 observed, from simulation results, that a transfer function with a large absolute value could give rise to a triggering phenomenon. At the time, he discarded the solution since the quasi steady theory would require non physical values (see section 3.1.2 for more details about stability boundaries) of the coefficients in the *AB* form of the response. In our case, such a response function is physical and justified by the presence of a surface layer. The explanation of the triggering has been given recently by Ananthkrishnan 2001, and is based on the fact that such a large value of the response causes a change of sign in one of the coefficients of the gasdynamics equations, and hence produces the correct dynamics for triggering.

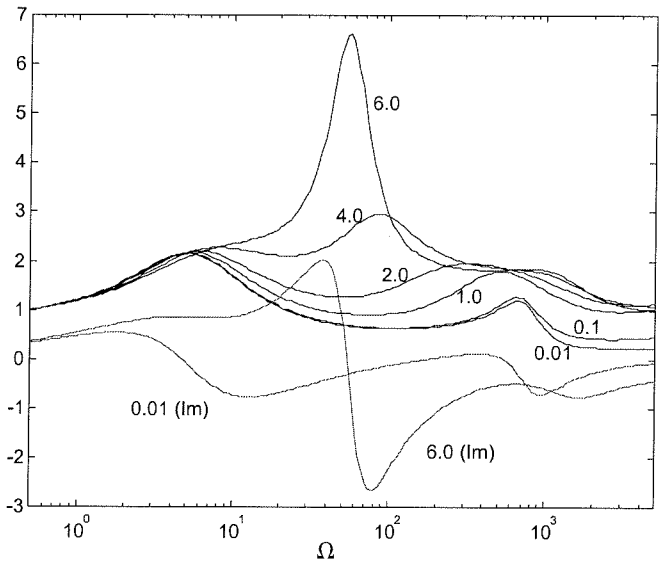

Figure 3.16. Variation of the response function with ρ_1.

The activation energy (Figure 3.17) influences only the amplitude of the peaks. This can be explained by observing that the value of the activation energy sets the importance of each particular section in the energy balance. Hence, a large value of the activation energy in the surface layer (compared to the value in the solid phase) would make this zone more dominant.

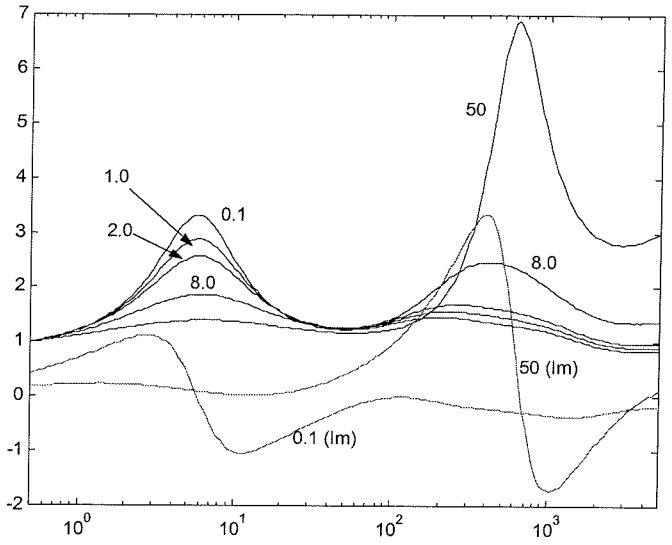

Figure 3.17. Variation of the response function with E_l.

The same conclusion is reached in the case of the latent heat, shown in Figure 3.18. A large value of this parameter makes the surface layer dominant in the response.

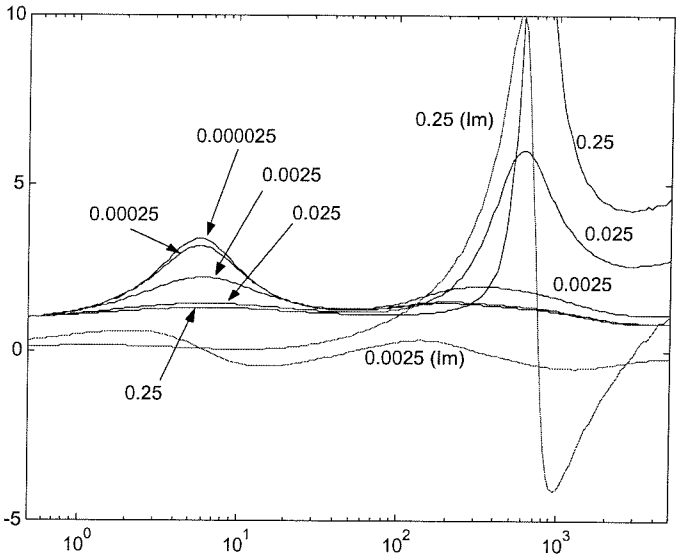

Figure 3.18. Variation of the response function with L_l.

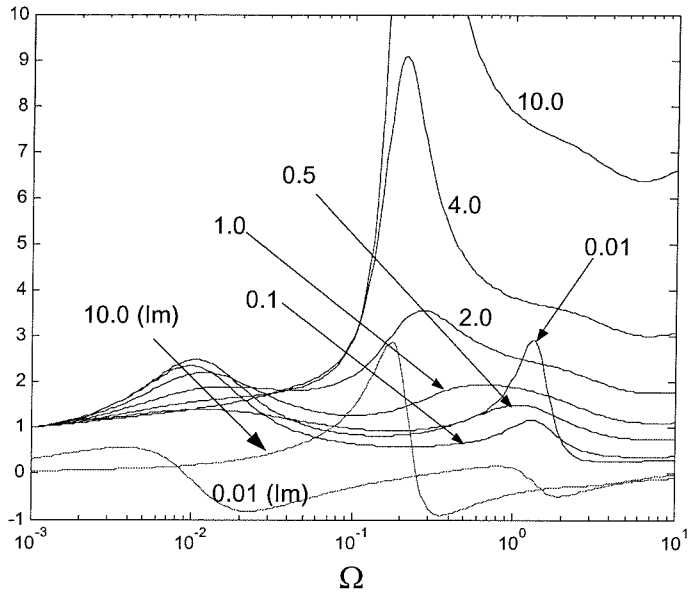

Figure 3.19. Variation of the response function with χ_i.

As expected, the thickness of the surface layer does not have a major effect on the results, since all the chemical reactions remain concentrated in the gas phase by assumption.

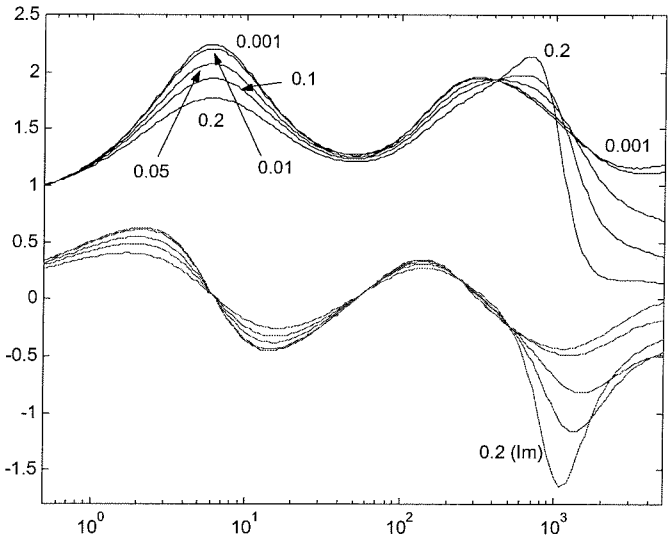

Figure 3.20. Variation of the response function with x_i.

3.3.1 Reduction to Transfer-Function Model

In order to analyze the effect of the various sections of the propellant on the total response, we will now divide the contribution of each zone of the propellant into a separate transfer function. For the purpose of this chapter, we will use a representation more typical of the control literature and present the plots of the transfer functions as magnitude and phase, so the effect of combustion is more immediately apparent from the analysis of the graphs. The 'Solid phase' line in Figure 3.21 shows the quasi-steady response under this convention.

By using the numerical solution for the case with full dynamics, we can now evaluate the response of each phase in terms of a transfer function (Figure 3.21).

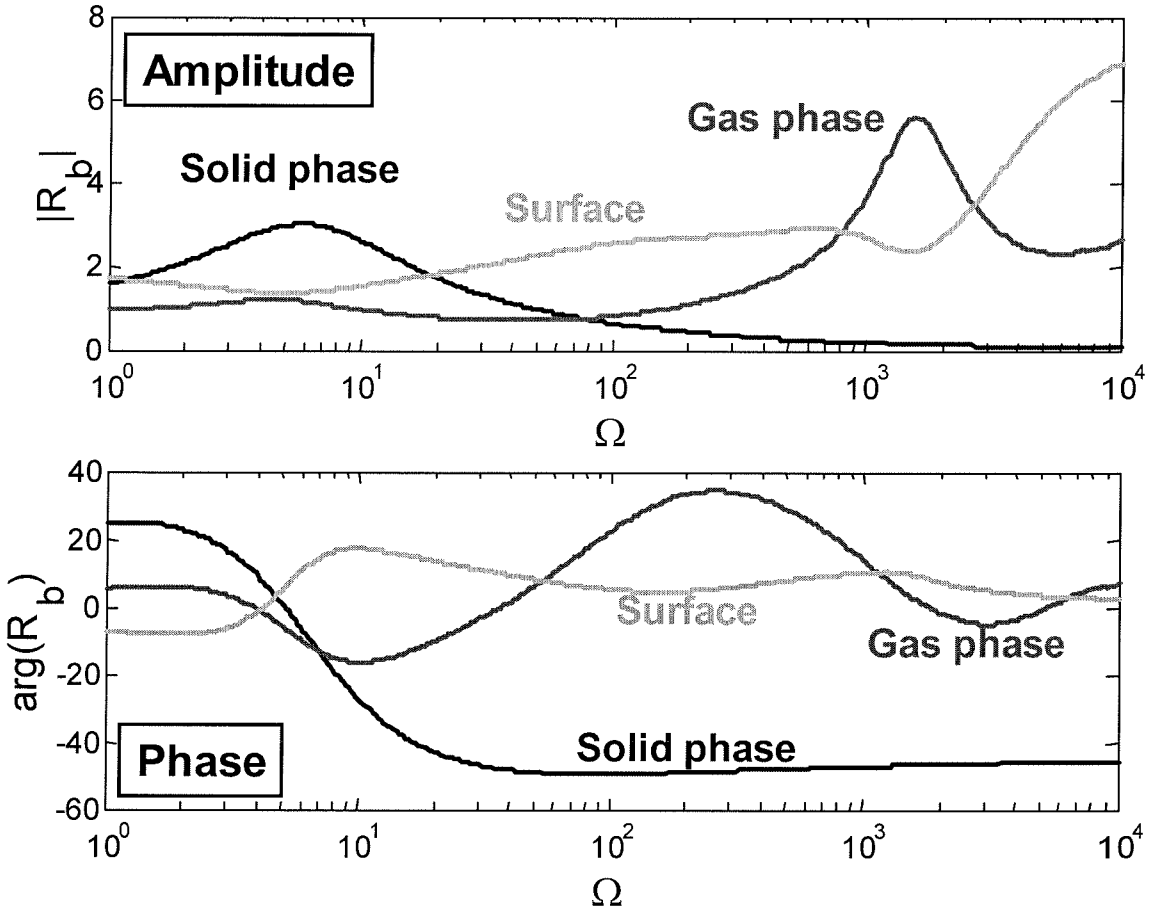

Figure 3.21. Response in terms of transfer functions (in deg).

We note that the gas phase dynamics adds a peak at high frequency. Also it has an effect on the phase at low frequency. Also there is a significant effect of the surface layer at higher frequency than the limit of the quasi steady response.

Regarding the sensitivity of the response functions to variation of the physical parameters in the surface layer or solid phase, we can qualitatively refer to the figures from Figure 3.16 to Figure 3.20. Different transfer functions for different values of the parameters are not reported, but can be easily calculated following the method described here.

The purpose of describing each 'section' (cf. Figure 3.1) of the propellant with a transfer function was described in more detail in section 3.1.3; in brief, it allows to separate and identify the effects of the various propellant zones on the dynamics of the combustion chamber. Furthermore, it is very convenient for parametric studies and the introduction of different models of a particular zone, since the new model can be just plugged in without recalculating the whole system.

3.4 Pressure Coupling - Results

This section presents the dynamical analysis of a small rocket motor to illustrate the consequences of the combustion dynamics for the stability and nonlinear behavior of unsteady motions in a motor. The simulated combustion chamber is $0.6\ m$ long, $0.025\ m$ in diameter and has a throat radius of $0.009\ m$; the mean pressure in the chamber is $1.06 \times 10^7\ Pa$. Figure 3.22 presents the results of the simulation for system with a combustion response based on the quasi-steady theory. The top section presents the combustion response function; the vertical lines mark the frequencies of the first acoustic modes of the combustion chamber. The bottom half shows the time evolution of the amplitude of each mode. The values of the parameters are: $A = 7.0$, $B = 0.60$, $n = 0.80$.

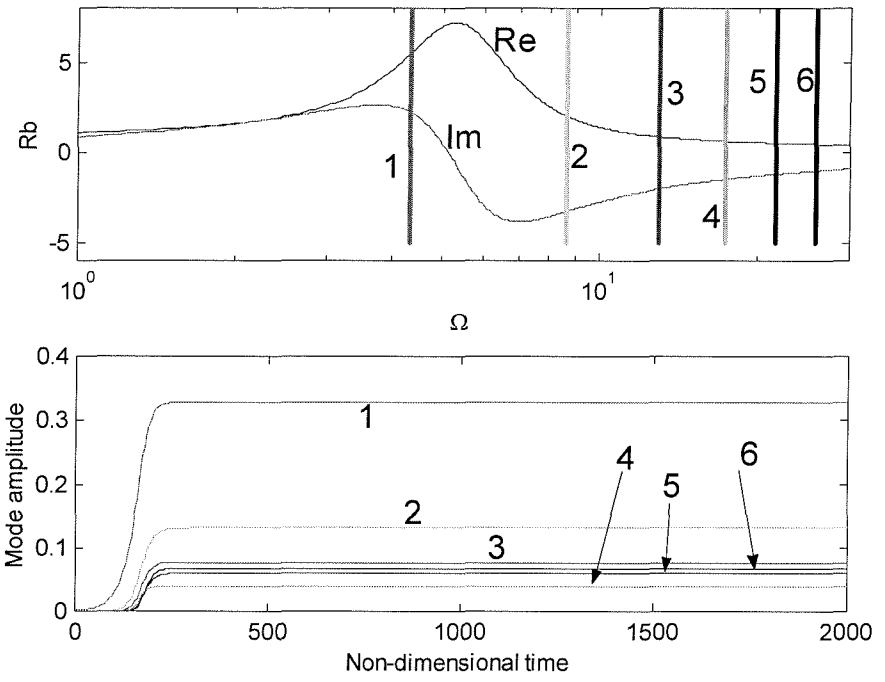

Figure 3.22. Simulation results for QSHOD combustion response.

The first mode is unstable and rapidly grows to a limit amplitude, while the other modes are all stable, and draw energy from the first mode (allowing the system to enter a limit cycle).

Figure 3.23 shows the same simulation for the case of a delayed combustion response function: note that the dynamic behavior of the system is richer. The limit cycle is reached later and the first two modes (both unstable) have a more complex interplay. The values of the parameters for this case is: $A = 8.0$, $B = 0.60$, $n = 0.80$, $\tau = 1.5$ (non-dimensional units). For some particular values of the parameters, we also observed a switching of the most unstable mode after a (long) period of time, which indicates that the system is close to a bifurcation where the period of the limit cycle becomes influenced by both the first two modes, a case similar to period doubling.

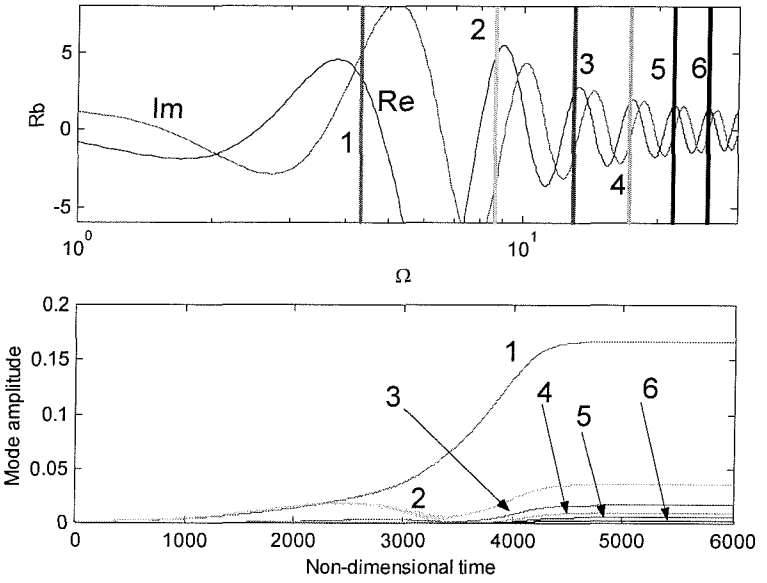

Figure 3.23. Simulation with time delay.

Figure 3.24 shows a similar calculation using the response including the dynamics of the surface layer: the higher values of the response function at high frequency produce a very different time-evolution of the amplitude of the modes before reaching the limit cycle values.

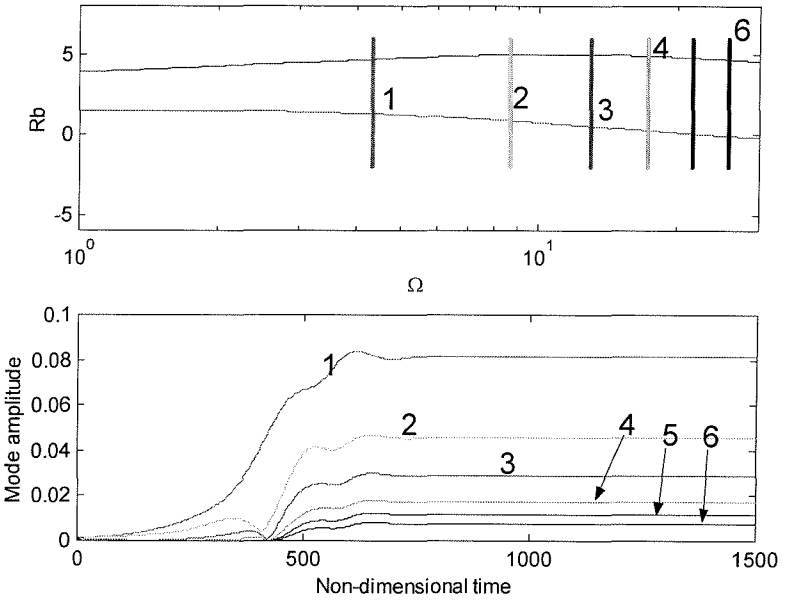

Figure 3.24. Simulation with surface layer.

Figure 3.25 presents the same simulation with surface layer and gas-phase dynamics. The response function has a higher value than in the previous cases at high frequency. This has the effect of driving the higher modes to a larger value. The effect on the response is not very dramatic because the model used for the particle damping (Culick and Yang 1992) produces a damping rapidly increasing with frequency, and, from the third mode, that constitutes the dominating effect on the dynamic of the system.

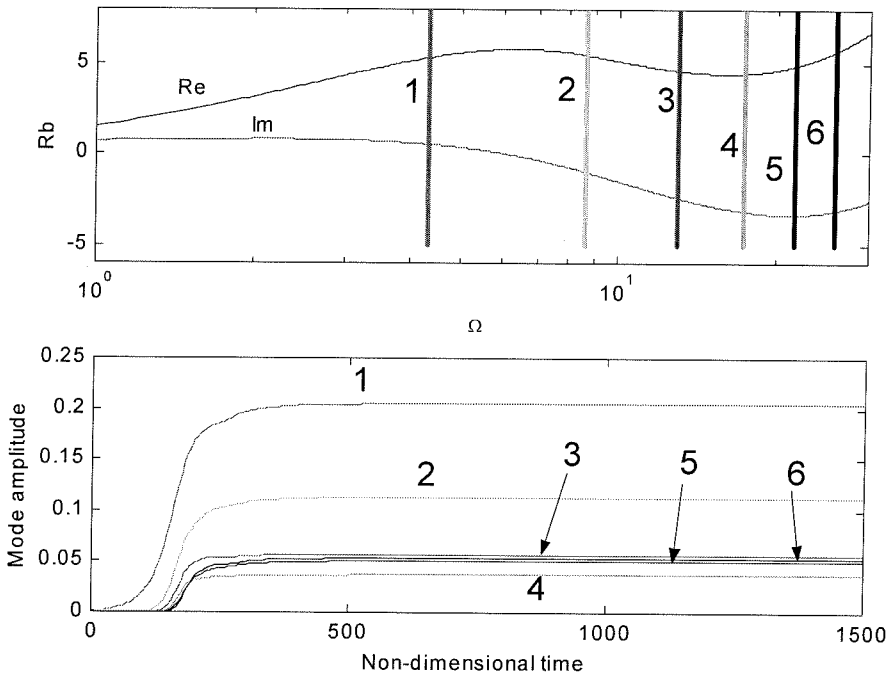

Figure 3.25. Simulations with gas-phase and surface layer.

Figure 3.26 shows the same case with a *10%* reduction in the particle damping. In this case the final amplitude of each mode is consistently larger. Large values of high frequency modes cause quite a marked difference in the shape of the pressure waveform in the limit cycle, as shown in Figure 3.27.

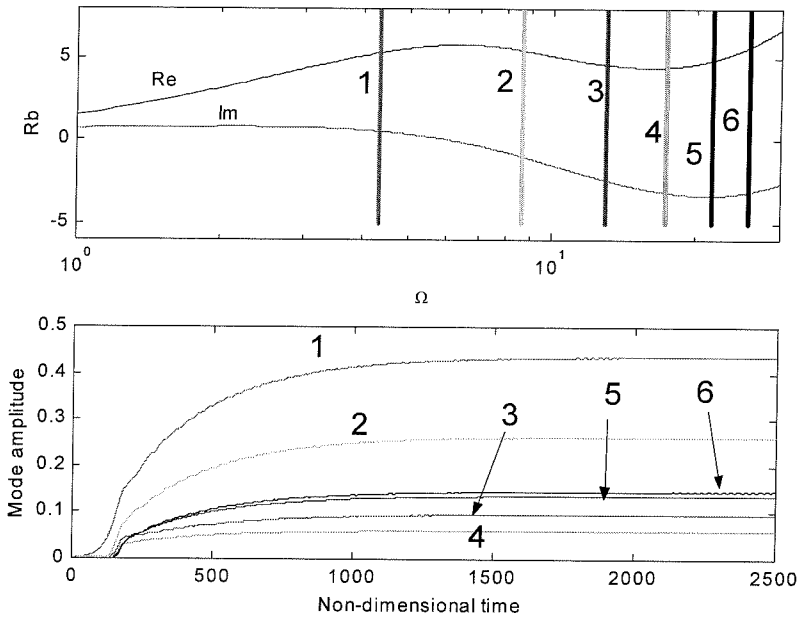

Figure 3.26. Simulations with gas-phase and surface layer, with reduced particle damping (constant 10% reduction over all the frequency range).

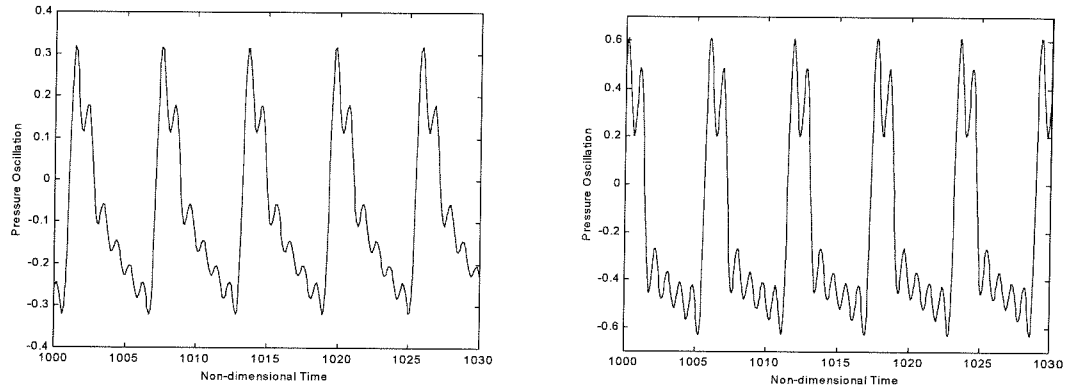

(a) (b)

Figure 3.27. Pressure waveforms for the limit cycles of (a): Figure 3.25 and (b): Figure 3.26.

3.5 Pressure Coupling - Discussion

The examples presented in the previous section show the influence of including the dynamics of the surface layer in the modeling of the burning of a solid propellant. Two simple models representing the dynamics of the surface layer are introduced. One simply adds a time lag to the conventional quasi-steady theory, the other introduces a layer with different properties.

The time lag model gives rise to a combustion response function that presents several peaks, and hence it is not very realistic. The peaks could be eliminated by choosing a time lag dependent on frequency (Grad 1949), but that choice does not have a physical justification and it reduces the model to curve fitting with experimental data.

With the second model, the effect of the surface layer on the combustion response function consists in the reduction of the peak induced by the solid phase, and in the appearance of another peak (of higher absolute value) at higher frequency, due to the response of the surface layer to the heat feedback from the combustion zone. The relative density of the surface layer seems to have an effect on the response function that is larger than that of the activation energy.

The combustion model is also applied to an example computation of the dynamics of a rocket motor, to show the effect of the combustion response function on the dynamics of the system. For the examples chosen here, the waveforms in the limit cycles are similar whether or not dynamics of the surface layer and gas phase are accounted for. This is a consequence of the heavy damping in the higher harmonics introduced by the model used (Culick and Yang 1992).

Calculations with less damping of the higher modes show larger amplitudes of those modes in the limit cycle. This affects the amplitude and the harmonic content of the waveforms in the limit cycles.

In general, models based on pressure coupling do not show a dramatic sensitivity of the propellant response to changes in composition, especially when compared with the introduction of another coupling mechanism, based on velocity coupling, presented in the following section.

3.6 Velocity Coupling (Continuation Method)

The idea of velocity coupling is based on the model introduced by Levine and Baum 1983. The principle is that the velocity parallel to the propellant surface gives a contribution to the mass burning rate of the propellant. This can be justified by the convective heat transfer, that becomes particularly important if the flow is turbulent.

The total mass burning rate can now be written as

(3.68) $$\dot{m} = \dot{m}_{pc}\left\{1 + \tilde{R}_{vc} F(\mathbf{u})\right\}$$

where $\dot{m}_{pc}$ is the mass flux due to pressure coupling, $\tilde{R}_{vc}$ is a coupling coefficient and $F(\boldsymbol{u})$ is the velocity coupling function.

A simple model is to use the oscillating velocity as coupling function. Neglecting the mean flow velocity, equation (3.68) becomes

(3.69) $$\dot{m} = \dot{m}_{pc}\left(1 + \tilde{R}_{vc}|\mathbf{u}'|\right)$$

This expression can be easily introduced in the formalisms presented in chapter 2 to perform the simulations (Burnley 1996).

As also noted by Levine and Baum 1983, and Burnley 1996, velocity coupling has a significant effect on the global dynamics of the system.

Similarly to Burnley 1996, in order to use a method based on solution continuation to study the dynamics of the system, a continuous approximation is introduced in equation (3.69) to substitute the absolute value. According to Burnley 1996, it is this approximation that produces a 'threshold' effect responsible for the incurrence of a subcritical bifurcation, as shown in Figure 3.28, where α is the growth rate of the first mode. The results presented in the figure are obtained by using a solution continuation method (described in Appendix A), using the growth rate of the first mode is used as a parameter in the continuation (x-axis in Figure 3.30).

Some recent work done on the dynamics resulting from the functional form of the equations used in the analysis by Ananthkrishnan 2001 seems to prove that the absolute value function in itself, as it appears in a simple model of velocity coupling, is sufficient to produce a subcritical bifurcation (pitchfork) followed by a fold (saddle-node bifurcation).

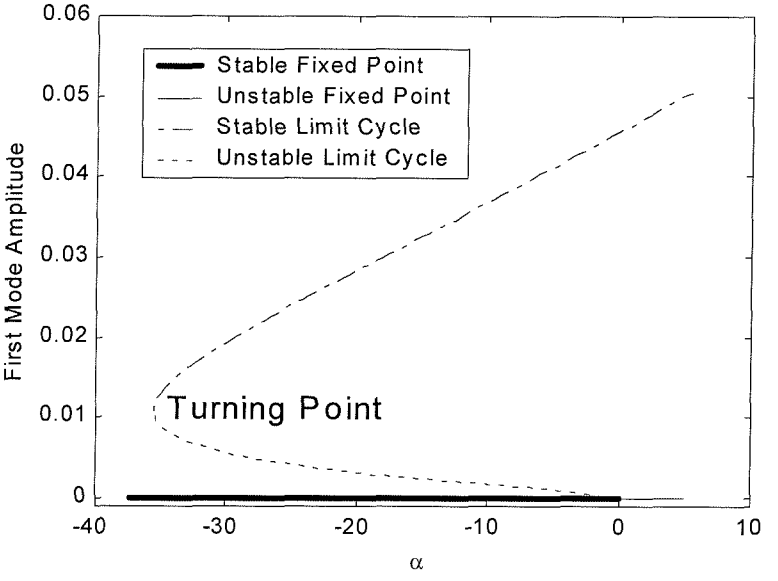

Figure 3.28. Bifurcation diagram.

In order to analyze the effect of velocity coupling on the overall dynamics, the following two relative sensitivities are defined:

(3.70)
$$S_{\tilde{R}_{vc}}^{A_{LC}} = \frac{1}{A_{LC}} \frac{\partial A_{LC}}{\partial \tilde{R}_{vc}}$$

(3.71)
$$S_{\tilde{R}_{vc}}^{\alpha_{BP}} = \frac{1}{\alpha_{BP}} \frac{\partial \alpha_{BP}}{\partial \tilde{R}_{vc}}$$

where A_{LC} is the amplitude of the limit cycle (defined at a fixed value of α), and α_{BP} is the value of the growth rate at which the unstable fold turns to a stable fold. Equation (3.70) defines the relative sensitivity of the amplitude of the limit cycle to variations in the velocity coupling coefficient; equation (3.71) refers to the sensitivity of the turning point to the same coefficient.

Figure 3.29 shows a plot of the sensitivities, calculated for the combustion chamber used in the examples of the previous section, and using a six mode approximation of the system. Note that the sensitivity of the turning point is very high, and also the sensitivity of the amplitude of the limit cycle is quite large in the range 0.15 to 0.25 of the coupling coefficient.

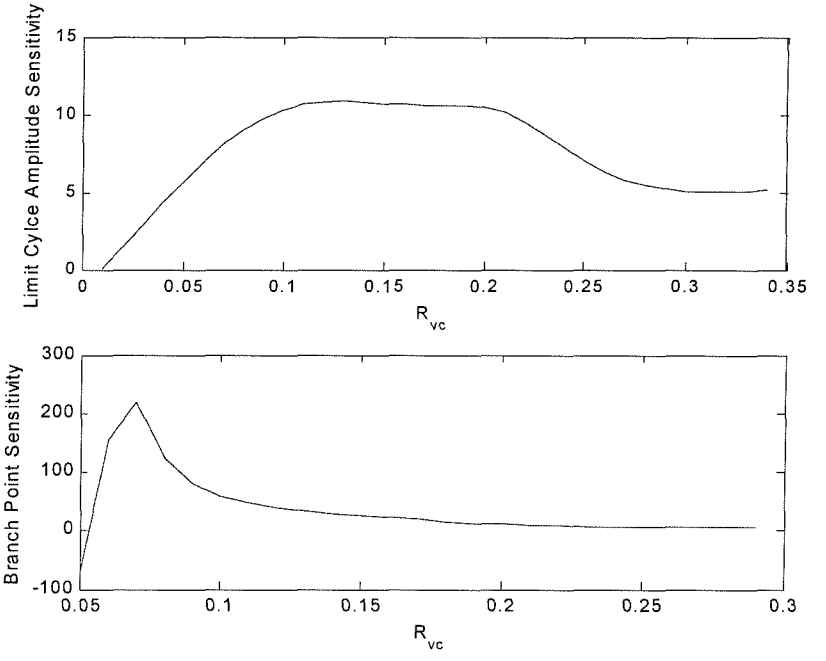

Figure 3.29. Sensitivity of global dynamics to variations of the coupling coefficient.

3.7 Velocity Coupling - Results

We now analyze the same combustor described in section 3.4, with the introduction of the extra terms due to velocity coupling.

For reference, Figure 3.30 presents the results of the simulation for the system with a combustion response based on the quasi-steady theory. The top section presents the combustion response function; the vertical lines mark the non-dimensional frequencies of the acoustic modes of the combustion chamber considered in the simulations. The bottom half shows the time evolution of the amplitude of each mode. The values of the parameters are: $A = 6.0$, $B = 0.55$, $n = 0.50$.

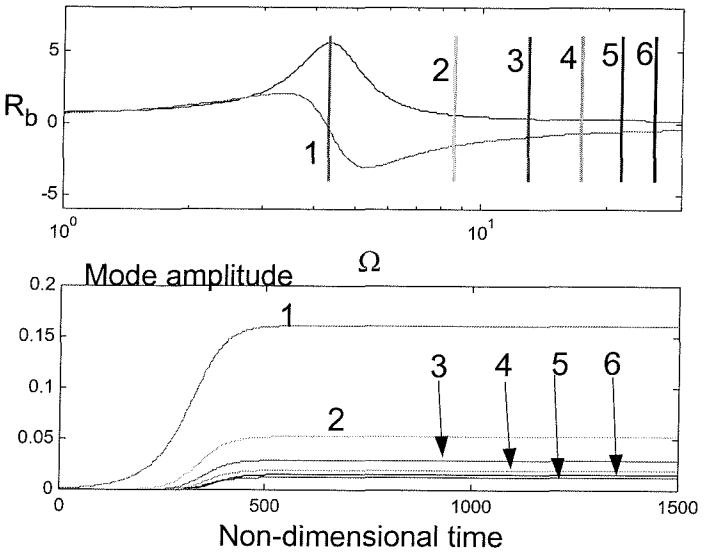

Figure 3.30. Simulation results for QSHOD combustion response.

The first mode is unstable and rapidly grows to a limit amplitude, while the other modes are all stable, and draw energy from the first mode (allowing the system to enter a limit cycle).

Figure 3.29 shows that there is a region of high sensitivity of the amplitude of the limit cycle for variations in the velocity coupling coefficient. Figure 3.31 presents the global response for a small variation of the velocity coupling coefficient ($\tilde{R}_{vc} = 0.15$ and $\tilde{R}_{vc} = 0.165$).

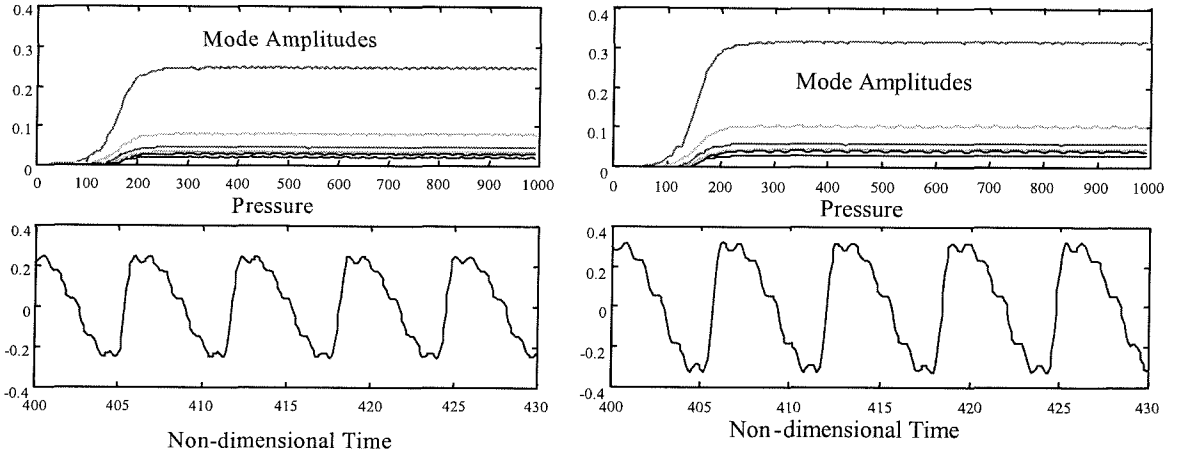

Figure 3.31. Simulations with velocity coupling for: (a) $\tilde{R}_{vc} = 0.15$, (b) $\tilde{R}_{vc} = 0.165$.

The simulation uses the same coefficients for the pressure coupling as in the results of Figure 3.30, with the addition of the velocity coupling terms. Figure 3.32 and Figure 3.33 show the pressure trace and the harmonic content for the same two cases.

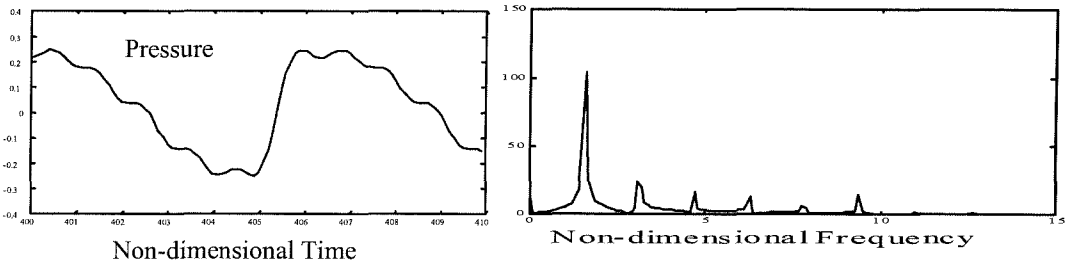

Figure 3.32. Pressure trace and harmonic content for the case $\widetilde{R}_{vc} = 0.15$.

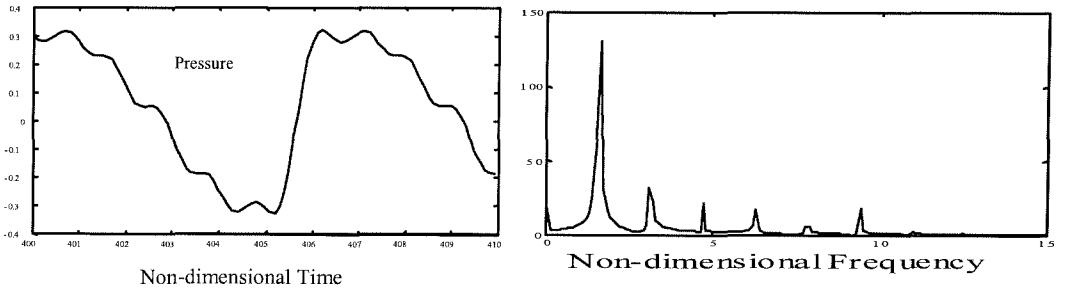

Figure 3.33. Pressure trace and harmonic content for the case $\widetilde{R}_{vc} = 0.165$.

Note that the combustor shows a quite large sensitivity on a small variation in the velocity coupling parameter; this is shown by the final amplitude of the limit cycles that develop in both cases.

Particle damping has a significant effect on the growth rate of the various modes. Figure 3.34 shows the same calculation as Figure 3.31 (a) but with the condensed matter damping calculated according to the particle distribution of Kraeutle 1978 (see Figure 3.11 in section 3.2). Note the considerably lower value of the limit cycle amplitude, a consequence of the fact that the first mode, which is the only one having a positive growth rate exponent (hence it is linearly unstable), is subjected to larger damping than before, and hence the absolute value of the growth rate is

smaller. On the other hand, the influence of the higher frequency modes in the waveform is more pronounced, as clearly shown, for a different example, by the amplitudes in the Fourier spectrum of Figure 3.35.

It is interesting to show a result for the response using the combustion response including the surface layer and the gas phase dynamics (as in section 3.3) and velocity coupling plus the damping model with distributed size (Figure 3.35).

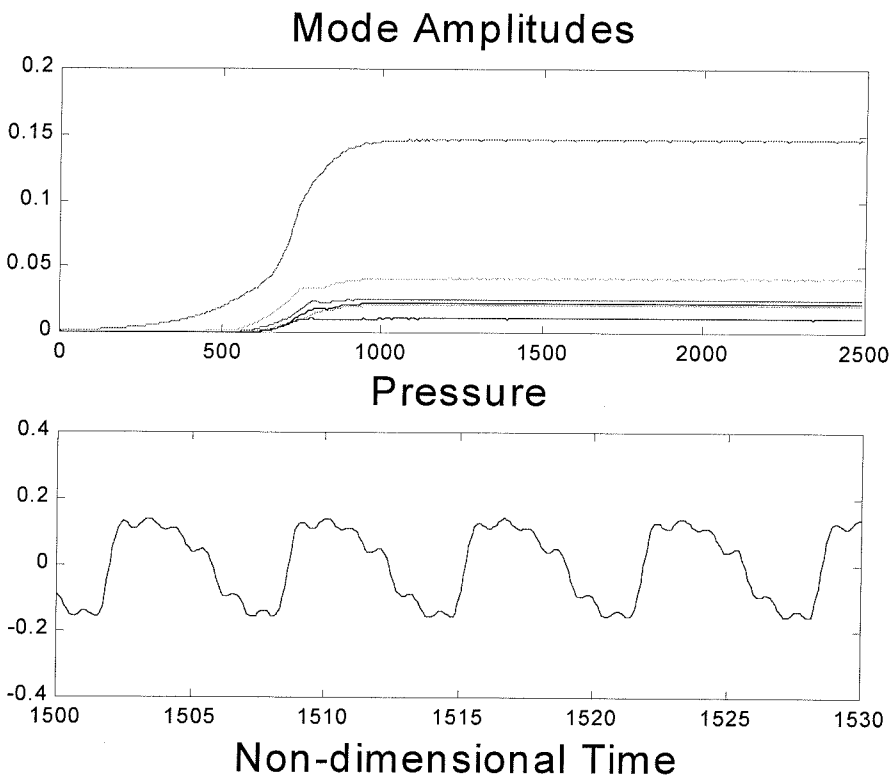

Figure 3.34. Simulations with particle damping calculated according to the experimental size distribution.

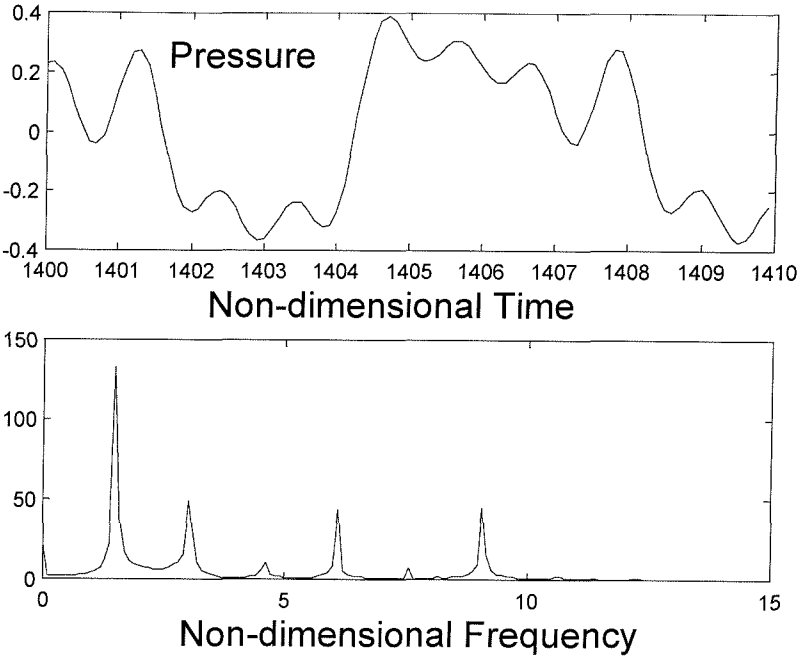

Figure 3.35. Global dynamics with full combustion response and particle damping according to the experimental size distribution.

In this case the first two modes are unstable, and the higher frequency modes are much less damped (due to a combustion response function with higher values than the QSHOD response at high frequency). The result is a higher value of the limit cycle amplitude and a richer harmonic content.

3.8 Velocity Coupling - Discussion

The purpose of the analysis of velocity coupling is to investigate the sensitivity of global dynamics to small changes in the propellant physical and chemical composition.

In section 3.5 it was shown that a model including combustion response based on pressure coupling only is not sufficient to produce large effects in the global dynamics of the system. The only exception is when the combustion response function has values near the boundary for intrinsic stability (see section 3.1.2 for a detailed discussion).

The results of the simulations including velocity coupling suggest that unsteady surface combustion responsive to velocity fluctuations parallel to the surface leads to a combustion dynamics sensitive to small compositional changes.

We also show that particle damping is in effect an important factor in the simulations; changes in composition of the propellant that would lead to changes in the size (or distribution of sizes) of the condensed material after burning will have a great effect on the global dynamics of the chamber. This is an important point and must be kept into consideration when detailed simulation of combustion chambers is performed.

3.9 Sensitivity of Combustion Chamber Dynamics to Propellant Characteristics

In this chapter we constructed a model of the combustion of solid propellant and analyzed two possible coupling mechanisms between combustor and propellant. The main objective is to construct a formalism that allows simulation and testing of combustors and to identify the possible causes of the observed sensitivity of combustion chamber dynamics to propellant characteristics.

The conclusions of the present analysis, regarding sensitivity, can be categorized within two groups: sensitivity of the propellant characteristics, analyzed through its effect on the combustion response function, and sensitivity of the coupling mechanism between propellant and chamber dynamics.

Regarding the propellant sensitivity, within the quasi steady theory, propellants exhibit a high sensitivity to small variations in their parameters only when close to the intrinsic stability limit. Even though potentially this mechanism could give rise to very sensible variations in the response functions, it is unlikely to be the one responsible for the behavior observed experimentally, since common propellants are mixed to stay away from intrinsic instabilities, and hence this mechanism does not commonly appear in practice.

If we abandon the quasi steady approximation and include gas phase dynamics, we observe a response of the propellant at higher frequency than the QS predictions; this corresponds to some of the experimental data available (see Baum et al. 1982) and hence it is a better model for the propellant combustion, but still it does not justify any stronger sensitivity. The introduction of the dynamics of the surface layer, beside considering solid phase and gas phase, introduces a very interesting sensitivity of the propellant response function to the characteristic of the surface layer itself. As shown above, the surface layer introduces the possibility for very different response functions, which, for some values of the parameters, present large peaks at moderately low frequencies and hence could justify some phenomena observed in rocket firing experiments (like triggering).

Regarding the second mechanism, i.e., the coupling between propellant and combustion chamber, we can summarize the results as follows. The traditional coupling mechanism, based on pressure, does not show the capability of justifying a high sensitivity of chamber dynamics on propellant characteristics. Simulations show that, even with large variations in the combustion response function, the chamber dynamics is not strongly affected. On the other hand, the introduction of velocity coupling, i.e., a dependence of the combustion response also on the velocity parallel to the propellant grain, shows a path for a more direct connection between chamber and propellant dynamics. It also introduces the possibility of explaining some observed dynamics (like triggering) without recurring to excessively high values for the combustion response function.

Another point worth mentioning regarding the coupling between propellant and chamber regards the effect of the solid particles on the dynamics. It is well known that particles introduce a considerable amount of damping in the dynamics; this damping is a function of the frequency and depends mainly on the size of the particles. All of the work done previously on reduced order modeling and simulations used a single size distribution for the particles; our simulations show, by introducing a realistic particle distribution, that previous analysis might have introduced too

much damping of the high frequency modes, and hence underestimated some of the dynamics coming from those modes. This is to say that some of the effects of a larger response function at high frequency, introduced by considering gas phase and surface layer dynamics, might have been filtered away in previous simulation by the excessive damping introduced by assuming an incorrect particle size distribution in the computations.

4 Control of Instabilities in Combustion Chambers

Even before the development of models including combustor dynamics and feedback control, experimental application of feedback control of combustion instabilities was successfully tested on small systems (mainly using loudspeakers as actuators). Those laboratory demonstrations report examples in which the amplitudes of limit cycles in linearly unstable combustors have been significantly reduced, sometimes even to vanishingly small values (Poinsot, Bourienne, Candel and Esposito 1987, Gulati and Mani 1992). In most cases, the 'practical' controller was a simple proportional feedback or a variation of a *PID* (Proportional-Integral-Derivative) controller. One might wonder why that simple approach works or, conversely, ask why we need more sophisticated control methods. From a general viewpoint, experiments show that an unstable combustion chamber is a system exhibiting a linear instability (rapidly) growing to a limit cycle (defined by the nonlinearities) that typically shows a marked predominant frequency.

In terms of dynamical systems, the combustor is characterized by two unstable complex-conjugate poles and then a series of stable poles with relatively large damping. Provided that the combustor is observable and controllable, for this kind of system, a proportional feedback or a *PID* controller can be successfully tuned to obtain a stable feedback loop (Franklin et al. 1995). Regarding the issue of controllability (and observability) of the system, for the purpose of this argument, we will say that controllability has been proved in practice for those systems by the success of the experiments cited. A detailed analysis of this point would allow optimization of the position of actuators and sensors, but that is out of the scope of the present discussion.

The need for more sophisticated control methods derives mainly from two aspects: first, one might want to impose performance specifications on the controller, for example on the maximum control action, or on the noise or disturbance rejection. Second, combustion systems show a high degree of uncertainty and variability (Lieuwen and Zinn 2000), and a controller 'tuned' on a particular operating point does not guarantee a reliable performance. Modern control design methods allow for the introduction of this kind of consideration during the synthesis of the controller.

All the considerations above and most of the design methods and examples found in the literature are generally based on a linear model of the combustor. On the other hand, the real system is manifestly nonlinear: the main indication of that is the fact that the pressure oscillations in the combustion chamber rapidly reach a limit cycle. A complete understanding of the dynamics of the combustor would allow tracing the source of the nonlinear behavior observed in the experiments (limit cycles, hysteresis, as in Isella et al. 1997 and Lieuwen and Zinn 2000) to its origin: nonlinear gasdynamics or nonlinear combustion. In that case nonlinearities in the system could be exploited by an 'ad hoc' form of (nonlinear) control to overcome the main limitations of linear control: requirement of a relatively high control effort and actuation frequency at the same frequency of the instability.

Since such a complete model is not available (except for special cases), controller synthesis is generally based on a linear model. Note that the linear model of the combustion chamber presented in the section 4.1 is actually a linearization of the full model (ideally, of the real system) around the operating point. Since the main purpose here is to keep the system 'stable', i.e., as close as possible to the linearized equilibrium point, the linear model and simulation is a valid and realistic approximation to the real case, provided that the nonlinearities do not give rise to a subcritical bifurcation (Wang 2000). Note that nonlinearities have the effect of limiting the

amplitude of the oscillations: hence the linear model is in this sense a 'conservative' approach to the problem (for example, in terms of required control action, we will find an upper limit).

In short, within the present approach, nonlinearities can actually be neglected, except as a formal vehicle for rigorously introducing noise sources. As a consequence, we will not be able to capture the effects of any instability mechanism different from the linear growth and phase shifting included in the model presented below.

On the other hand, the present approach allows for a clear distinction of the effects of uncertainties, intrinsic noise sources, external noise sources, unmodeled dynamics and time-delay (Seywert, Isella and Culick 2000).

4.1 Reduction of the Equations to State-space With Control

The approximate analysis outlined in chapter 2 leads to a set of equations representing the dynamics of the combustion chamber that can be easily cast in the traditional control theory form. To reduce the set of equations (2.20) to state-space form, we separate the linear terms from the nonlinear

$$\ddot{\eta}_n + \omega_n^2 \eta_n + \sum_{i=1}^{k} \left(D_{ni}\dot{\eta}_i + E_{ni}\eta_i \right) + F_n^{NL}(\ldots) = w_n(t) + U_n(t) \qquad n = 1,\ldots,k \tag{4.1}$$

where we have added two extra terms on the right-hand side: w_n to represent the additive noise input, and U_n to represent the control input. The expression of the linear coefficients D_{ni} and E_{ni} is reported by Kim 1989; for longitudinal one-dimensional motion they reduce to the simple expressions:

$$D_{ni} = \frac{1}{E_n^2} \int A(x) \left[\left(1 + \frac{k_n^2}{k_i^2} \right) \psi_n \bar{u} \frac{\partial}{\partial x} \psi_i + \bar{\gamma} \psi_i \psi_n \frac{\partial}{\partial x} \bar{u} \right] dx \tag{4.2}$$

$$E_{ni} = \frac{1}{E_n^2} \int A(x) \left(\psi_i \bar{u} \frac{\partial}{\partial x} \bar{u} \frac{\partial}{\partial x} \psi_n \right) dx, \qquad E_n^2 = \iiint \psi_n^2 dV \tag{4.3}$$

Recall that the central idea of the approximate analysis is that combustion instabilities are dominated by acoustic waves and hence we neglected entropy and vorticity components in the expansion for the pressure. These extra contributions can be retained, and give rise to some extra linear terms in the equations that can be treated as stochastic sources (Seywert et al. 2000); here, we lump these contributions as unmodeled dynamics and ignore their explicit contribution to the system. Also the contribution due to linear combustion is lumped together with linear gasdynamics in the linear coefficients; in particular, it is the linear combustion that makes the system unstable in the first place. This is a valid approximation within the approach described; for a detailed analysis of the effect of this approximation, see Wang 2000.

For the purpose of linear control, we neglect non linear terms in (4.1) and we reduce the set of differential equation to first order, similarly to chapter 2.3.1. Define

(4.4)
$$\mathbf{x} = \begin{bmatrix} \eta_1 \\ \dot{\eta}_1 \\ \dots \\ \dot{\eta}_n \end{bmatrix}$$

as the state vector. And

(4.5)
$$\mathbf{A} = \begin{bmatrix} 0 & 1 & \dots & 0 \\ -\omega_1^2 + E_{11} & D_{11} & \dots & D_{1n} \\ \dots & \dots & \dots & \dots \\ E_{n1} & D_{n1} & \dots & D_{nn} \end{bmatrix}$$

(4.6)
$$\mathbf{B} = \frac{\bar{a}^2}{\bar{p}} \begin{bmatrix} 0 & 0 & 0 \\ \dfrac{\psi_1(x_a)}{E_1^2} & W_{1_{input\ noise}} & 0 \\ \dots & \dots & \dots \\ 0 & 0 & 0 \\ \dfrac{\psi_n(x_a)}{E_n^2} & W_{2_{input\ noise}} & 0 \end{bmatrix}$$

(4.7)
$$\mathbf{C} = K_m \bar{p} \begin{bmatrix} \psi_1(x_m) & \dots & \psi_n(x_m) & 0 \end{bmatrix}$$

$$\mathbf{D} = \begin{bmatrix} 0 & 0 & W_{sensor\ noise} \end{bmatrix} \tag{4.8}$$

where we assumed a system with one actuator at position x_a and one sensor at position x_m, and W is the weight associated to the noise input into the system and in the sensor. With this notation, the set of equations (4.1) becomes equivalent to

$$\begin{aligned} \dot{\mathbf{x}} &= \mathbf{A}\mathbf{x} + \mathbf{B}\mathbf{u} \\ \mathbf{y} &= \mathbf{C}\mathbf{x} + \mathbf{D}\mathbf{u} \end{aligned} \tag{4.9}$$

where **u** includes the control input and the additive noise terms.

There are some basic issues associated with introducing control into a system, namely the observability and controllability of the system. For our case, where we chose to represent the system with a (finite) sum of acoustic modes, the state of the system is not readily available as an output, since the typical output would be just a pressure pick up, or a temperature measurement. By following control system theory, it is possible to explicitly compute the controllability and observability matrices for the system and check that the system is indeed controllable and observable (provided that actuator and sensor are conveniently placed inside the chamber). In the same manner, since, by using our approach we produce a simple model of the system, it can be shown that we can estimate the model system from the pressure reading. An important question is whether this can be always done in practice or not. A precise answer to this question would require some experimental work that is currently planned; for now, we can say that, since our control analysis and modeling work is based on the observation that similar control systems have been applied to real system and shown to be effective, we work under the implicit assumption that the real system are indeed controllable and observable.

4.2 Sensor and Actuator Modeling

Experimental work on active control of combustion instabilities has been so far mainly concentrated on laboratory combustors, with some examples, in more recent years, on full scale items.

Regarding possible sensors for control purposes, from experimental work, it results that the most reliable sensing can be done with the use of pressure sensors. Heat release measurements or temperature measurements are less reliable and more complex/costly: they remain very important as a tool for developing and testing models, but not for control feedback.

In our simulations, following common practice in combustion control literature (Fung 1992, Haddad et al. 1997), we model the pressure sensor as a pure gain between the measured pressure and the output voltage of the microphone. Possible time delays are lumped together in a single delay for the whole system, as explained later. For simulation purposes, such model can be immediately introduced in our formalism, since the pressure in the chamber can be immediately written as a synthesis of the acoustic modes, as in equation (2.18).

Typical actuators present more variety than the sensors. The most commonly used include: loudspeakers (especially for laboratory combustors), secondary fuel injection/modulation, primary fuel modulation.

The typical model of a speaker is given in Haddad et al. 1997, and uses a second order transfer function between speaker voltage input and velocity induced by the speaker baffle. This model lends itself naturally to the introduction in the model of the system within our formalism, and simulation is simply done by augmenting the system states with the actuator states. As noted later, even the actuation from a loudspeaker has a time delay (that can become significant) due to the traveling time of the acoustic waves in the chamber. Again, this delay is lumped as a system

delay and treated separately. This actuator model is the most commonly used in the combustion control literature.

More complex is the modeling of a liquid fuel injector. In this case we give an example of a simulation that includes a liquid injector actuator, modeled from the results presented in Neumeier, Nabi et al. 1997. The data reported make it is possible (with a few assumptions) to identify the characteristics (transfer function) of a fuel injector.

Figure 4.1 presents the experimental injector transfer function and the corresponding model. Note the scale factor on the gain, inferred from other data (not clearly specified by the authors in Neumeier, Nabi et al. 1997). The frequency axis is in non-dimensional units.

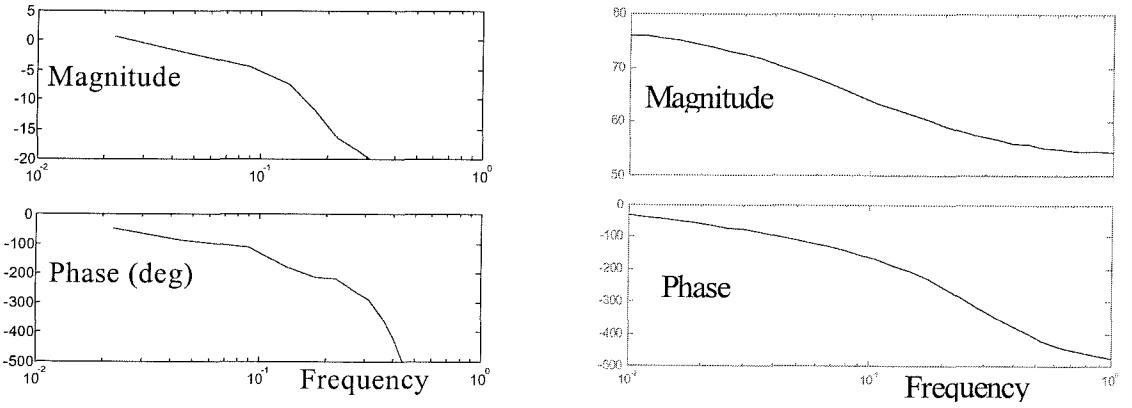

Figure 4.1. Experimental characterization of the injector versus identified model.

The model of the injector is the following transfer function:

$$inj = 300\frac{s+700}{s+50}e^{-0.008s} \tag{12}$$

Figure 4.2 presents the comparison of a run using the loudspeaker model and the injector model; the combustor is based on the 'standard' test combustor, described in Seywert 2001. Delay compensation is performed by using a predictive model, as explained in section 4.4.

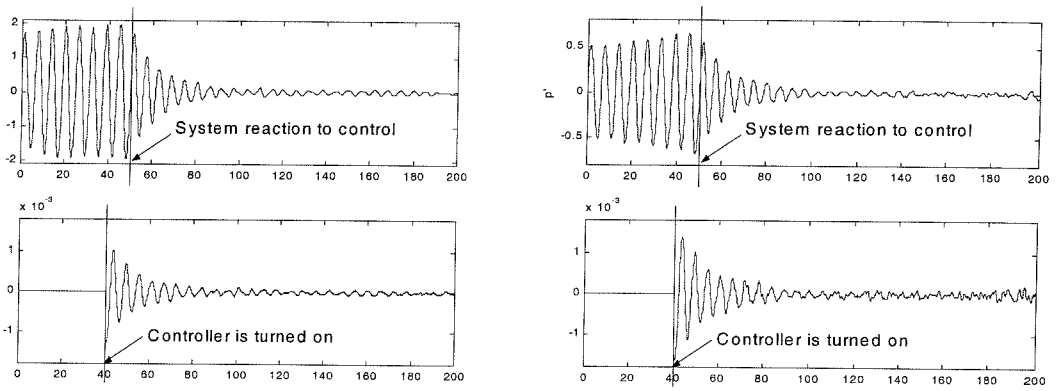

(a) (b)

Figure 4.2. Control with time-delay, (τ=*10*). Top half: system response. Bottom half: control action. (a): Loudspeaker actuator; (b): Injector actuator

An interesting point is to compare what is the necessary (used by this controller) injector authority versus the amplitude of *natural* oscillations in the chamber; the comparison is presented in Figure 4.3. The top half shows amplitude of the pressure oscillations and amplitude of the control effort; the lower half is the ratio of control and pressure.

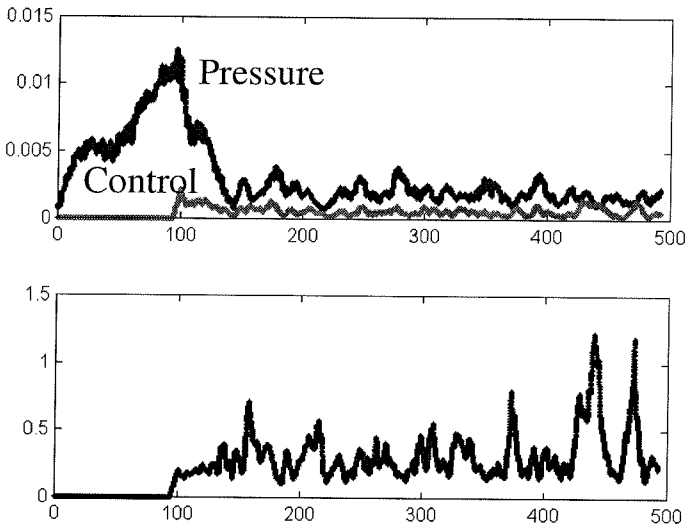

Figure 4.3. Injector heat release vs. *mean* heat release.

This assures that the actuator would be in practice able to perform the required control. A similar comparison obtained from experimental data, presented in Neumeier et al. 1997, shows that the ratio presented in the bottom half of Figure 4.3 ranges from 0.55 to about 0.80, and is hence consistent with the numbers obtained in our simulation.

More recently, an example of control using fuel injection is given by Hathout, Annswamy and Ghoniem 2000. In this work, starting from a physical model of a generic 'proportional' liquid fuel injector, the authors produce a third order model of the injector, which is then immediately simplified to a first order system. In this paper, the authors also analyze the possibility of using the same model for an on/off injector (like the one used for the experiments described in chapter 5). Control design is done as for a linear system, and the on/off characteristic is added during simulations.

An open question is the scaling of the actuators from laboratory combustors to industrial size systems. As long as the systems are linear, the answer is obvious, but there is evidence that nonlinearities in the flame dynamics might be responsible for some of the observed effects, and hence scaling would be an issue.

4.3 "PID"-like Control

We dedicate a short mention to this kind of control, since it is the most commonly used for laboratory applications, and it appears to be effective in most cases. One of the first applications can be found in Poinsot et al. 1987, where the authors describe a feedback control example with proportional feedback based on the observation of the unstable mode.

This method includes the common experimental approach of measuring an output from the system (typically pressure) and using it as a feed-back input after filtering, phase-shifting and amplifying. The only design variables are the gain of the amplification and the phase shift. This method is shown to work in a variety of circumstances; the disadvantage is that it does not give

much insight into the system and also it is not possible to impose some a priori performance specification on the control design. Moreover, stability is typically not very robust, and hence is not suitable for general applications, since combustion systems have large uncertainties on the parameters, large noise in the sensors, actuators and system, and the models have to neglect or approximate part of dynamics.

A detailed analysis of control algorithms, effects of residual dynamics, truncation, etc., is presented in Seywert 2001 and is not repeated here. For the purpose of the examples, we use a controller similar to the one used by Seywert et al. 2000, and we limit the analysis to the effects of time delay in the controlled system.

4.4 Issues Relative to Control of Combustors: Time Delay

Time delays often arise in combustion systems: for example, even when no control is present, there is delay between injection of the fuel mixture and fully developed combustion for the case of liquid or gas combustors, as a consequence of transport and chemical mixing. When feedback control is present, there are further delays intrinsic to the controller due to finite rates of actuators and sensors, time spent for signal acquisition and processing, and clock time in case a digital computer is used.

Even for the typical laboratory-scale combustor, when a loudspeaker is used as an actuator, time delays might play an important role: suppose the first unstable acoustic mode has a frequency of 1 *kHz*, then a typical reaction time for the controller (if we consider linear approach, the bandwidth of the controller should at least match the typical frequencies of the instability in the plant) is of the order of 1 *ms*. Modern electronic equipment can certainly process the required computation for determining the control input much faster than that; the bottleneck for this case is the time it takes for the pressure input (from the loudspeaker) to influence the chamber acoustic response. A similar situation would be present in the case of control based on fuel (primary or

secondary) modulation: in this case, the longer delay would be the time elapsed between injection and combustion and, consequently, the effect on the combustion chamber.

This time, for a 50 *cm* chamber, is of the order of 1-2 *ms*, just the same order of the instability.

In the case of industrial scale combustors, or when using secondary fuel injection as control actuation, the necessity of considering time delays becomes even more compelling, since in these cases the time delay can easily be larger than the characteristic timescale of the instability.

Time delays always reduce the stability of a system (Franklin et al. 1995), hence it is very important to take them into consideration when simulating a realistic combustor and when designing a suitable controller.

Regarding the controller design phase, three general approaches are possible.

- *Classical Control.* If we look at the transfer function of the system, and indicate with τ the time delay, the problem with time delay is reduced to a conventional one by expressing the nonrational function $e^{\tau s}$ in terms of a rational function. Note that the function $e^{\tau s}$ is analytic (for finite values of s), so approximation with a rational function is allowed. A typical approach is to use a Padé approximant, based on a McLauren series expansion of the exponential function. The value of the method is limited by two factors. First, the rational approximation of the delay rapidly increases the effective order of the plant, making the control design problematic. Second, large values of time delay will decrease the available phase margin to the point where it is no longer possible to design a stabilizing controller. Also, in Wang 2000, the author shows that a low order polynomial approximation of the time delay is not enough to have a satisfactory model in terms of dynamical behavior of the original system. In the present paper we do not take this

method into consideration, since we focus our attention on control design methods capable of incorporating robustness requirements.

- *Modern Control.* In this case, time delay can be viewed as an uncertainty in the system and incorporated in the design as a perturbation to the original plant. More details are given in the following section.

- *Delay Compensation.* This category includes all the other methods used to compensate for time delay. An important group includes compensation networks that bring the delay 'out of the loop', and hence allow to design the controller using conventional methods applied to the plant without time delay. A typical example is the Smith Regulator. A caveat here is constituted by the fact that most networks based on linear elements generally do not modify the eigenvalues of the original plant, so they only apply to stable (or marginally stable) plants. On the other hand, by using these methods, arbitrarily large time delays can be accounted for without loss of stability margin.

4.4.1 Modern Control

Time delay can be incorporated in the design of a controller by considering the time delay as a multiplicative perturbation to the plant. Let $\tilde{P}(s) = P(s)e^{-\tau s}$ be the perturbed plant. The perturbed plant can be included in the set

(4.10) $$\left\{(1+\Delta_{Plant}W_{unc})P : \|\Delta_{Plant}\|_{\infty} \le 1\right\}$$

In order to obtain that, the weight function W_{unc} is chosen so that

(4.11) $$\left|\frac{\tilde{P}(j\omega)}{P(j\omega)} - 1\right| \le |W_{unc}(j\omega)| \qquad \forall \omega, \tau$$

or

$$\left|e^{-\tau j\omega}-1\right| \le \left|W_{unc}(j\omega)\right| \qquad \forall \omega, \tau \tag{4.12}$$

The design of the controller then proceeds in the same way as before. Note that, if the time delay is 'large', condition (4.12) typically imposes a significant limitation on the controller; in general performance is degraded and, if τ is large enough, it might be impossible to design a stabilizing controller for the delayed system. On the other hand, when a solution exists, stability and performance are guaranteed according to the design. Uncertainty in the numerical value of the time delay, as it is typical in combustion systems, is automatically taken into consideration by the design method. Application of this approach is included in the example presented later.

4.4.2 Delay Compensation

In this section we will examine a method based on *predictive control*: the time delay is compensated by a predictor that acts on the measured or estimated state and feeds the controller with the appropriate signal to perform the feedback action at the compensated time.

Smith Compensator

The idea is to bring the delay out of the feedback loop, so that traditional design methods can be used.

Figure 4.4 shows a block diagram of a system with pure time delay.

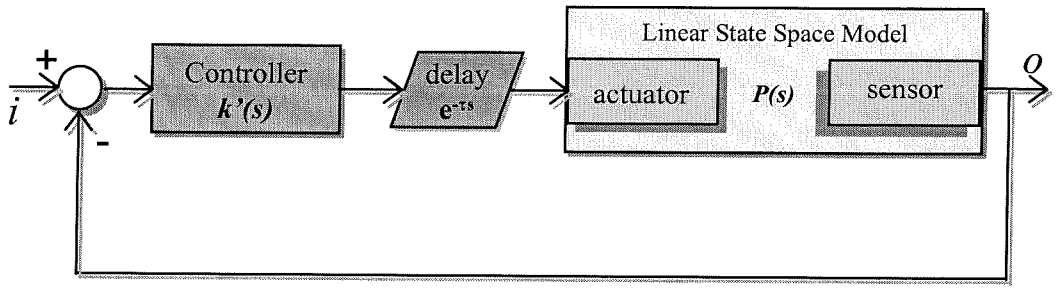

Figure 4.4. System with pure time delay.

The input-output transfer function of the system is set equal to a transfer function of a system with the delay out of the loop, as shown in equation (4.13), and then the equation is solved for the appropriate regulator *k'(s)*, given by equation (4.14).

(4.13)
$$\frac{o(s)}{i(s)} = \frac{k'(s)e^{-\tau s}P(s)}{1+k'(s)e^{-\tau s}P(s)} = \frac{k(s)P(s)}{1+k(s)P(s)}e^{-\tau s}$$

(4.14)
$$k'(s) = \frac{k(s)}{1+k(s)P(s)\left(1-e^{-\tau s}\right)}$$

Figure 4.5 shows a block diagram of equation (4.14), and expands the controller box of Figure 4.4.

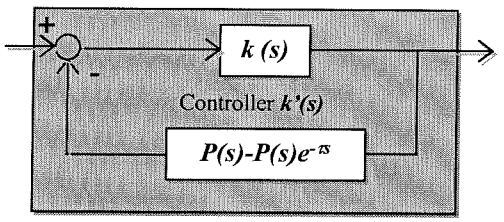

Figure 4.5. The Smith compensator.

In other words, Smith's scheme utilizes two feedback loops to control the system: the inner (or minor) feedback takes care of the delay, the outer (or major) loop is the normal control feedback.

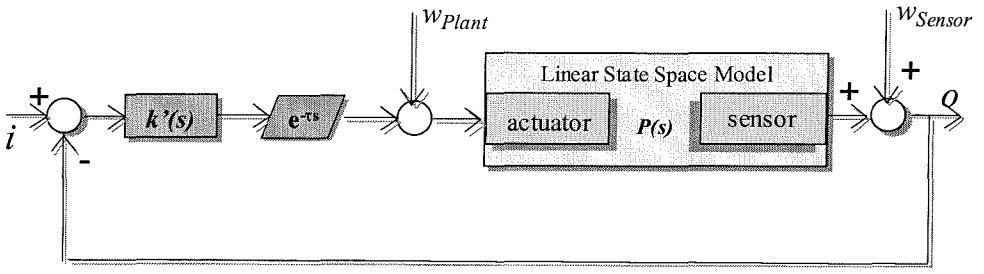

Figure 4.6. Disturbance sources into the system.

Note that the noise rejection properties of the Smith's compensator are not good

(4.15)
$$\frac{o}{w_{Sensor}} = \frac{1+kP\left(1-e^{-\tau s}\right)}{1+kP}; \qquad \frac{o}{w_{Plant}} = P\frac{1+kP\left(1-e^{-\tau s}\right)}{1+kP}$$

As shown by equations (4.15), the compensator loop brings the controller gain on the numerator. It is interesting to note that the noise rejection characteristics actually depend on the time delay. As expected, in the limit of $\tau \to 0$, the system behaves as if the Smith Compensator were not present, while with increasing τ, the noise rejection worsens.

Since the frequency range of interest for the dynamics of the combustor is limited, the noise rejection properties can be drastically improved by adding a low-pass filter in the loop (the noise is just random white noise).

For the case of a perturbation of the plant, where *P(s)*, in Figure 4.4, is substituted by $\tilde{P}(s)$, the "model" of the plant acts as an ulterior perturbation, weighted by the time delay:

(4.16)
$$\frac{o(s)}{i(s)} = \frac{k\tilde{P}}{1+k\left[\tilde{P}e^{-\tau s}+P\left(1-e^{-\tau s}\right)\right]}e^{-\tau s}$$

Stability Properties of the Smith Compensator

One important problem with the Smith scheme is represented by its stability properties. Furukawa et al. 1983, presented an argument, based on a State-Space representation of the system, to show

that the controller can not effectively modify the eigenvalues of the closed loop system. A similar conclusion can be obtained from the following argument.

Considering the transfer function for the whole system, expressed by the last of (4.13), the characteristic equation is

(4.17) $$1+k(s)P(s) = 0$$

If the plant is unstable, i.e., $P(s)$ has poles with positive real part, on the condition that the system is controllable and observable, by pole placement it is possible to find a controller $k(s)$ such that equation (4.17) has roots in the left half of the complex plane, and hence the closed-loop interconnection appears to be stable.

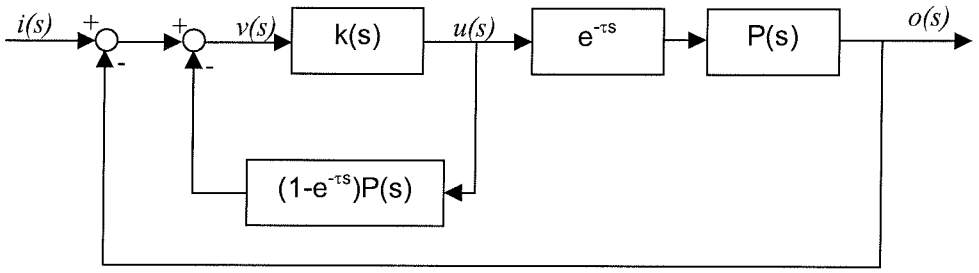

Figure 4.7. Smith Compensator with Minor and Major feedback loops explicitly drawn.

Let us now consider some of the internal transfer functions, in particular, with the notation of Figure 4.7, the relationship between input, $i(s)$ and controller output, $u(s)$.

(4.18) $$u = kv = -ukP(1-e^{-\varpi}) + i - o = -u\,P(1-e^{-\varpi}) + i - uP\,e^{-\varpi}$$

Hence

(4.19) $$\frac{u(s)}{i(s)} = \frac{1}{1+kP\left(1-e^{-\varpi}\right)+Pe^{-\varpi}}$$

Now the characteristic equation for this part of the system includes the plant itself; the poles of the term:

(4.20) $$1+kP\left(1-e^{-\varpi}\right)$$

are placed in the left-hand side of the complex plane by the controller design, while nothing can be done to the original (unstable by assumption) poles in the extra term:

(4.21) $$Pe^{-\varpi}$$

Hence this part of the internal loop of the system is unstable. In other words, the spectrum of the closed loop system contains all the original eigenvalues of *P*, plus the ones modified by the presence of the controller. The same conclusion can be obtained by conducting the analysis with a State-Space representation of the system. This fact prevents using the Smith Regulator in the case of unstable plants and makes its value for our case rather marginal.

Other Predictive Control Schemes

The control system consists of a predictor and a controller; the closed loop equations for a generic input-delayed system can be written as

(4.22) $$\begin{cases} \dot{\mathbf{x}}(t) = \mathbf{A}\mathbf{x}(t) - \mathbf{B}\mathbf{u}(t-\tau) \\ \mathbf{y}(t) = \mathbf{C}\mathbf{x}(t) \end{cases}$$

(4.23) $$\mathbf{p}(t) = e^{A\tau}\mathbf{x}(t) + \int_{-\tau}^{0} e^{-A\tau} B\mathbf{u}(t+\tilde{t})d\tilde{t}$$

(4.24) $$\mathbf{u}(t) = \mathbf{K}\mathbf{p}(t) + \mathbf{i}(t)$$

where $\mathbf{i}(t)$ is the external input to the system and might not be present, and, without loss of generality, **D** is assumed to be zero. The predictor written as in (4.23) is simply derived by integrating (4.22) from the current time t to the time $t+\tau$. A change of variables produces the form (4.23), which contains information only up to the current time and consequently it can be physically implemented.

In Furukawa and Shimemura 1983, the authors prove (by directly computing the closed-loop characteristic equation) that if the pair (**A, B**) is controllable, then the predictor (4.23) and the controller (4.22) yield a finite spectrum of the closed-loop system, located at arbitrarily pre-assigned points in the complex plane.

Note that the predictor (4.23) contains an integral term up to the current time. It is impossible to integrate up to current time without solving an integral equation, or iterating on the solution, but it can be shown (Manitius and Olbrot 1979) that the limits in the integral term appearing in (4.23) can be substituted by -τ-ε and -ε if ε is sufficiently small.

Let us now consider the following scheme

$$\begin{aligned}
&\dot{\mathbf{x}}(t) = \mathbf{A}\mathbf{x}(t) - \mathbf{B}\mathbf{u}(t-\tau) \\
&\begin{cases}
\dot{\tilde{\mathbf{z}}}(t) = \mathbf{A}\tilde{\mathbf{z}}(t) - \mathbf{B}\mathbf{u}(t) \\
\mathbf{z}(t) = \tilde{\mathbf{z}}(t) - e^{\mathbf{A}\tau}\tilde{\mathbf{z}}(t-\tau) \\
\mathbf{p}(t) = e^{\mathbf{A}\tau}\mathbf{x}(t) + \mathbf{z}(t)
\end{cases} \\
&\mathbf{u}(t) = \mathbf{K}\mathbf{p}(t)
\end{aligned} \tag{4.25}$$

A simple substitution shows that computing $\mathbf{z}(t)$ from the equations above results in the evaluation of the correct predictor term (4.23). The scheme (4.25) can be physically implemented in Simulink by using the network connection presented in Figure 4.8, where symbols refer to the letters used in (4.25) and p is the signal sent to the controller.

Since the time delay is compensated in this secondary predictor-loop, application of this scheme to the plant presented above allows including significant time delays in the system without compromising performance in the design of the controller. On the other hand, the use of a second loop reduces the robustness of the system to uncertainties in the value of the parameters.

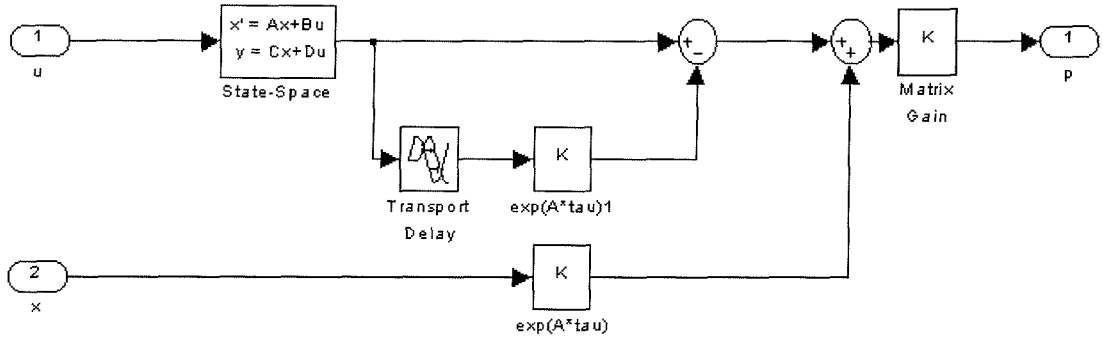

Figure 4.8. SIMULINK realization of the *predictor* block, equations (4.25).

4.4.3 Application and Discussion

By using the standard model for the plant (cf. Fung 1992, Haddad et al. 1997, Seywert 2001) we can demonstrate an application of the predictive control scheme described above. Figure 4.9 presents the result; the simulation refers to the plant described in detail by Seywert 2001, and includes additive noise but no uncertainty into the system.

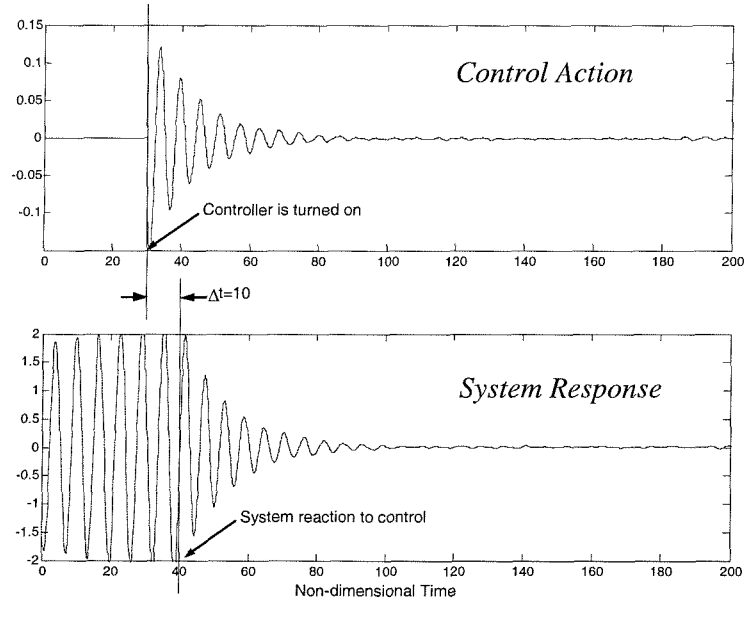

Figure 4.9. Example of control with time delay.

The non-dimensional time delay is chosen to be $\tau = 10$, which corresponds to a delay of about $10ms$, i.e., 5 periods of an oscillation at 500 Hz and constitutes a reasonable upper limit to the delay that can be expected in a real combustor controlled by modulating the injection of secondary fuel. Note how the predictor works: the controller (control action is plotted in the top half of Figure 4.9) starts sending commands immediately when activated. The control is computed on a prediction of the future state of the system, i.e., the state of the system when the control signal will effectively reach the plant. The system response, plotted in the bottom half of the figure, shows that the system effectively starts reacting to the control at a non-dimensional time of 40, when the controller is put on line at a non-dimensional time of 30.

Figure 4.9 presents the results of a simulation with exact knowledge of both plant and time delay. An important question is whether this compensation network would tolerate the presence of uncertainty. A numerical evaluation of the stability region is presented in Figure 4.10, where we used multiplicative uncertainty on the state matrix and uncertainty in the time delay as parameters.

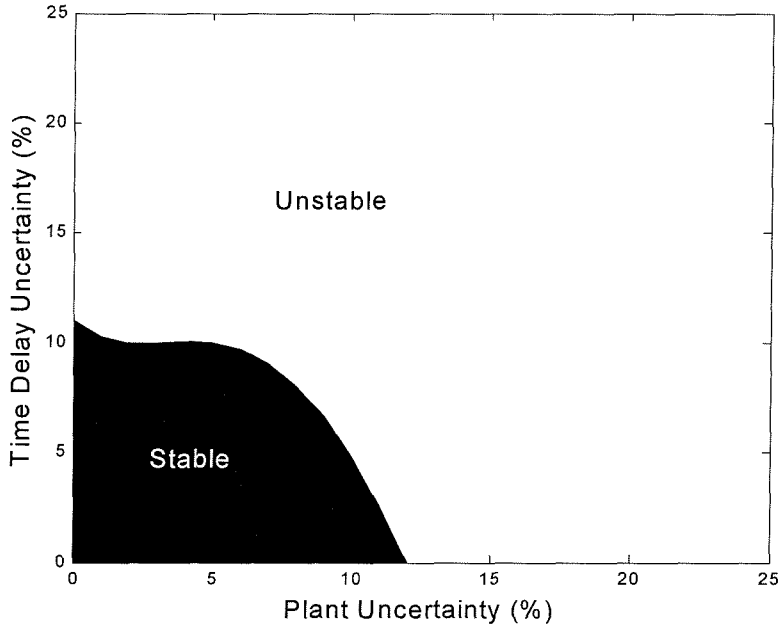

Figure 4.10. Plant and time delay uncertainty.

Simulations show that the limit uncertainty is not symmetrical, i.e., the results differ from overestimating or underestimating any of the two parameters. The figure presents the worst case, and shows that a modest uncertainty will rapidly bring the system to instability. The real test of the effectiveness of this approach will be the application to an actual combustor, where it would be possible to estimate the uncertainty in the parameters.

Inclusion of the time delay in the modern design framework as an uncertainty is adequate when the time-delay is of the same order of the characteristic time of the instability, defined as the inverse of the frequency of the unstable mode. Cases with longer time delays, as it might be the case in full scale combustors, can be treated by adding a second loop to compensate for the delay: simulation shows very good performance, but issues about robustness to uncertainty and perturbation need to be addressed carefully. Since a good model of the system is needed to perform the prediction, performance degrades rapidly if the time delay is long (unless the model is perfect) or if the model is not very accurate. Some degree of capability to adapt on line might be needed for application to real systems.

Some recent work by Evesque, Dowling, Annaswamy, 2000 and Hathout et al. 2000, also makes use of the concept of predictive control to compensate for the time delay and also uses an adaptive regulator (with fixed, and known, time delay). The approach is substantially the same as the one presented here, and the authors reach similar conclusions.

5 Experimental Investigation of a Dump Combustor with Pulsed Secondary Fuel Control

Hysteretic behavior, as found in the dump combustor facility at GALCIT, allows nonlinear active control of the instability, demonstrated first by Knoop, Culick and Zukoski (1996).

As in that work, pulses of secondary fuel, based on a simple on/off control law, have been successfully used to drive the transition between the two modes present in the hysteretic region, thereby reducing the amplitude of the pressure oscillations with minimal use of fuel.

In order to clarify the origin of the phenomenon, high speed shadowgraph images of the flowfield during the transition between 'unstable' and stable burning have been taken, showing distinctive features that may help in modeling the observed behavior. A preliminary parametric study (type of injector, duration of pulses, type of secondary flow) has also been conducted, showing that the transition can be obtained over a broad range of conditions.

5.1 Dump Combustor[1]

A vast variety of approaches to active control of combustion instabilities has been proposed; McManus, Poinsot and Candel (1992) give a review of those strategies: the main feature is to act on the system at the frequency of the instability without however taking advantage of the underlying characteristics (non-linearities) of those systems. In this work, the idea proposed by Knoop, Culick and Zukoski (1996), of using hysteretic behavior to perform a non-linear low

---

[1] The work described in this section was performed in collaboration (50%) with Claude Seywert.

frequency control of the unsteady motions in a combustor is pursued further. Some of the hypotheses presented in Knoop et al. (1996) are confirmed here and extended by the results obtained in further experiments, conducted in the dump combustor facility at the Graduate Aeronautical Laboratories, California Institute of Technology (GALCIT).

5.1.1 Experimental Apparatus and Procedure

The experimental apparatus (Figure 5.2) is essentially the same as that used by Knoop et al. (1996); the combustor was originally designed by Smith, and details of the design and operation of the facility are discussed in Smith (1985); an overall layout of the facility is presented in Figure 5.1. A high speed motion picture camera was added in order to visualize (by using shadowgraph technique) the transition between the two burning modes of the combustor.

The system consists of a blowdown supply of air and fuel (methane) controlled by dome regulators. A three-way valve allows fuel and air lines to be pressurized separately or equally in a 'paired mode' of operation. This permits mixtures of any stoichiometry to be used (the nozzles have been designed in such a way that 'paired operation' gives a stoichiometric mixture).

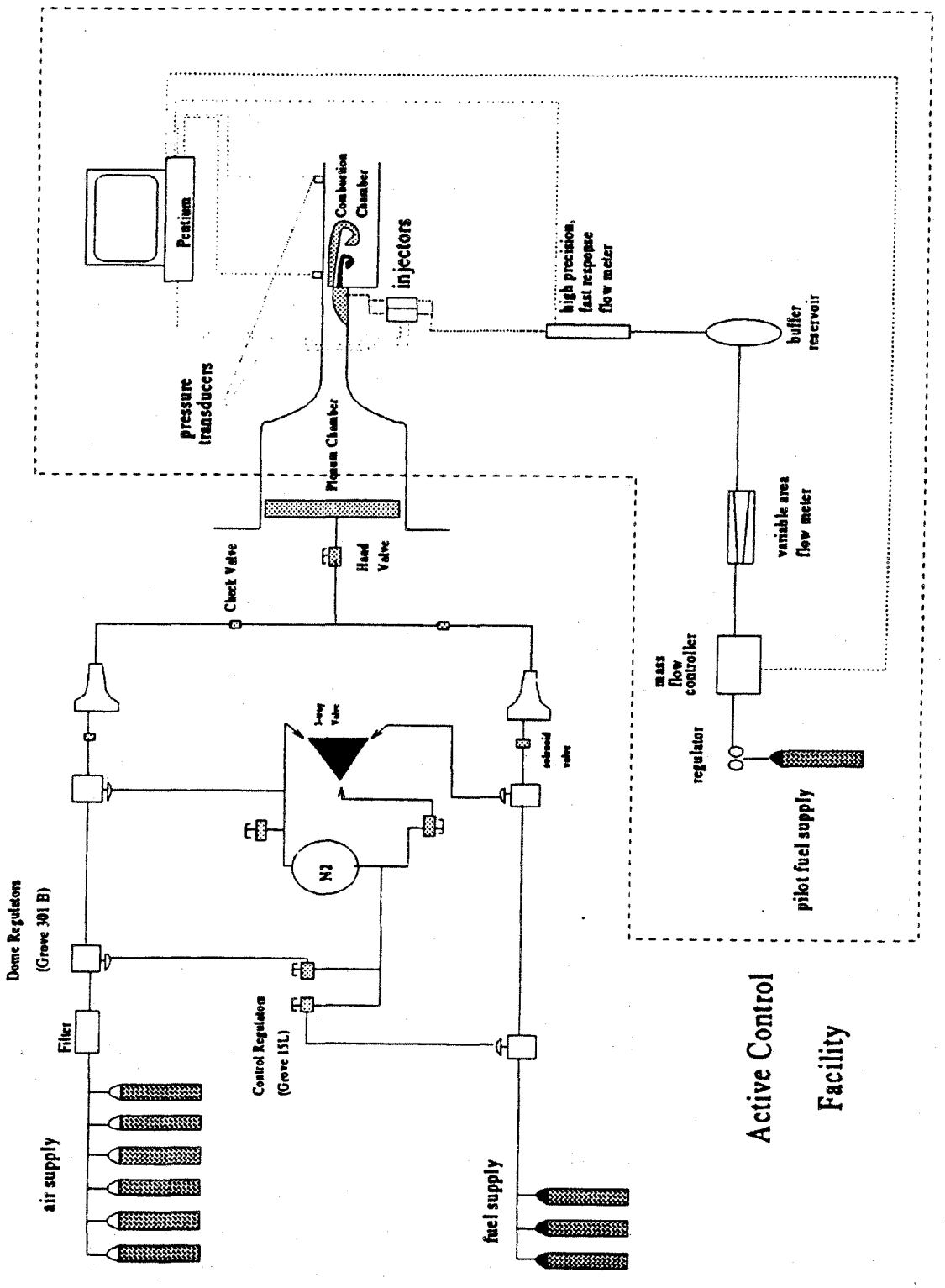

Figure 5.1. Layout of the Dump Combustor Facility.

Figure 5.2 shows a schematic of the combustor with the dimensions expressed in millimeters. The section immediately following the expansion (which acts as flameholder) is water cooled and has optical access from both sides through Vycor glass windows. Combustion is initiated by a spark igniter located at the bottom of the chamber.

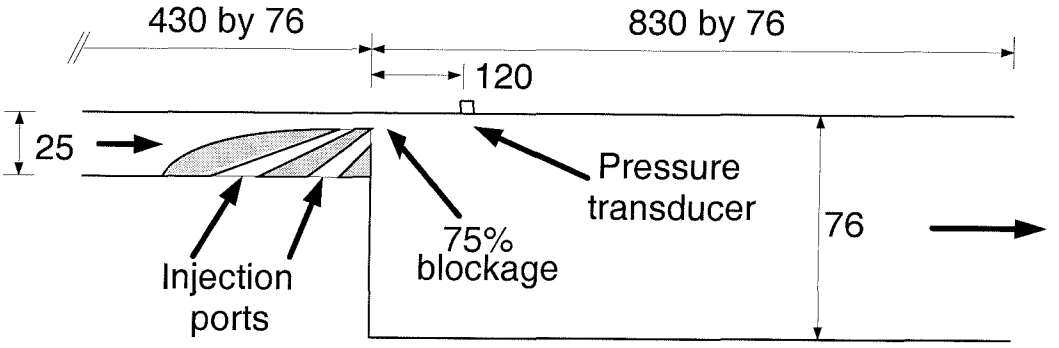

Figure 5.2. Experimental apparatus (measurements in mm).

Once the system has reached the desired operating condition, control is performed by injecting a pulse of pilot gas (methane, hydrogen or nitrogen) whenever the combustion chamber exhibits pressure oscillations surpassing a predefined threshold. The pulses are generated by using commercial diesel engine injectors, and fed into the combustion chamber through two different ports: either into the boundary layer of the incoming fuel-air mixture or immediately into the recirculation zone behind the rearward facing step (Figure 5.2). The injectors line is pressurized separately from the other lines and can be set in the range 0-15 *psig*. Two injectors are used and can be commanded asynchronously to increase injection frequency.

The pressure is recorded by using a PCB model 106B piezoelectric pressure transducer mounted in a small water cooled cavity on the top of the combustion chamber at a distance of 12 *cm* from the dump plane. The cavity was designed so that its resonant frequency (5500 *Hz*) is well above any acoustic frequency of the duct (the first observed mode is at 234 *Hz*) and there are no phase or magnitude adjustments for frequencies below 800 *Hz*.

The differences in pressure amplitude and frequency content of the two burning modes can be seen by comparing Figure 5.3 and Figure 5.4; the two modes will be referred as *stable* (the one with the lowest amplitude of pressure oscillations) and *unstable* (combustor operating on a limit cycle, with large oscillations).

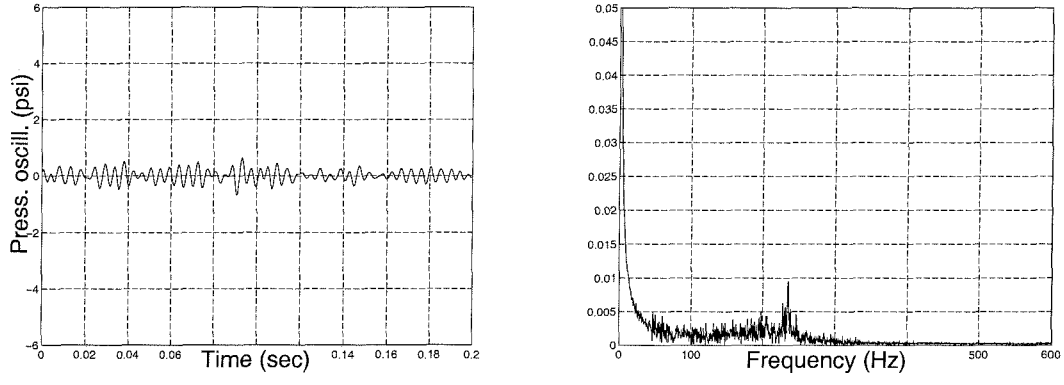

Figure 5.3. Pressure and trace of the stable burning mode.

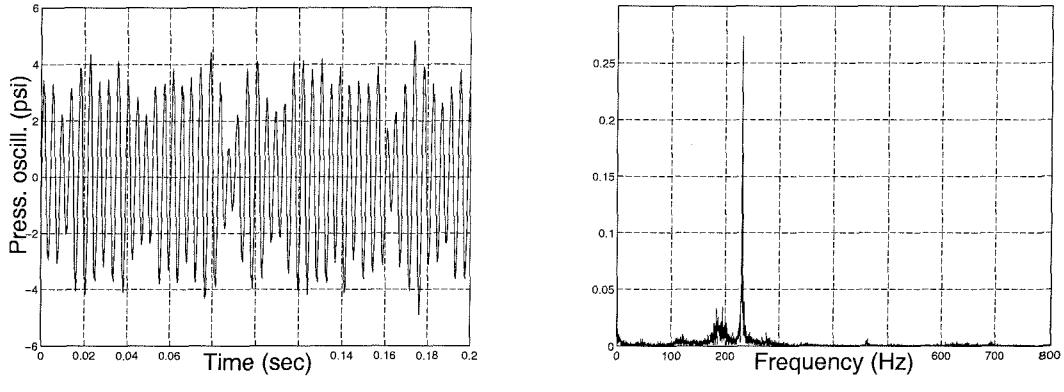

Figure 5.4. Pressure trace and spectrum of the unstable burning mode.

Sterling 1987 shows a high speed shadowgraph sequence of the flow field for both the stable and unstable burning conditions.

Two independent flow meters are used to monitor the pilot gas rate. A variable are flowmeter (Matheson Gas Products, model FM-1050) located on the control panel allows accurate measurement of the steady flow. A Honeywell Mass Airflow Sensor (model AWM5101VN),

located immediately upstream of the injectors, is used for measuring time variations in the pilot fuel flow.

The possibility of stabilizing the combustion by this simple means relies on the fact that the amplitude of pressure oscillations in the combustor exhibits an extended hysteresis loop when the equivalence ratio ϕ is varied. Figure 5.5 clearly shows that for $0.75 \leq \phi \leq 0.9$ two possible states (stable and 'unstable') exist in the combustor. Which of these states is actually present depends on the history. Thus if the combustor turns unstable (to be more precise: if it reaches the stable limit cycle characterized by large oscillations) within this substantial region of values of the equivalence ratio (ϕ), it should be possible to force it from the upper branch of the hysteresis to the lower one (stable combustion). This transition can be consistently achieved, as demonstrated by the experiments described later, by injection of secondary fuel into the chamber at the dump plane.

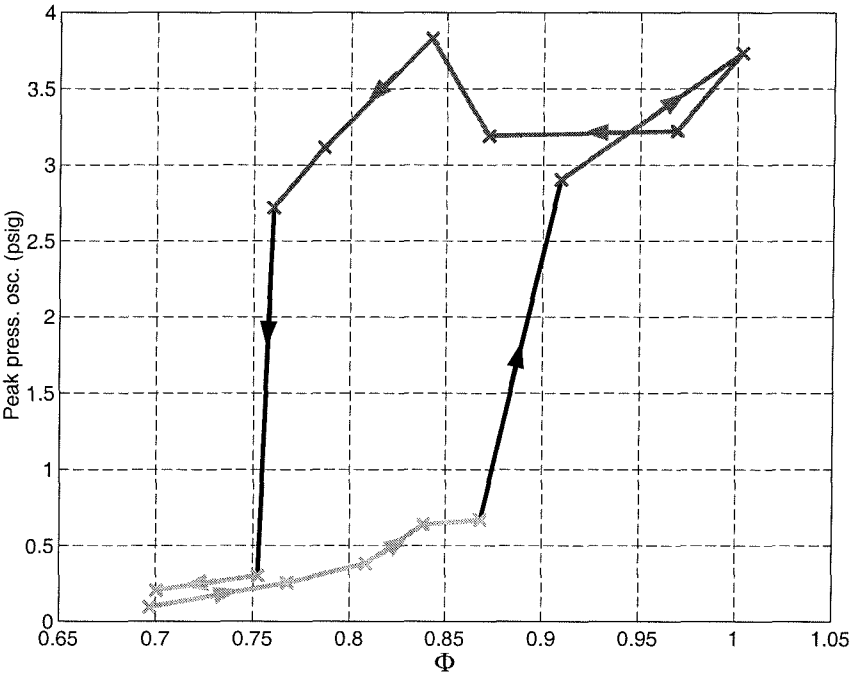

Figure 5.5. Hysteresis of the combustor.

The flowfield in the combustion chamber is recorded using a standard Z-configuration shadowgraph arrangement with a high speed camera and a high intensity Hg continuous light source. The geometrical configuration of the elements in the setup can be seen in Figure 5.6.

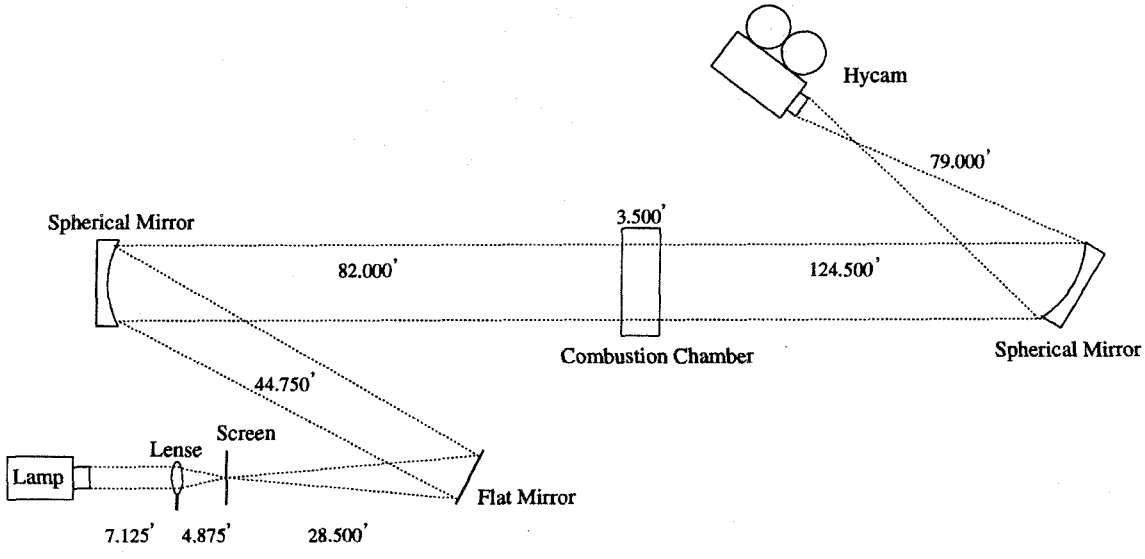

Figure 5.6. Setup of the shadowgraph imaging system.

The camera is a HycamII, 16mm, high speed motion picture camera, manufactured by Visual Instrumentation Corporation. It allows continuous speed regulation up to a top speed of 1100 frames per second. In this investigation recording was done at a rate of 5000 frames per second, using 100 ft rolls of Kodak-Eastmann 7222 DoubleX negative film (black and white).

The camera takes about 40 *ft* of film to reach the desired speed, and the remaining 60 *ft* provide 0.4 seconds of useful recording at 5000 *fps*. To achieve synchronization, a triggering circuit has been added to the facility. The combustor is brought to its unstable mode and data acquisition started. As soon as the camera reaches the preset constant speed, it sends a signal to the controlling workstation that starts operating the injectors in order to achieve transition to the stable mode. This event takes place in a time of the order of milliseconds, and hence the camera has enough time to record the complete event in a single run.

The control software has been developed using Sparrow (Murray, 1995), and it allows real time data acquisition and analysis. Analog signals are acquired using a 16 channel A/D converter board model CIO-DAS 1600. The sampling frequency used in this investigation was 2000 *Hz*.

The feedback control law is based on the pressure signal: whenever amplitude of the pressure oscillations in the combustion chamber reaches a defined threshold, the pilot fuel injectors are opened for a defined amount of time. The parameters of the system are: threshold pressure, duration of the pulse, phase between triggering and pulse, pressure in the pilot fuel line.

5.1.2 Experimental Observations

As mentioned above, the transition is driven by the pulsed injection of a small amount of gas near the dump plane.

For a given fuel, the main parameters in the control law are: injection port, flow rate, length of the pilot fuel pulse and pressure threshold used to trigger the action. Experiments show that both injection ports are effective for control; the pulse duration is not critical as long as it doesn't reach the `blow-out' limit: long (more than 0.1 s) continuous injection of pilot fuel causes the flame to be blown out of the combustion chamber. Also the pressure threshold (i.e., the minimum amplitude of pressure oscillation required to trigger the control action) does not have a major role: its sole purpose is to distinguish between 'unstable' and stable burning. The combination of pulse duration and threshold value sets, as a consequence, the number of pulses required to obtain the transition (in general, the shorter the pulse - with fixed threshold - the more pulses are required).

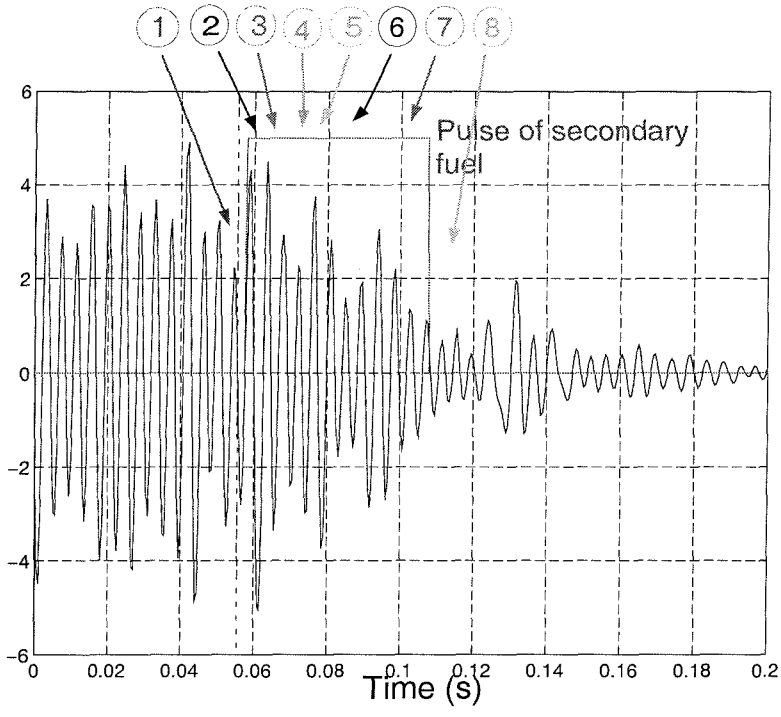

Figure 5.7. Typical control run, pulse duration: 50 ms (pressure oscillations in psig).

Figure 5.7 presents the typical output of a controlled run of the combustor. Triggering time and position of the injectors are marked in the figure; pressure oscillations are plotted in *psig*. During the opening time of the injectors, methane is injected into the recirculation zone downstream of the step. In this combustor, 50 ms is the minimum opening time required to achieve control with a single pulse. The data of Figure 5.7 correspond to the shadowgraph pictures presented in Figure 5.8 (1)-(8). The premixed flow enters the chamber at the top left of the picture; the geometry of the system is presented in Figure 5.2.

These pictures are taken from a high-speed movie (shot at 5000 frames per second) that clearly shows that a large scale recirculation zone, nonexistent in either of the two steady burning modes, dominates the flowfield during transition and appears to be the major driving force enabling the control. In stable burning, the recirculation zone is limited to a small section of the upper part of the combustion chamber, cf. Figure 5.8-(8). During 'unstable' burning, the large vortex shedding,

Figure 5.8 (1), produces a recirculation zone which extends 20 cm downstream of the step and occupies the whole height of the chamber.

(1)

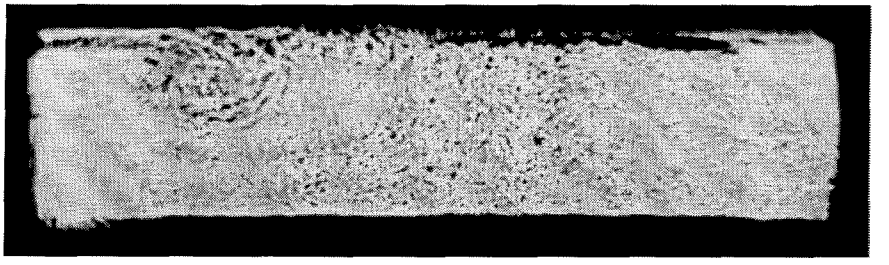

(2)

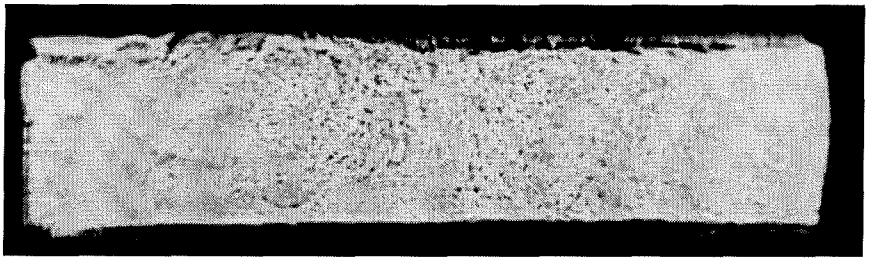

(3)

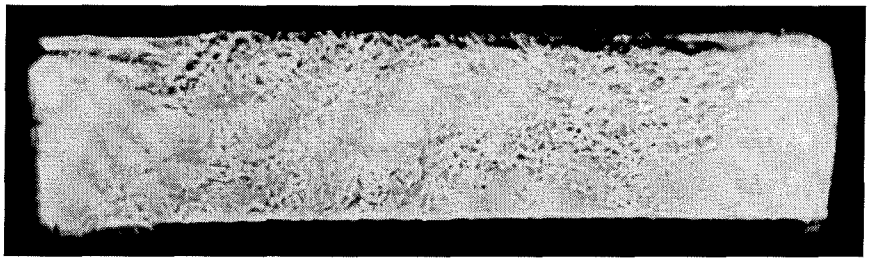

(4)

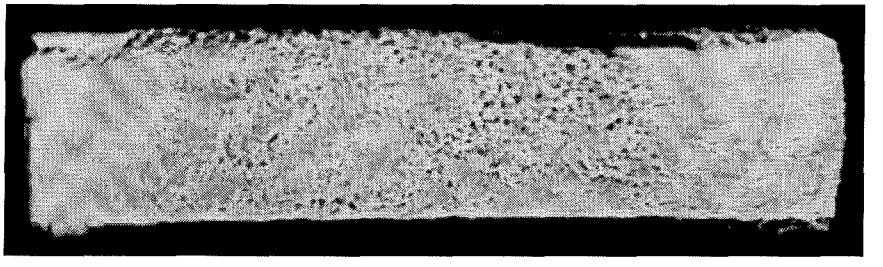

(5)

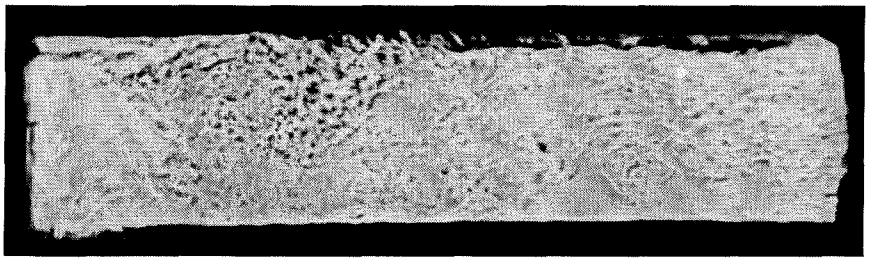

(6)

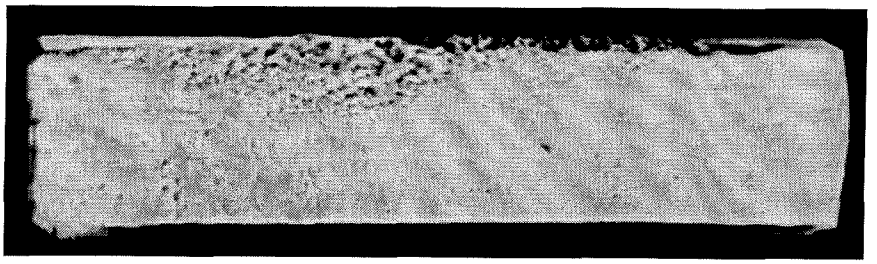

(7)

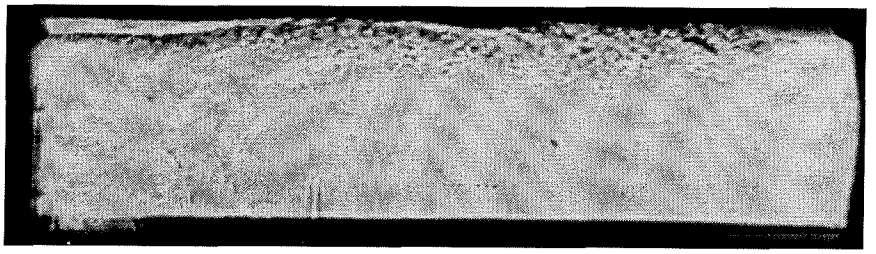

(8)

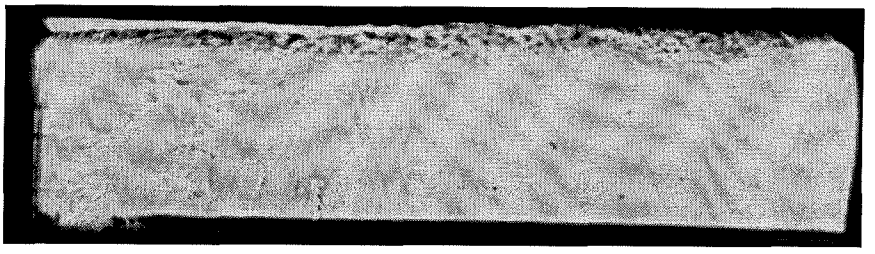

Figure 5.8. Behavior of the flow near the step during a *transition* from the unstable mode to the stable mode.

The pulse of injected fuel begins at t=0. (1) **t = -3 ms: Start in the unstable burning mode: large vortex shedding.** (2) **t = 0: Injection of secondary fuel.** (3) **t = 1.4 ms: The next vortex still forms but is not allowed to develop fully.** (4) **t = 8 ms: Instead, a recirculation zone appears next to the dump plane.** (5) **t = 14 ms: The recirculation zone is now occupying all the chamber.** (6) **t = 18 ms: The strength of the recirculation is fading and the size is shrinking.** (7)-(8) **t = 30 ms, 56 ms: The last disturbances get 'washed' away, the recirculation zone has disappeared and the combustor will eventually reach the state of stable burning where only a turbulent burning boundary layer can be seen.**

Note that Figure 5.8-(7) and (8) show a clear example of a wall jet developing along the upper surface of the combustion chamber.

Stabilizing the motions has also been achieved by injecting nitrogen into the recirculation zone. It is not clear whether the same effect can be achieved by injection into the shear layer. Contrary to methane injection, successful control seems to be very sensitive to the amount, and possibly the phase, of nitrogen injection. It should be noted that, while with fuel the repeatability of the control is high (100% over more than 40 runs of the combustor), with nitrogen the rate of success is much lower (about 45%).

It has also been noted that the presence of water droplets in the bottom of the combustion chamber reduces, or even prevents, the instability in the combustor.

5.1.3 Discussion of Experimental Observations

In this investigation active control has been used to stimulate transition from an unstable state of a combustor to a stable state:

- Control can be achieved by a simple feedback-loop monitoring the pressure oscillations in the combustion chamber. The injection of pilot fuel need not take place at the same frequency as the pressure oscillations; a pulse, extended over several periods of the pressure oscillations (see Figure 5.7), is sufficient.
- Control by injection of secondary fuel over several periods of the oscillation has also been reported by Richards et al. (1995) using entirely different apparatus. The character of those results suggests that the mechanism is not that established here.
- The number of pulses needed to achieve control depends strongly on the length of the pulses. Very long pulses (0.1 s for the combustor studied here) blow the flame out and can not be used. On the other hand, very short pulses appear to be less effective than the pulse of the minimum duration required to achieve control with a single pulse, i.e., the

sum of the duration of the multiple pulses normally is higher than the minimum single pulse length.

- The flowrate of pilot fuel needed to stimulate the transition is substantial. Contrary to Knoop et al. (1996), we find that the amount of fuel needed to achieve control is approximately 25% of the primary fuel flow rate; the actual mass of injected fuel is nevertheless low, due to the very short duration of the pulse. However, there is a significant uncertainty due to the difficulty of measuring low flow rates on such a short time scale.
- The possibility of control with nitrogen suggests that the action is partly dependent on the flow-field modification induced by the pilot gas *blowing*. However, the low effectiveness of the control with nitrogen, and the stabilizing effect of the presence of liquid water in the chamber, indicate that the mechanism related to the energy transfer between the fluid present in the combustion chamber and the fresh mixture coming into the combustor is the dominant one.

Several high-speed shadowgraphs of the transition have been recorded. The most distinguishing features of the transition are

- The flowfield changes completely during the transition phase. It is neither dominated by the large vortex shedding of the unstable state nor by the turbulent boundary layer of the stable mode. Instead a large recirculation zone occupying the entire combustion chamber appears. On the time-scale of the whole transition process, this large-scale recirculation is dominant for approximately one-fifth of the total duration.

The transition is extremely fast: barely a dozen cycles of the pressure oscillations are enough for the combustor to become stable; the same is true for the onset of the limit cycle, when the critical value of ϕ along the lower branch of the hysteresis cycle is reached (cf. Figure 5.5).

5.1.4 Conclusions

The possibility of initiating and controlling the transition from 'unstable' to stable burning through the injection of pilot fuel into the combustor has been thoroughly confirmed with several experiments, under a wide set of different operating conditions.

Two different mechanisms seem to be participating in the transition: one is the perturbation of the local energy balance; the other is the perturbation of the flow field due to the blowing of the secondary fuel. Experimental observations suggest that the first mechanism is by far the most significant. An important feature is that both the addition and removal of energy in the recirculating gas, if persistent for sufficient time, are able to drive the transition to the stable state. The required time (cf. Figure 5.7) is about 50 ms, whereas the period of shedding large vortices is about 4.3 ms: the fuel pulse covers 8-10 cycles.

The sequence of shadowgraph images of the transition shows that a distinctive feature of the process is the presence, for a substantial time, of a large recirculation area, occupying the whole combustor: that feature is not present in neither of the two 'stationary' modes, characterized by large vortex shedding (the 'unstable' mode) and a small turbulent burning layer (stable mode).

How general the existence of hysteresis is in combustors remains a matter to be investigated: the geometry has been fixed in all these tests. Moreover, at least three additional significant questions are raised, and not answered by these results:

- How significant is the purely fluid dynamic effect of injecting pulses of secondary fuel or nitrogen?
- What determines the required length of the pulses and why must they last for several cycles of the oscillation?

- What conditions must be met to ensure that the injected pulses do not cause a perturbed state that simply decays to the initial oscillation or limit cycle, but do cause the desired transition?

6 Concluding Remarks

The present work describes a framework to perform the analysis and simulation of the dynamics of an actively controlled combustion chamber with a detailed description of a model for the combustion of solid propellant, including the dynamics of the solid phase, surface layer and gas phase.

Different coupling mechanisms between combustor and propellant have been analyzed, as well as different models for the propellant. The purpose of the analysis is both to establish a framework to identify the possible sources of the observed sensitivity of chamber dynamics to propellant characteristics.

We also show that the same framework can be extended to include active control. Detailed analysis of some of the principal issues regarding control are described elsewhere (Seywert 2001). This work concentrates on some issues regarding the compensation of time delay in an unstable system and a short overview of the sensors and actuator models currently used in combustion literature.

Some experimental results are presented for the case of a dump combustor, where we analyze a possible control scheme and show experimental evidence of the mechanisms responsible for some of the dynamics observed in the combustor.

The effect of the dynamics of the surface layer on the chamber dynamics was previously neglected. Here we analyze two simple models representing the dynamics of the surface layer.

One simply adds a time lag to the conventional quasi-steady theory, and the other introduces a layer with different properties.

The time lag model gives rise to a combustion response function that presents several peaks, and hence it is not very realistic. The peaks could be eliminated by choosing a time lag dependent on frequency (Grad 1949), but that choice does not have a physical justification and it reduces the model to curve fitting with experimental data. Also this model does not add any significant behavior to the dynamics observed when using the traditional quasi steady approach.

With the second model, the effect of the surface layer on the combustion response function can be summarized in the reduction of the peak induced by the solid phase, and in the appearance of another peak (of higher absolute value) at higher frequency, due to the response of the surface layer to the heat feedback from the combustion zone. The relative density of the surface layer seems to have an effect on the response function that is larger than that of the activation energy and the other parameters describing the characteristics of the surface layer.

The combustion model is applied to an example computation of the dynamics of a rocket motor, to show the effect of the combustion response function on the dynamics of the system. For the examples chosen here, the waveforms in the limit cycles are similar whether or not dynamics of the surface layer and gas phase are accounted for. This is a consequence of the heavy damping in the higher harmonics introduced by the model used and of the coupling mechanism between combustion and combustor (pressure coupling).

In general, models based on pressure coupling do not show a dramatic sensitivity of the propellant response to changes in composition, especially when compared with the introduction of a second coupling mechanism, based on velocity coupling between combustion and the velocity parallel to the propellant grain.

The results of the simulations including velocity coupling suggest that unsteady surface combustion responsive to velocity fluctuations parallel to the surface leads to a combustion dynamics sensitive to small compositional changes in the propellant.

We also show that particle damping is in effect an important factor in the simulations; changes in composition of the propellant that would lead to changes in the size (or distribution of sizes) of the condensed material after burning will have a great effect on the global dynamics of the chamber. This is an important point and must be kept into consideration when detailed simulation of combustion chambers is performed.

Regarding the sensitivity of the chamber dynamics, results can be categorized within two groups: sensitivity of the propellant characteristics, analyzed through its effect on the combustion response function, and sensitivity of the coupling mechanism between propellant and chamber dynamics.

Regarding the propellant sensitivity, within the quasi steady theory, propellants exhibit a high sensitivity to small variations in their parameters only when close to the intrinsic stability limit. Even though potentially this mechanism could give rise to very sensible variations in the response functions, it is unlikely to be the one responsible for the behavior observed experimentally, since common propellants are mixed to stay away from intrinsic instabilities, and hence this mechanism does not commonly appear in practice.

If we abandon the quasi steady approximation and include gas phase dynamics, we observe a response of the propellant at higher frequency than the QS predictions; this corresponds to some of the experimental data available (see Baum et al. 1982) and hence it is a better model for the propellant combustion, but still it does not justify any stronger sensitivity. The introduction of the dynamics of the surface layer, beside considering solid phase and gas phase, adds a sensitivity of

the propellant response function to the characteristic of the surface layer itself, and hence to the propellant composition.

Regarding the second mechanism, i.e., the coupling between propellant and combustion chamber, we can summarize the results as follows. The traditional coupling mechanism, based on pressure, does not show the capability of justifying a high sensitivity of chamber dynamics on propellant characteristics. Simulations show that, even with large variations in the combustion response function, the chamber dynamics is not strongly affected. On the other hand, the introduction of velocity coupling, i.e., a dependence of the combustion response also on the velocity parallel to the propellant grain, introduces a path for a more direct connection between chamber and propellant dynamics. It also introduces the possibility of explaining some observed dynamics (like triggering) without recurring to excessively high values for the combustion response function.

Some further sensitivity is also introduced by the consideration of a realistic particle size distribution; this results in less damping of the higher frequency modes, which are also subjected to more excitation than previously considered because of the presence of surface and gas phase dynamics that contribute to the response at high frequency.

Regarding active control, we analyzed the possibility of time delay compensation. We observe that inclusion of the time delay in the modern design framework as an uncertainty is adequate when the time-delay is of the same order of the characteristic time of the instability, defined as the inverse of the frequency of the unstable mode. Cases with longer time delays, as it might be the case in full scale combustors, can be treated by adding a second loop to compensate for the delay: simulation shows very good performance, but issues about robustness to uncertainty and perturbation need to be addressed carefully. Since a good model of the system is needed to perform the prediction, performance degrades rapidly if the time delay is long (unless the model

is perfect) or if the model is not very accurate. Some degree of capability to adapt on line might be needed for application to real systems.

The experimental results presented confirm the possibility of initiating and controlling the transition from 'unstable' to stable burning through the injection of pilot fuel into our laboratory combustor.

Two different mechanisms seem to be participating in the transition: one is the perturbation of the local energy balance; the other is the perturbation of the flow field due to the blowing of the secondary fuel. Experimental observations suggest that the first mechanism is by far the most significant. An important feature is that both the addition and removal of energy in the recirculating gas, if persistent for sufficient time, are able to drive the transition to the stable state. The required time is about 50 ms, whereas the period of shedding large vortices is about 4.3 ms: the fuel pulse covers 8-10 cycles.

A distinctive feature of the process is the presence, for a substantial time, of a large recirculation area, occupying the whole combustor: that feature is not present in neither of the two 'stationary' modes, characterized by large vortex shedding (the 'unstable' mode) and a small turbulent burning layer (stable mode).

Future Directions

Several interesting questions are posed and left unanswered by the current work. These are some of the possible future developments that will greatly contribute to their answer.

We have shown that the combustion response function for a solid propellant shows a large amplitude at a frequency higher than the one predicted by quasi steady theory. Unfortunately experimental data in a useful range of frequencies are very scarce and carry large uncertainties. To that purpose we are currently proposing a new experimental method, based on LDV

measurement, that will hopefully enable us to perform accurate (and direct) measurements of the response for a large range of frequencies.

Regarding solid propellant, more work is needed in the modeling and experimental characterization of the surface layer. More analysis is also required regarding velocity coupling: it would be very helpful to have experimental results to validate our hypotheses.

Regarding control, we are at a point where there is a need of experimental validation of the methods we describe and propose. Some work is being currently done to this purpose.

The dump combustor experiment also leaves some questions open; particularly important is to obtain a quantitative theory to explain and justify the experimental observation.

Appendix A Dynamical Systems and Continuation Method (AUTO)

Dynamical systems theory provides a systematic approach to study the behavior of systems described by differential equations. This method was first applied to the study of combustion instabilities by Jahnke and Culick 1993, and it allows for determining regions of similar dynamic behavior of the solution of the approximate system of differential equations describing the combustion chamber.

As outlined in chapter 2, the acoustic equations, including combustion and, if present, control and actuation, can be written in the form (2.27), i.e., as a system of first order differential equations:

(A.1)
$$\frac{d\mathbf{x}}{dt} = f(\mathbf{x}, \mu)$$

Where $\boldsymbol{x}$ is the vector describing the system and μ is a parameter of interest.

For a moment, we consider the value of the parameter as given; the study of the dynamics of such a system starts with the determination of the steady states, defined by simply setting the derivatives to zero. In the general case, determination of the steady states (since the system is non linear) might not be trivial. In our case, since the equations for the combustion chamber describe the amplitude of an oscillation over a mean value, subtracted from the equations, we have the advantage of knowing that $\boldsymbol{x} = 0$ is always a physical steady state that the system will exhibit.

The next step consists in studying the local stability of the steady state: for this purpose, the linearization theorem (Hartman-Grobman, Wiggins 1996) establishes that the flow (i.e., the solution) generated by (A1.1) is $\mathbf{C}^0$ conjugate to the flow generated by the linearized system, provided that the Jacobian of the system has no eigenvalues on the imaginary axis. This means that we are allowed to simply consider the eigenvalues of the linearized system to draw

conclusions regarding the original non linear system. This is the basis for the validity of linear stability analysis.

When the eigenvalues have a vanishing real part, the system might undergo a qualitative change in its dynamics; cases where this happens are called bifurcations, and the value of the parameter for which this happens is called bifurcation point (Strogatz 1994). A typical example of a simple system exhibiting a bifurcation is the instability of a beam loaded in compression: the control parameter in this case is the value of the compressive load.

The most common bifurcations encountered in the case of combustion systems are the Hopf and the turning point bifurcation, which are characterized, respectively, by the presence of a pair of imaginary eigenvalues and a non null Jacobian and a point for which the gradient of the parameter with respect to x changes sign.

Bifurcation diagrams are created using a program (XPPAUT) based on AUTO, a package developed by Doedel, and based on the continuation method developed by Keller and Doedel.

The software package XPPAUT, by Ermentrout 1998, allows to numerically integrate differential systems in time domain, determine nullclines, direction fields and analyze phase plots. It also includes a continuation package based on AUTO.

The continuation method is based on the use of the implicit function theorem, which determines that the solutions of a continuously differentiable system are continuous functions of the parameters. This fact allows the program to "continue" a steady state for incremental values of a chosen parameter. During the continuation, the eigenvalues of the Jacobian are computed at every step, thus allowing AUTO to identify the stability characteristics of the solution, and to identify possible branches following a bifurcation.

AUTO is also capable of continuing periodic solutions: in order to do this, a procedure similar to the construction of a Poincarè map is applied (Wiggins 1996). The periodic solution is discretized in time and continuation is performed as if it were a steady state. The effectiveness of this method

depends critically on the accuracy of the estimate of the period: this is the source of the difficulties described by Burnley 1996 when starting a continuation from a periodic solution.

The nature of bifurcations arising from periodic orbits is determined by using Floquet multipliers (Guckenheimer and Holmes, 1983); namely, the number of multiplier with unitary modulus determine the type of bifurcation. The limit cycles will be stable only if all the other multipliers have absolute value less than 1.

Floquet theory is based on the construction of a matrix called "fundamental solution matrix" of the system.

Given a differential system:

(A.2) $$\mathbf{V}' = \mathbf{F}(\mathbf{V})$$

that has a periodic solution $\mathbf{V}(t)$ with period T, its stability can be studied by looking at the perturbation

(A.3) $$\mathbf{v}(t) = \mathbf{V}(t) + \mathbf{w}(t)$$

where $\mathbf{w}(t)$ is small. It can be shown (Levinson and Coddington 1955) that the evolution of $\mathbf{w}(t)$ is determined by the linear system of equations:

(A.4) $$\mathbf{w}' = \mathbf{A}(t)\mathbf{w}$$

where $\mathbf{A}$ is periodic of the same period of $\mathbf{V}$. The solution of (A.4) can be arranged as vectors in a matrix $\mathbf{Y}(t)$, called the *fundamental solution matrix*. Two important properties of this matrix are:

(A.5) $$\begin{aligned} \mathbf{Y}(t+T) &= \mathbf{Y}(t)\mathbf{K} \\ \mathbf{Y}(nT) &= \mathbf{Y}^n(T) \end{aligned}$$

where $\mathbf{K}$ is a constant matrix. For proofs and other properties of this matrix, see, for example, Levinson and Coddington 1955.

The eigenvalues (λ_i) of this matrix are called Floquet multipliers. If we denote the corresponding eigenvectors with the symbol $\mathbf{X_i}$, the solutions of (A.4) can be written as

(A.6) $$\mathbf{w}(t) = \mathbf{Y}(t) \cdot \mathbf{X}$$

We can now study the stability of the solution $\mathbf{w}(t)$, that, according to equation (A.3), represents the perturbation to the periodic solution of the original differential system;

(A.7) $$\mathbf{w}(t + nT) = \mathbf{Y}(t + nT) \cdot \mathbf{X} = \lambda^n \mathbf{Y}(t) \cdot \mathbf{X}$$

Hence, if $|\lambda| > 1$ then as $t \to \infty$, $\mathbf{w}(t) \to \infty$ and the periodic solution $\mathbf{V}(t)$ is unstable; on the other hand, if $|\lambda| < 1$, then the solution is stable.

Appendix B

In this appendix, we report the expression of the temperature gradient boundary condition for the case of the model of the burning of a solid propellant with the presence of a surface layer with different physical properties. This corresponds to the term $F(\Omega)$ in equation (3.40).

We start from the energy equation for the temperature in the surface layer, expressed by equation (3.36). The general solution for the oscillating temperature at position x within the layer is given by solving the equation assuming oscillating solutions and the appropriate boundary conditions at the two sides (see chapter 3.1.3 for more details). The solution is

(B.1)
$$\hat{T}(x) = \hat{T}(x_1)\left\{\left[\Xi + \chi_l\right]\Theta e^{\frac{1+\sqrt{1+4\chi_l\rho_l i\Omega}}{2\chi_l}x} + \Theta e^{\frac{1-\sqrt{1+4\chi_l\rho_l i\Omega}}{2\chi_l}x} - \frac{\Psi_l}{i\Omega\rho_l}e^{\frac{x}{\chi_l}}\right\} \quad (0 \le x \le x_l)$$

where:

(B.2)
$$\Psi_l = \frac{E_l}{\overline{T}_l^2}\frac{\overline{T}_l - \overline{T}_s}{\chi_l}$$
$$\Xi = 1 + \frac{1}{i\Omega\rho_l}\Psi_l$$
$$\Theta = \frac{K(\Omega) + \frac{\Psi_l}{i\Omega\rho_l} - \frac{1+\sqrt{1+4\chi_l\rho_l i\Omega}}{2\chi_l}(\Xi)}{\sqrt{1+4\chi_l\rho_l i\Omega}}$$

and

(B.3)

$$K(\Omega)=\frac{1}{i\Omega\rho_c\chi_l}\left[(i\Omega\rho_c+\Psi)\frac{1+\sqrt{1+4\chi_c i\Omega\rho_c}}{2\chi_c}-\frac{\Psi}{\chi_c}+i\Omega\rho_c\frac{E_s}{\overline{T}_s^2}L_c\chi_l\right]$$

$$\Psi=\frac{E_c}{\overline{T}_1^2}\frac{\overline{T}_1-T_0}{\chi_c}$$

This last expression derives from consideration of the solid boundary, equation (3.11). Considering the unsteady energy balance at the boundary between liquid layer and gas zone (boundary 1), we have

(B.4)

$$\left.\frac{d\hat{T}}{dx}\right|_{x_1^+}=\frac{1}{\chi_g}\left.\frac{d\hat{T}}{dx}\right|_{x_1^-}+E_l\frac{\hat{T}(x_0)}{\overline{T}_1^2}L_l$$

We can now substitute expression (B.1) into (B.4) to obtain the required relation:

(B.5)

$$\left.\frac{d\hat{T}}{dx}\right|_{x_1}=\frac{\hat{T}(x_1)}{\chi_l\chi_g}\left\{\frac{1+\sqrt{1+i4\chi_l\rho\Omega}}{2}\left[\Xi+\chi_l\Theta\right]e^{\frac{1+\sqrt{1+4\chi_l\rho i\Omega}}{2\chi_l}x_1}+\frac{1-\sqrt{1+4\chi_l\rho i\Omega}}{2}\Theta e^{\frac{1-\sqrt{1+4\chi_l\rho i\Omega}}{2\chi_l}x_1}\right.$$

$$\left.-\frac{\Psi_l}{i\Omega\rho_l}e^{\frac{x_1}{\chi_l}}+\chi_l\chi_g\frac{E_s}{\overline{T}_s^2}\frac{\hat{T}(0)}{\hat{T}(x_1)}L_l\right\}=F(\Omega)\hat{T}(x_1)$$

Note that if we let the surface layer vanish, $\Psi_l\to 0$, $\Xi\to 1$, $\Theta\to K(\Omega)-\frac{1}{\chi_l}$, and hence expression (B.5) reduces to the form (3.11) that includes only the surface dynamics.

Appendix C

Combustor and propellant data used in the examples reported in the previous chapters.

Geometrical Properties

Combustor length	$L = 0.60\ m$
Combustor radius	$r_c = 0.025\ m$

Characteristics and geometrical configuration of the sensors/actuators for control are specified case by case.

Combustion Properties

Mean pressure	$\overline{p} = 1.06 \times 10^7\ Pa$
Linear burning rate	$\overline{r}_b = 0.0078\left(\frac{\overline{p}}{3.0 \times 10^6}\right)^{0.3} m/s = 0.01145 m/s$
Flame temperature	$\overline{T} = 3540K$
Non dimensional prop. temperature	$\overline{T}_s = 0.15$
Non dimensional surf. temperature	$\overline{T}_s = 0.35$
Mass particles/mass gas	0.36
Particle diameter	$\sigma = 2 \times 10^{-6}\ m$

Parameters in the combustion response for quasi-steady response are specified case by case.

Propellant and Gas Physical Properties

Thermal diffusivity of

propellant	$\kappa_p = 1.0 \times 10^{-7}\, m^2/s$
Specific heat (gas)	$C_p = 2020 J/Kg\ K$
Specific heat (cond.)	$C = 1400 J/Kg\ K$
Viscosity	$\mu = 8.925 \times 10^{-5}\, Kg/m\ s$
Particle density	$4 \times 10^3\, Kg/m^3$
Propellant density	$1750\, Kg/m^3$
Gas density	$7.97\, Kg/m^3$
Mixture specific heat ratio	$\bar{\gamma} = 1.18$
Gas constant	$R = 377.8 J/Kg\ K$

Other characteristics are listed in Table 3-2.

Appendix D Review of Published Work about Dynamics and Control of Combustion Processes at Georgia Institute of Technology

The Jet Propulsion Center has an ongoing effort to review the work of research groups in other universities on the subject of control of combustion instabilities. The report on the work done at Georgia Institute of Technology is included in this appendix. Other reviews describe the combustion control work done at Cambridge University, included in Poncia 1998, and Massachusetts Institute of Technology, included in Seywert 2001.

D.1 Introduction

Modeling and control of combustion instabilities in various systems has been investigated at the Georgia Institute of Technology in the last twelve-fifteen years, mainly by the group of B. T. Zinn.

The activity started in the late eighties with experimental investigation of the instability in ramjet combustors. With the advent of Y. Neumeier in the group (1991-1992), the interest shifted towards numerical and analytical modeling, and development of simple control schemes based on a nonlinear observer. More recently (1996-1999) the interest moved towards modern control and the investigation of the effect of the equivalence ratio oscillations on the driving of the instability and emission of NO_x.

From the published work, it seems quite evident that no specific coherent program for the investigation of control of combustion instability was carried on during these years. Control was

often introduced as a side effort in the main investigation regarding the mechanism of the instabilities. As a result, control approaches are tailored to the particular case and often there is no consideration toward the extension of the control strategy to a wide range of operating conditions or different scale problems.

This appendix presents a thorough review of the work published on modeling and control of combustion instabilities by the group at Georgia Institute of Technology. The review is divided in two parts: the first section is a description of some work done between 1990 and 1994-95; the second part is an analysis of more recent studies (1996-1999). Some general comments are made at the end the last section.

The early work was mostly experimental and dealt with ramjet combustors (Hegde, Reuter, Daniel, Zinn 1987). In this part, the main interest was in gathering data and modeling the acoustics of the system (Hegde, Reuter, Zinn 1988, 1990). The first application of a control system is described by Menon and Yang (1993) and tested on a numerical experiment. The interest of the authors is not in the control strategy (they use a simple proportional law), but in trying to develop a low order model that can reproduce the system behavior correctly.

With Neumeier, Zinn and Jagoda 1993, the more analytical part of the work starts: the interest is now in the modeling from first principles and analysis of different control strategies. The group declared goal is to develop an adaptive controller based on secondary fuel injection (Zinn, Daniel, Neumeier 1994): this is considered the most viable solution for real systems.

In Neumeier, Zinn (1996b) and Neumeier, Markopoulos, Zinn (1997), the authors describe an interesting control strategy, based on a non-linear observer (that follows the most-unstable mode) and (simple) linear control. The controller is tested on numerical examples and shows very good performance, even though many questions are left unanswered, especially regarding the performance of the controller on a real system, with noise and perturbations.

Neumeier, Nabi, Arbel, Vertzbeger, Zinn (1997) contains an interesting characterization of a fuel injector, from a "control" point of view: the data provided there can be used to implement a simulation using the experimentally derived characteristic of such an injector.

A change of perspective comes with Haddad, Leonessa, Corrado, Kapila (1997), written by a group in the control department of Georgia Tech, with the collaboration of Dr. Zinn and Dr. Neumeier. A complete design (tested on numerical examples) of a robust controller is presented, with noise and perturbation added to the system. The system and the controller are linear, and a speaker is used as actuator.

As said before, it is not easy to trace a unitary path followed through the years in the control studies: it is more a collection of trials in different directions, starting from a common interest: combustion instabilities.

D.2 Early Work

There are a few works published around 1990 related to control of combustion: the main theme of the research is the investigation of instabilities (mostly longitudinal) in dump type ramjet combustors. Both experimental and theoretical analysis has been performed as part of this investigation. Figure D.1 (from Hegde et al. 1987) presents a schematic of the experimental apparatus developed for these studies. A mixture of air and propane is introduced into the combustor through the injector, built in sintered stainless steel; the flame is stabilized in the combustor section (7.5 *cm* x 5 cm^2) on a 0.8 *mm* diameter nichrome wire. A fine wire mesh grid is located 8 *cm* upstream of the stabilizing wire and acts as a flame arrestor in case of a flashback. The exhaust section is equipped with two acoustic drivers, used to excite a standing acoustic wave of desired amplitude and frequency in the system. The injector can be moved axially so that the stabilizing wire can be placed on any part of the standing wave; the maximum length of the apparatus is 3 *m*. Pressure and temperature are measured along the combustor walls (water

cooled); space-time resolved measurements of *CH* species radiation also allows quantitative measurement of the reaction rate and hence of the heat release.

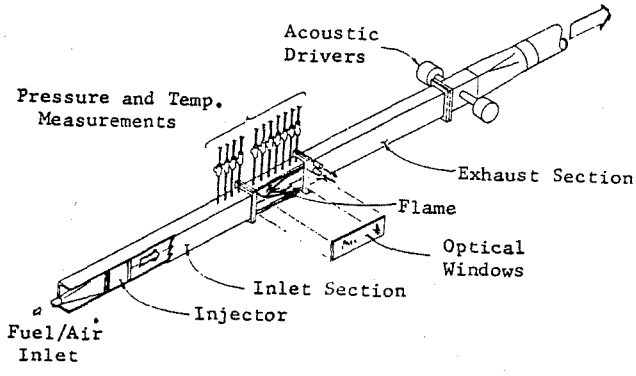

Figure D.1. Experimental apparatus (from Hegde et al. 1987).

The acoustic behavior of the set-up was tested in cold flow conditions, and the authors determined that the system behaves like a closed-open organ pipe, *i.e,*. the injector side behaves like a closed end (Hegde et al. 1987).

Experiments conducted in this facility reveal the presence of a spontaneous instability of the first acoustic mode (the quarter wave mode). The flame is stable when close to the lean flammability limit, becomes unstable when increasing the fuel fraction and then stable again when the fuel fraction is further increased, approaching the rich flammability limit. In a region around unitary stoichiometric ratio, the flame is "blown-back" from the wire to the screen placed upstream, and returns to the wire when operating in the fuel rich region. The instability is characterized by an increase in the amplitude of the fundamental acoustic mode; pressure in the chamber reaches levels of 140-150 *dB*, when the flame is back onto the screen. The instability, however, starts with the flame still stabilized on the wire, and the results reported refer to experiments conducted with the flame on the wire.

The presence of the instability is explained through an experimental investigation of the characteristics of the flow behind the flameholder (Hegde et al. 1987), conducted by measuring heat release and pressure (magnitude and phase) and a series of shadowgraph images.

Rayleigh's criterion can be written in a form suitable for flame driving:

(D.1)
$$\int_{flame} |S_{pq}| \cos \vartheta_{pq} dV > 0 \quad \textbf{(for driving)}$$

Where S_{pq} is the cross-spectrum between pressure and heat release, ϑ_{pq} is the phase between the unsteady heat release and the pressure and the integral is performed over the flame volume.

By calculating the integral (D.1) with the experimental data, the presence of the instability at the fundamental frequency is justified.

The main characteristic of the flow field in this combustor is the presence of a small recirculation zone behind the wire that acts as a flameholder and the periodic shedding of burning vortices behind it. This feature is clearly visualized by shadowgraph images and inferred through *CH* measurements (Hegde et al. 1987).

External forcing was also applied by the acoustic drivers (see Figure D.1), with acoustic excitation driving a harmonic, a sub-harmonic or a random frequency. Note that the combustor presents a spontaneous instability, and the acoustic driving at different frequencies was only used to study its effect on frequency and characteristics of the vortex shedding from the flameholder; no control of the instability is attempted.

Results show that the frequency of the vortex shedding is not affected by the external excitation frequency (it remains at the first natural frequency). The propagation velocity of the vortices (computed from the shadowgraph film and the phase of the CH emissions) is also unaffected by the external driving.

The authors found that only in a small region behind the flame holder (the "near wake region," about *5* flameholder diameters long) the heat release spectrum is dominated by a component at the external driving frequency (especially evident for frequencies in the range 200-500 *Hz*, compared to a natural frequency of 80 *Hz*).

The amplitude of the forcing is not specified: it might be that the acoustic forcing was too weak to have any other significant effect, when compared to the dominant first mode instability reaching peaks of 130 *dB* in the conditions at which the experiments where conducted.

Two conclusions can be drawn from this work:

1. The interaction between fluid mechanical instability of the flame and acoustic field provides a mechanism (vortex shedding at the flameholder) for driving longitudinal mode instability.
2. The fact that external driving affects the recirculation region in the wake of the flameholder might offer a way of controlling the instability by disrupting the vortices (non-linear control).

Two later works (Hegde et al. 1988, 1990) introduce some comparisons between theoretical models and the experiment just described.

The first (Hgde et al. 1988) develops a theory for predicting the sound generated by a flame in an enclosed duct.

The model assumes a rectangular duct, premixed reactants, small (zero) Mach number of the mean flow, and a given axial temperature profile. By expanding the flow variables in mean and fluctuating part, and assuming small fluctuations, a wave equation for the pressure is derived:

(D.2)
$$\nabla \cdot \left(\overline{T} \nabla p'\right) - \frac{\overline{T}}{a^2} \frac{\partial^2 p'}{\partial t^2} = -\frac{1}{C_p} \frac{\partial q'}{\partial t}$$

Where $\overline{T}$ is the average temperature, p' and q' are the unsteady pressure and heat release; C_p is the specific heat at constant pressure, a is the speed of sound.

The derivation makes use of the equation of state for a perfect gas, and takes into account the heat release from the combustion process (q') and the spatial variations of temperature.

Equation (D.2) is solved under the hypothesis of harmonic longitudinal motion in the case when the length of the combustion zone is small compared to the acoustic wavelength. The solution yields the pressure amplitude at a certain frequency (p_ω) as a function of the heat release (q_ω),

wall losses, acoustic impedance at the boundaries and geometry of the system (see Hegde et al. 1988 for details):

(D.3)
$$p_\omega(x) = \frac{i\omega q_\omega(L_1)G(x,L_1)}{C_p}$$

Where G is the appropriate Green's function satisfying the wave equation, boundary and jump condition across the discontinuity at the flame position (L_1). For the results presented in Hegde et al. 1988, the temperature is assumed to be the cold gas temperature up to the flame, and the flame temperature from the flame location on.

This model applies directly to the experimental setup presented in Figure D.1; in order to compare the results for the pressure spectra, unknown coefficients (like wall losses) were determined via a "best fit" method between data and theoretical prediction, and kept fixed during successive runs of the combustor.

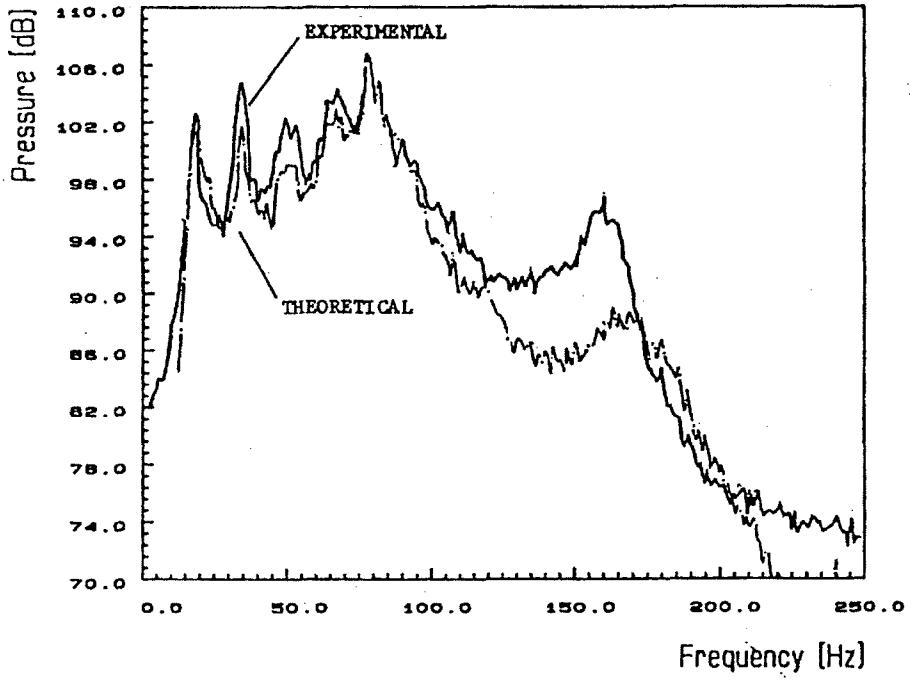

Figure D.2. Comparison of experimental and theoretical pressure spectra (from Hegde et al. 1988).

Figure D.2 presents a comparison between theoretical prediction and experimental pressure spectrum, and shows a very good agreement. This is actually not surprising, since:

- the position of the peaks defines the natural (longitudinal) acoustic modes, and these are almost exclusively functions of the geometry and are not much affected by the flame zone (this is one of the results of Hegde et al. 1987);
- the spectra of the heat release, which affects directly the pressure spectra -see equation (D.3)- is actually measured from the experiment and used into the theoretical solution: no dynamical modeling of the flame is done;
- the amplitude of the predicted oscillations is adjusted via a preliminary "best fit" evaluation of coefficients appearing in the formulation.

In any case, the main result is the agreement between the model and the experiment. The claim of the authors that "a theoretical model capable of predicting the sound generated by confined flames" has been developed is excessive: the model by itself only predicts the frequency of the natural longitudinal modes (in a simple rectangular duct). It does not include any flow-field effect caused by the flame, it does not have any flame dynamics, and relies on the measurement of the complete heat release spectrum from the system that should be predicted. This poses a severe limitation on the utility of the study. It might be more useful as an inverse method: to back up coefficients from the experiment (wall loss coefficients), to determine the heat release spectrum from the measured pressure spectrum, or to use as a model for simple numerical experiments.

A third paper (Hegde et al. 1990) investigates the effect of the phase of the unsteady heat release on the dynamic behavior of the same combustor presented in Figure D.1. The phase of the heat release is changed by varying the geometry of the flame zone: a *W* shaped flame is stabilized over two cylindrical flameholders, *5 mm* in diameter. The flameholders are located *1 m* downstream of the injection plane and can be moved vertically; see Figure D.3 for a schematic showing the flameholder disposition.

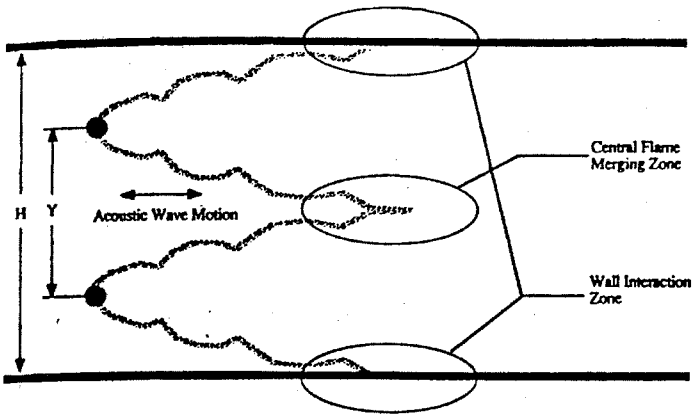

Figure D.3. Disposition of the flameholders (from Hegde et al. 1990).

The position of the flameholders is defined by the ratio *Y/H*. A value of zero indicates only one flameholder in the middle, and *1* indicates that the flameholders are on the external walls (they are always moved symmetrically).

The experimental results are somehow strange: the amplitude of the pressure oscillations, frequency of the instability and phase between CH radiation and pressure oscillations are a weird function of the separation distance (normalized by *H*); see Figure D.4 for an example.

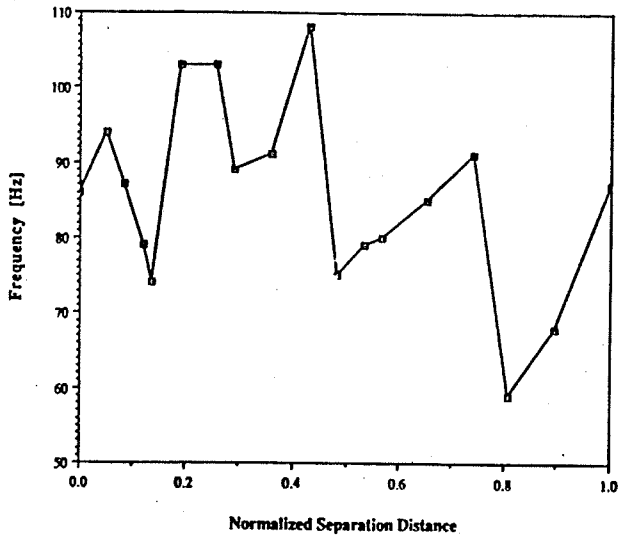

Figure D.4. Frequency of instability versus separation distance *Y/H* (from Hegde et al. 1990).

The authors do not give any explanation for that sort of behavior, consistently found in all the measurements presented. The data are used to plot phase difference (*CH* radiation phase minus pressure phase) versus frequency, to show that when *CH* radiation leads pressure oscillations the frequency of the instability is increased and vice versa when radiation lags.

A theoretical investigation of this last phenomenon is presented. Using the solution (D.3), and applying a method based on the one presented in Hegde et al. 1988, the authors study the effect of an oscillating heat source (considered as a small perturbation) on the acoustic modes. As a result, they obtain an expression, which is in good agreement with the measured behavior, for the frequency shift due to the out-of-phase heat radiation. Again, as in Hegde et al. 1988, a key point is represented by the flame dynamics (here referred to as "combustor process response") that is not modeled but based on direct experimental determination, so that it only allows analysis of the experiment, but no prediction.

In all the three previous works, no attention is devoted to the possibility of controlling the instability: all the interest is given to modeling.

A 1993 paper (Menon and Yang 1993), written in collaboration with Dr. V. Yang of Pennsylvania State University, addresses the issue of active control of combustion. The system under consideration is a generic ramjet engine, where low frequency (200-800 *Hz*) and high amplitude pressure oscillations can develop. Also in this case, like in the combustor of Figure D.1, the instability is attributed to a complex nonlinear coupling between the shear flow, the pressure oscillations and the unsteady heat release. This mechanism manifests itself as a large-scale vortex/flame structure propagating in the combustor at the same frequency of the instability (this conclusion is based on previous works cited in Menon and Yang 1993).

After a brief discussion of previous work in the area, the authors conclude that secondary fuel injection is the method of choice when compared with acoustic feedback (typically a

loudspeaker) for real scale applications. Moreover, single frequency control approaches seem to be limited by the fact that real ramjets show several unstable modes, and controlling one has often led to amplification of other modes. Since the use of neural networks is very costly in terms of training time, the authors conclude that adaptive schemes and secondary fuel injection should constitute the appropriate approach for controlling a full-scale ramjet engine.

The theoretical analysis is based on the expansion in two parameters and derivation of an equation for the pressure oscillations (p') as in Culick 1976:

(D.4)
$$\nabla^2 p' - \frac{1}{a^2}\frac{\partial^2 p'}{\partial t^2} = h + h_c$$

$$\mathrm{n}\cdot\nabla p' = -f - f_c$$

Where h and f accommodate all acoustic, mean flow and combustion terms with no external forcing, h_c and f_c represent the control inputs; a is the speed of sound.

The control input is modeled as a secondary fuel injector by using a generalized time-lag theory. Ignoring the effects of the acoustic field on the injector, h_c can be written as

(D.5)
$$h_c(\mathrm{r},t) = -\frac{\overline{R}\Delta H_c}{a^2 C_v}\left[\frac{\partial \dot{m}_{in}(t-\tau)}{\partial t} R(\mathrm{r}(\tau),t-\tau)\right]$$

Where $\overline{R}$ is the gas constant, ΔH_c is the heat of formation of the fuel, C_v is the specific heat at constant volume and $R(r(\tau),t)$ characterizes the fraction of the fuel burned at position r with a time delay τ. For the purpose of calculation, the distributed action (represented by R) is approximated by the sum of M point actuators.

Following Culick 1976, all source terms in equation (D.4) are treated as small perturbation to the acoustic field, with second order accuracy. This allows using a synthesis of the non-perturbed acoustic modes of the chamber to represent the solution to the wave equation.

The state of the system (acoustic field) is determined by the use of a point pressure sensor that can be immediately written in terms of the modal expansion. Numerically, this is formulated just as the pressure value at the sensing point with a gain factor (no dynamics are associated to the pressure sensor).

The chosen control scheme is a fixed-gain *PD*; the parameters of the distributed control system (many actuators) are determined by averaging the optimization condition for individual point actuators. The optimization condition used in this case is

- performance of the controller is least sensitive to the variation of the actuator time delay;
- energy of the control input is minimized.

The averaging procedure (see Menon and Yang 1993 for details) produces an expression that defines the gains in terms of the linear growth rate and frequency shifts of the modes.

The design and test of a controller based on this idea is performed on the results of a numerical simulation of a ramjet combustor presenting a combustion instability leading to a limit cycle with pressure oscillation of about 15% at 234 *Hz*.

The theoretical model, based on equation (D.4), after spatial and time averaging, is first used to reproduce the limit cycle behavior found in the numerical model (by appropriately choosing the parameters). Then the controller parameters are selected and the controller tested, showing a reduction of the amplitude of the instability of about 35%.

A simplified version of the same controller (with only the proportional part) is then tested in the numerical simulation, with similar results (i.e., 35% reduction in the *rms*. amplitude of the unstable modes).

Many important details are missing in the paper, especially regarding the control section. The relationship between controller and combustor used in the simulations is not clear; also the parallel between theoretical analysis and numerical simulation seems based more on a parameter

matching rather than on an understanding of the physical system. The controller is very simple and based on a linear model for the system: this approach works reasonably on the particular numerical model but, as recognized by the authors, it is not likely to work in a real system.

The main result is the development of a theoretical model capable of incorporating control action in a natural way. The drawback is that the procedure requires parameters matching with real system (especially of the time delays), and does not allow any *a priori* prediction of the performance.

An interesting work is presented in Neumeier et al. 1993: the authors, starting from first principles, develop a complete model of a combustor in order to perform a *frequency domain* analysis of its behavior. The model uses a one-dimensional energy balance to obtain a closed expression and allow the analysis in frequency domain aimed to the development of a simple performance prediction method.

Figure D.5 presents a schematic of the combustor: the tailpipe is described by using linear acoustics and corresponds to the acoustic resonator of Figure D.6.

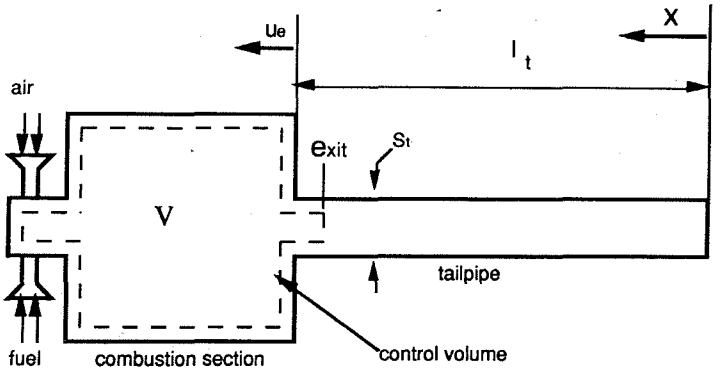

Figure D.5. Schematic of the combustor (from Neumeier et al. 1993).

The analysis is based on the integral energy equation written for the combustion section (the control volume is indicated by the dashed line in Figure D.5). Kinetic energy terms are neglected.

(D.6) $$\dot{q}_{reac} - \dot{q}_{loss} + \dot{m}_a h_a + \dot{m}_f h_f + \dot{m}_e h_e = \frac{d}{dt}\iiint \rho e dV$$

Where the subscript a refers to air, f to fuel and e to exit (tailpipe); $\dot{q}$ is the heat flux, e the internal energy and ρ the density (of the mixture). The integral on the right end side is eliminated by using perfect gas relations, and by assuming that the pressure is uniform inside the control volume. The tailpipe is described by the linear acoustics wave equation, and the solution is found by assuming periodic time dependence (see Neumeier et al. 1993 for details) and expressed in terms of frequency of the oscillations $H(\omega)$. The feedback from the resonator to the combustion and heat transfer process is through the boundary conditions at the combustion section exit. The feedback loop (see Figure D.6) represents the whole combustor.

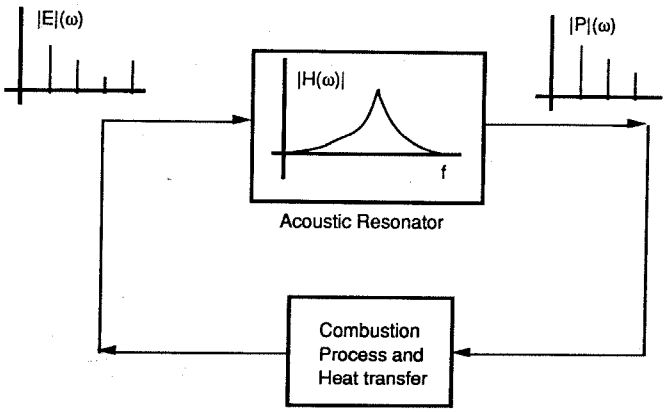

Figure D.6. Combustor as a feedback system (from Neumeier et al. 1993).

The solution is written as a combination of modes and harmonics; each of them satisfies the energy equation, and hence produces a transfer function in the frequency domain (i.e., a relation between amplitude and phases of the modes and oscillation of the energy input).

Further assumptions include the following:

- the pressure in the chamber is considered uniform to simplify the energy equation (i.e., the oscillations are neglected);
- the pressure oscillations are assumed to be sinusoidal;

- a temperature profile along the tailpipe is assumed.

The result of the analysis shows that most of the dynamics are associated with the fundamental mode and minimum energy input is needed to maintain oscillations when the input frequency is close to resonance. On the other hand, instability is completely damped when the energy input is out of phase by 90°, as also stated by Rayleigh's criterion.

The authors also include a discussion about the dissipation of the extra-energy produced by combustion when the chamber is near resonance: the model requires that either a significant amount of this energy is transferred to the tailpipe, or there is a large oscillatory heat dissipation in the combustion area. Experimental evidence, on the other hand, suggests that neither of these situations appear in real combustors. The conclusion of the authors is that there must be some kind of "high oscillatory loss" that can not be accounted for by any "known heat transfer mechanism." It is likely that the deficiency of the model comes from the original assumption that the pressure in the chamber is uniform: that limits the validity of the analysis to linear cases (very weak perturbations), while in the last part the model is used to analyze limit cycle behavior. Also, the only dynamics are associated with the tailpipe (linear acoustics), while the combustion volume is treated as a uniform region with instantaneous response.

Zinn et al. 1994 presents a brief progress report on some of the work concerning active control of instabilities. It is missing too many details to be of any use: the idea the authors intend to pursue is based on oscillating the fuel injection line in order to produce oscillation in the heat release and hence reduce instability.

D.3 Current Work

D.3.1 Experimental Work

D.3.1.1 Actuator Design

A short but quite complete review of the active and passive combustion control work (up to 1997) is presented in Neumeier and Zinn 1997. The authors again conclude that the most viable actuation method for active control of combustion instabilities in realistic systems seems fuel injection (compared to shakers and speakers) coupled with some kind of adaptive control, to compensate for the lack of complete understanding of combustion systems.

They also present some results referring to a test of the observer (Neumeier and Zinn 1996b) on a small Westinghouse combustor, but, apart from some plots, no detail is given.

Neumeier et al. 1997 presents the experimental study of a secondary fuel injector for the control of combustion instabilities. The experimental facility is presented in Figure D.7.

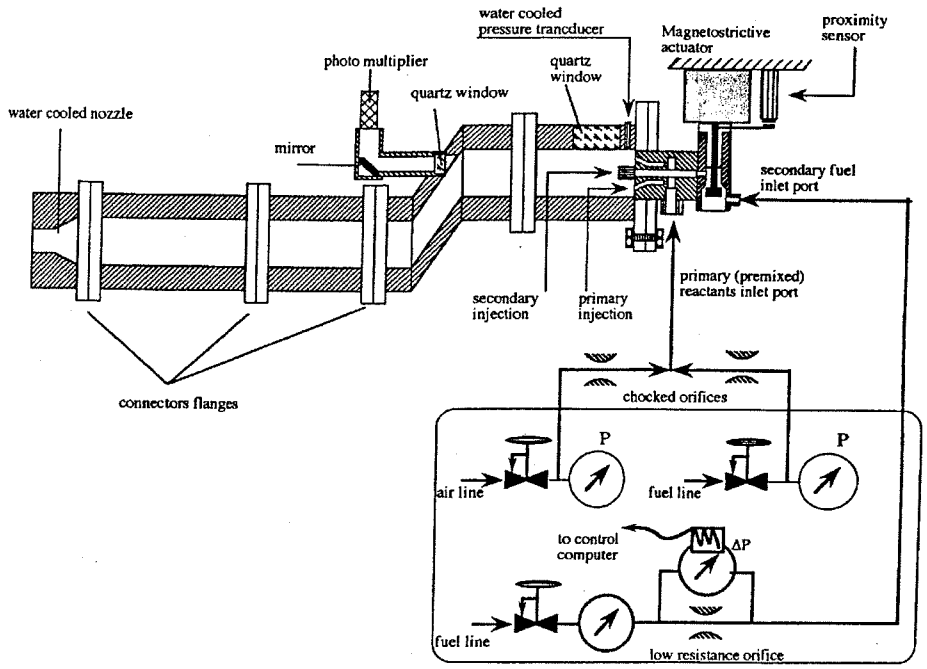

Figure D.7. Experimental Set-up (from Neumeier et al. 1997).

The primary reactants are air and methane; the secondary fuel is methane. Transducers monitor the pressure in different locations, while the photomultiplier is used to measure reaction rate. The proximity sensor accurately measures actuator motion. The internal diameter of the combustor segments is 1.44 *in*; the length varies depending on the number of pipe elements in the exhaust section. The natural frequency of the system is between 200 *Hz* (in the longest configuration) and 1800 *Hz* (shortest). The secondary fuel is modulated by the use of a magnetostrictive actuator connected to a needle: the axial motion changes the annular cross-sectional area between needle tip and its seat, resulting in a modulated flow rate.

The end nozzle is always choked during experiments.

The main characteristics are as follows:

- high pressure gas combustor (45 *psi*);
- primary fuel flow: 10 *g/s*;
- secondary fuel flow: up to 0.2-0.3 *g/s* (depending on the operating conditions), corresponding to a 20 *kW* peak-to-peak heat release oscillations;
- combustor power output: 55 *kW* (in nominal conditions);
- secondary fuel oscillation generated by using a magnetostrictive actuator, 1 *kHz* band;
- choked flow through injector plate (to prevent feed-back between the fuel supply lines and the combustor).

The major drawback of the facility is the very small size of the combustor; also, the study is more directed to rocket combustion chambers (very high pressure, choked nozzle) rather than gas turbine combustors.

Figure D.8 shows two different injector configurations tested by the authors. The first one (*a*) injects the secondary fuel directly into the combustion zone; the second (*b*) delivers the fuel in the primary reactants stream before combustion.

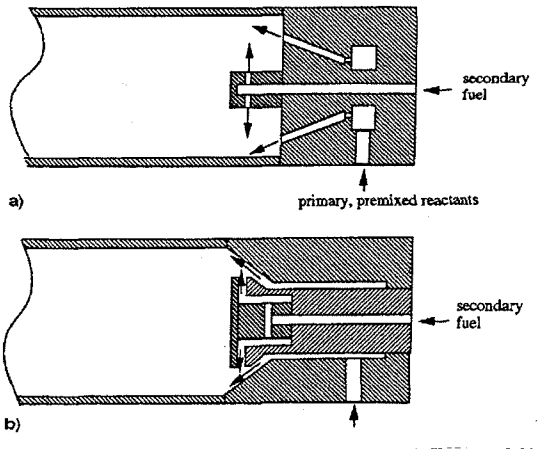

Figure D.8. Geometry of the fuel injectors (from Neumeier et al. 1997).

The performance of the injector is determined by open loop tests: the combustor (which presents several unstable modes) and the secondary injector are both run with their own independent fuel flow; pressure and radiation data are collected and then analyzed to identify the effect of the secondary fuel flow oscillation. Figure D.9 presents a result of that analysis, and shows that the lag between heat release and actuator displacement increases (in absolute value) with frequency. This suggests that a pure time delay is involved in this particular process.

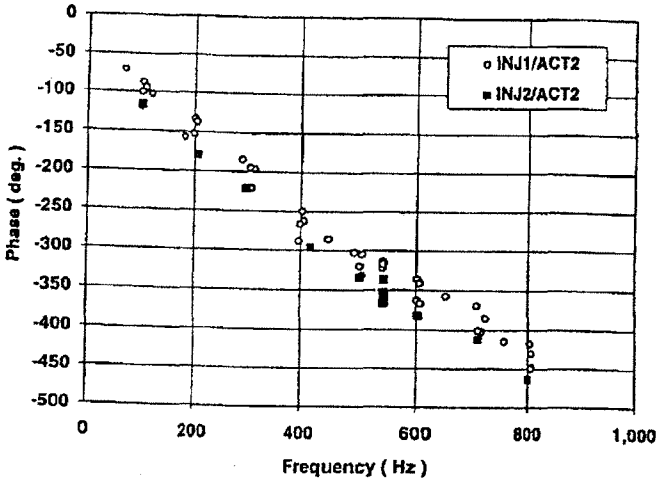

Figure D.9. Frequency dependence of the phase difference between heat release and actuator oscillations.

Another finding is that greater heat release oscillations were induced (at constant secondary fuel rate) when injecting directly into the primary combustion zone (injector *a* in Figure D.8).

No physical explanation is given for the phenomena observed. The authors did not try any flow visualization to characterize the differences between the two injectors analyzed; it is not clear how far these results can be extended to other configurations, or also how they would be affected by scaling (the test combustor was quite small). On the other hand, the data presented in the paper can be used to "identify" a suitable model for a realistic injector to be used in control simulations. Both relative magnitude and phase characteristics are provided; some guessing might be required on some parameters, but the description is fairly complete and detailed.

It seems that no further work has been published regarding experiments conducted in this facility.

D.3.1.2 Characterization of Combustion Instabilities

A new experimental facility for the study of low NO_x gas turbines (*LNGT*) has been recently set-up at the Georgia Institute of Technology. Figure D.10 shows a schematic of the facility, which is divided in several sections: air inlet, mixing, combustor and exhaust.

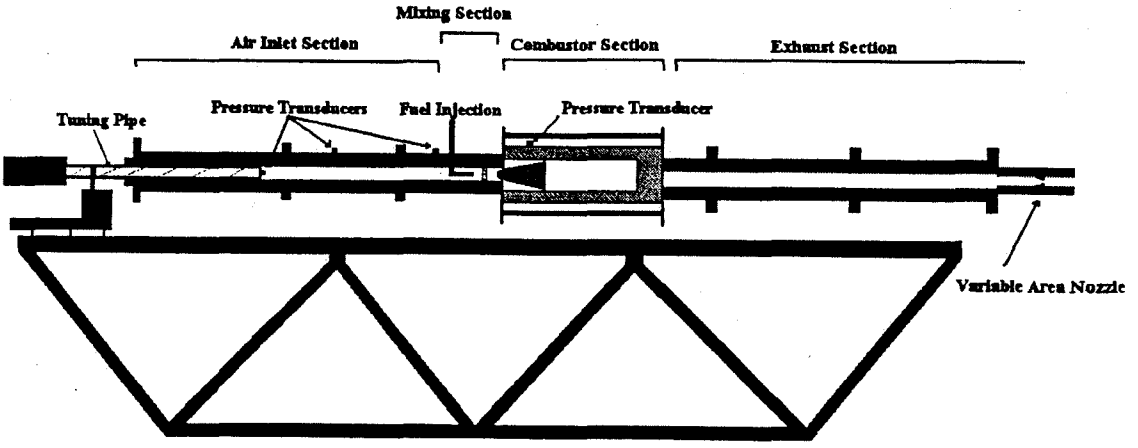

Figure D.10. *LNGT* simulator (from Torres et al. 1999).

The length of the air inlet can vary from 101.1 *cm* to 163.8 *cm*; the fuel is injected radially in the airflow upstream of the mixing section, and passes over 45° inclined swirl vanes before entering the combustor. Air and fuel (industrial grade methane) are choked upstream of the injectors to prevent coupling with the feed lines. The flame is stabilized by a conical bluff body, and the combustor is 47 *cm* long, with observation windows. The exhaust section length can vary from 192 *cm* to 350.5 *cm*, and is terminated by an adjustable throat nozzle, with a maximum area of 2.32 cm^2. The apparatus is equipped with several pressure transducers and a *CCD* camera capable of measuring *CH* radical chemiluminescence. Operating pressure range is 1-10 *atm*.

Depending on the operating conditions (mainly pressure and velocity, controlled by the area of the nozzle throat valve in the exhaust section) the combustor can exhibit instabilities from 100 *Hz* (fundamental mode) up to 700 *Hz* (7^{th} mode).

Several observations are presented:

- When sweeping the equivalence ratio from lean to rich and back, and when increasing and then decreasing the flow velocity, hysteresis was observed between stable and unstable burning (this point is not further investigated by the authors).
- The inlet section length has no influence on the amplitude of the pressure oscillations in the combustion region and on the frequency of instability. This is explained by the significant area constriction in the mixing section between inlet and combustion section. It has a little influence on the lean blowout limit. The same applies to the nozzle throat area.
- Three operating conditions are observed:
  1. Stable (low amplitude pressure oscillations).
  2. Unstable (large amplitude oscillations).
  3. Modulated Instability (intermittently alternated between the previous two).
- Images show that most of the chemical reactions occur in a thin annular region near the combustor walls. Also, the flame moves back and forth at the frequency of the instability;

the movement decreases when increasing the frequency. This clearly indicates an interaction with the flow field; it is not clear whether this is a cause or an effect of the instability.

The experimental data are used to test an interesting correlation between instability and equivalence ratio oscillation, resulting from a theory presented by the authors in Lieuwen, Neumeier, Zinn 1998. Figure D.11 presents the result of the test. Shaded areas are predicted to be unstable, white areas stable; the dark dots are the experimental data.

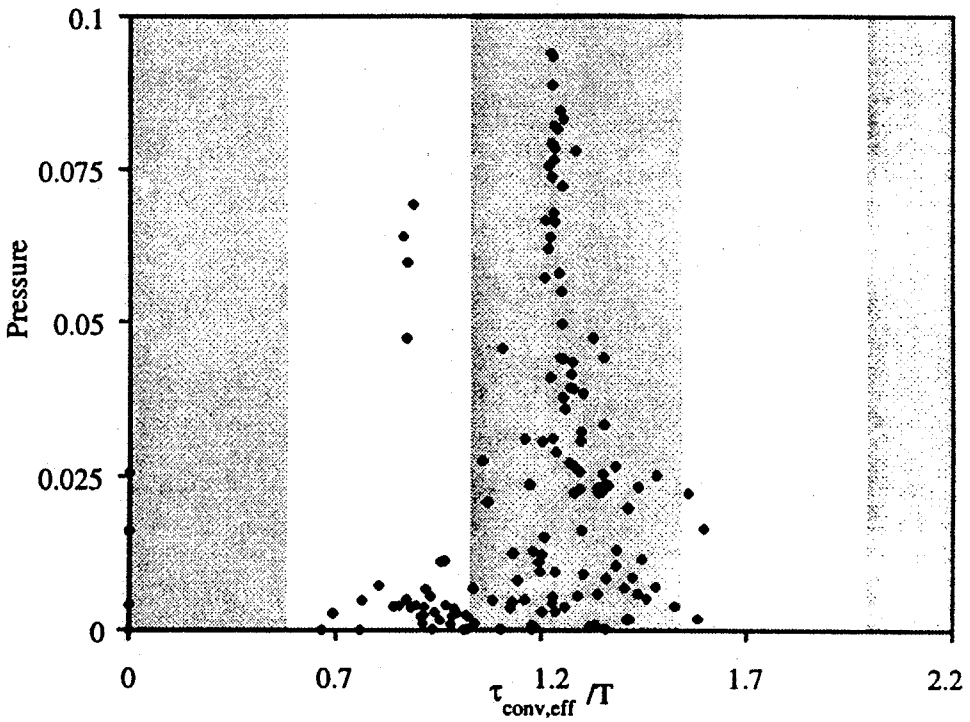

Figure D.11. Predicted stability limits and measured data (from Lieuwen et al. 1998).

The theory predicts that the sum of the convection time of the equivalence ratio perturbation (τ_{conv}) and the time required for the heat release to respond to the mixture perturbation at the base of the flame (τ_{eq}) divided by the period (T) is always close to some constant value (depending on the combustor).

Figure D.11 effectively shows that most of the unstable points lie inside the predicted (shaded) instability region. On the other hand:

- Some of the stable points are also inside the predicted instability region.
- No unstable points are in the other instability bands predicted by the theory.

The authors conclude that the condition is only necessary, but not sufficient, for the instability, and that some correction has to be made to the theory to forbid the other instability bands. Also, apparently unrelated experimental conditions (time of the day, weather, ...) seem to have a major impact on experiments (poor repeatability); this point is left unexplained in Torres et al. 1999.

Some recent experimental work conducted in the same facility (Zinn et al. 1999) shows that convective processes control the instability behavior. The instability is a consequence of a feedback loop between pressure oscillations, equivalence ratio oscillations and fluctuating heat release.

Also, experimental data show that the amplitude of the instability correlates with the ratio of the oscillating velocity in the combustor and the mean inlet velocity. This suggests that nonlinearities in the heat release response might be responsible for the limit cycle oscillations, while nonlinear gasdynamics does not play a major role (this conclusion is also supported by the observed increase in instability amplitude with frequency). In this experiment, the amplitudes of pressure oscillation were quite low (1-10% of the mean pressure).

D.3.1.3 Active Control

Zinn et al. 1999 gives a quick description of an experiment regarding active control of combustion instabilities. Very few details are given: the controller is adaptive, and it seems based on a frequency domain analysis. The actuation is performed by modulation of secondary fuel.

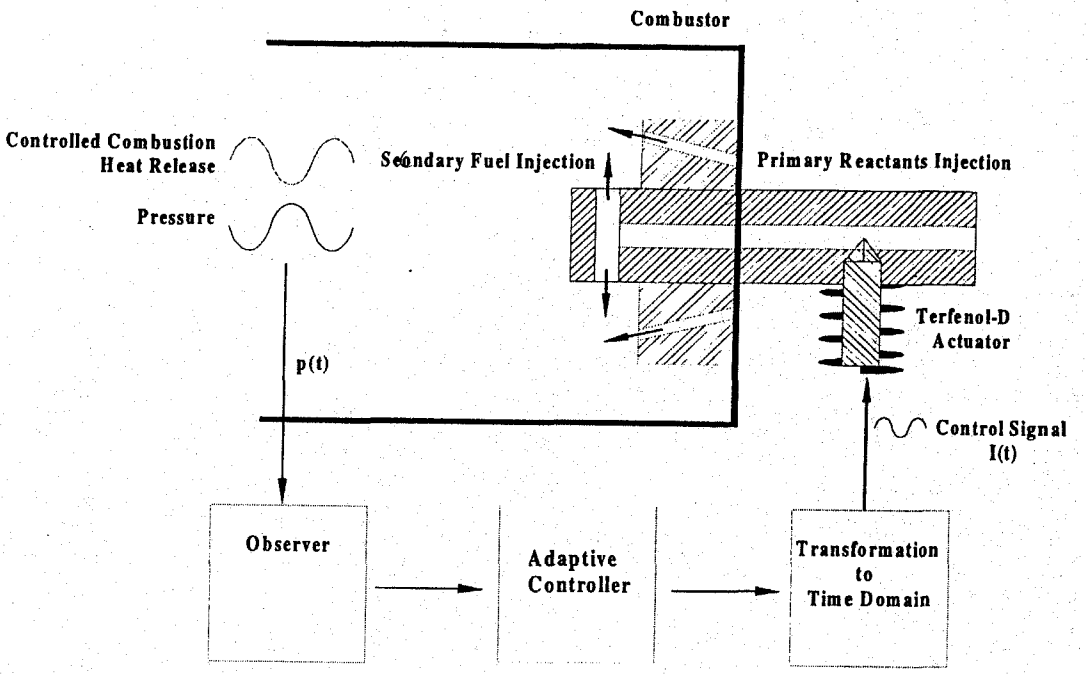

Figure D.12. Schematic of Control System (from Zinn et al. 1999).

The performance of the controller is successfully tested on an unstable speaker-microphone system, and then on an unstable combustor. The authors do not specify which combustor was used, and it seems that it is not the one described in Lieuwen et al. 1998 and Zinn et al. 1999 as the low NO_x simulator. In any case, the controller takes about 2 *s* for identification, and then, in 0.05 *s*, obtains a 50% attenuation of the pressure oscillations due to the unstable 110 *Hz* mode. No others details are given in those papers.

D.3.2 Theoretical Work

D.3.2.1 Observer Design

The idea is to use an observer to identify frequencies and amplitudes of the excited modes, which are not known in advance.

The observer assumes that the combustor oscillations are quasi-periodic, and can be expressed as a combination of several modes and harmonics. The pressure can be therefore expressed as a combination of K modes present in the combustor, and each mode can be written as a series expansion with M terms (Neumeier and Zinn 1996):

(D.7)
$$p(t)=\sum_{i=1}^{i=K} p_i(t)=\sum_{i=1}^{i=K}\sum_{n=1}^{n=M} A_{n,i}(t)\sin\left(n\omega_i t+\phi_{n,i}(t)\right)$$

Where $A_{n,i}$ and $\phi_{n,i}$ are given by expressions similar to the integrals used in Fourier series analysis:

(D.8)
$$\begin{aligned}
A_{n,i}(t)&=\sqrt{S_{n,i}(t)^2+C_{n,i}(t)^2}\\
\phi_{n,i}(t)&=\tan^{-1}\left(C_{n,i}(t)\Big/S_{n,i}(t)\right)\\
S_{n,i}(t)&=\frac{2}{T_i}\int_{-T_i} p_i(t)\sin(n\omega_i t)dt\\
C_{n,i}(t)&=\frac{2}{T_i}\int_{-T_i} p_i(t)\cos(n\omega_i t)dt
\end{aligned}$$

Note that the expressions in (D.8) differ from conventional Fourier integrals as their limits may vary with time. To reduce computation effort, the observer replaces (D.8) with the following expressions:

(D.9)
$$\begin{aligned}
S_{n,i}(t+dt)&=S_{n,i}(t)+\frac{2}{T_i}\left[p_i(t+dt)-p_i(t-T_i+dt)\right]\sin(n\omega_i t)dt\\
C_{n,i}(t+dt)&=C_{n,i}(t)+\frac{2}{T_i}\left[p_i(t+dt)-p_i(t-T_i+dt)\right]\cos(n\omega_i t)dt
\end{aligned}$$

The frequencies ω_i are not known at the beginning of the calculation, but it can be shown (Neumeier and Zinn 1996) that there exists a simple iterative relationship which quickly converges to the frequency of the dominant mode of the oscillation. Once this frequency is determined, the dominant oscillation can be subtracted from the signal, and the second mode can be determined, and so on. The computation is very quick and can be performed "on-line." Observer performance is successfully tested on several input cases both from synthesized signals and real data.

A more complete mathematical treatment of this approach is presented in Neumeier et al. 1997. The authors show the derivation of the observer and analyze and discuss various details missing in the previous papers, like the limits on the convergence of the series to the right frequency, the possibility of different equilibrium points for the observer, effect of noise and uncertainty in the parameters defining the system. There are also some notes regarding problems arising in the actual numerical implementation of the method.

It is important to note that the asymptotic stability of the observer (i.e., the fact that the equilibrium point corresponding to the right frequency in the observed signal is stable) can be proved only for the case of an input containing one sinusoid. It is not proved, but only induced from numerical experiments (the equilibrium points result locally asymptotically stable) for the general case of a signal composed of an arbitrary number (greater than 1) of sinusoids.

If the observer is used to identify a signal containing more modes than the "order" of the observer, i.e., $K>M$ in equation (D.7), it behaves chaotically, depending on the relative amplitude of the modes, and other features of the input signal. The observer is not always robust to this case; this is an important issue for real application, since this might imply the necessity of a very high order observer, depending on the specific case. The dynamic behavior of the observer is actually quite complex, and, by admission of the authors, "it is not fully understood, but it works well in numerical and laboratory applications" (Neumeier et al. 1997).

Two applications of the described observer to numerical examples are presented in Neumeier and Zinn 1996. In the first example an unstable system of six oscillators (the instability is artificially introduced by assuming positive growth constant for the 4^{th} and 6^{th} mode), representing a combustion system, is controlled by introducing an oscillation in the heat addition to the combustor. The controller (not specified in the paper) seems to be just a simple proportional controller, and is set so that it damps the most unstable mode, as identified by the observer. The instability is effectively damped quickly: when the controller is turned on, it takes about 40

oscillation cycles of the pressure (0.05 *s*) for the oscillation to virtually disappear. Figure D.13 is the trace of the observed frequency, and clearly shows the observer "jumping" between the two unstable modes.

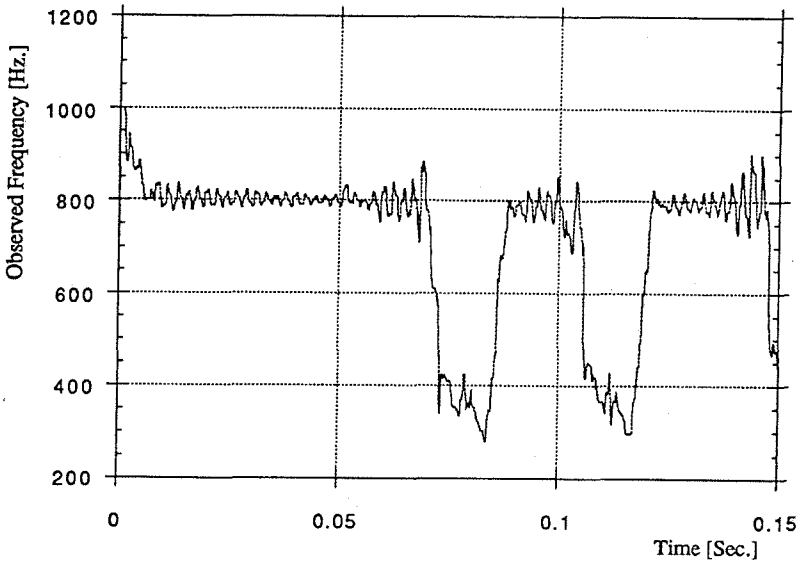

Figure D.13. Time dependence of the observed frequency of the dominant mode (Neumeier and Zinn 1996).

The second application is the control of an unstable rocket motor. The motor is simulated numerically by solving the one-dimensional conservation equations for mass, momentum and energy. Again, the heat addition in the combustion chamber is controlled proportionally (through a negative constant) to the observed pressure. The model for the motor also includes a time delay on the actuation line, which accounts for delays introduced in the actuation, fuel line and reaction rate.

The controller deals with the time delay by adding a frequency shift to the output before sending the signal to the actuator (this requires *a priori* knowledge of the exact time delay, and partially reduces the significance of the example).

For this example, the most unstable mode and its five harmonics are controlled simultaneously: Figure D.14 shows the results of the simulation.

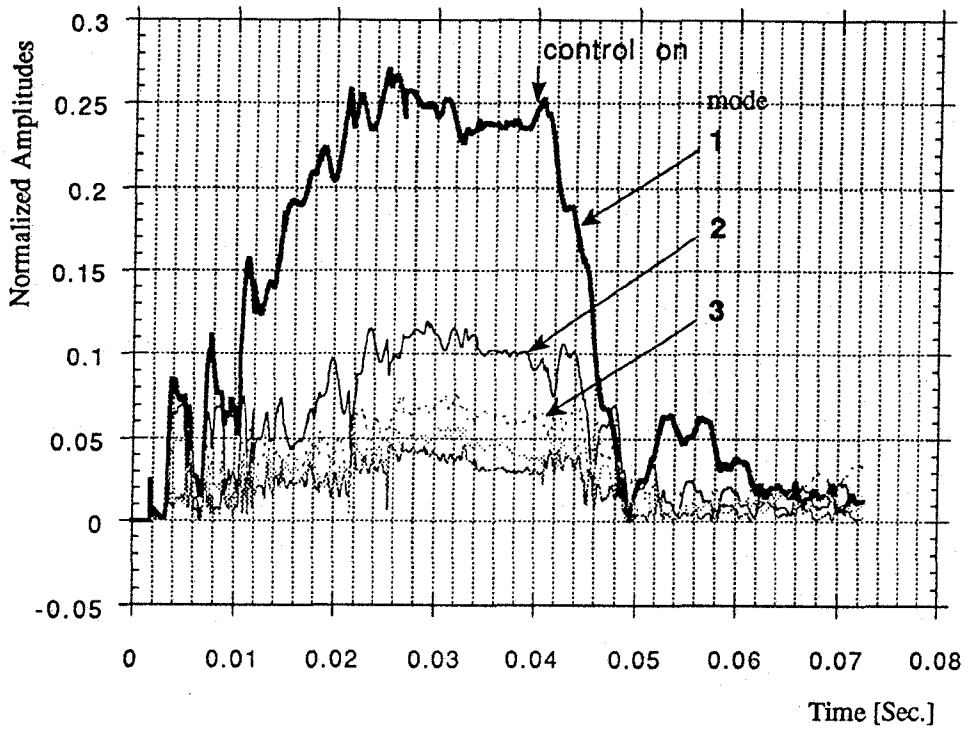

Figure D.14. Time dependence of the observed modes (Neumeier and Zinn 1996).

The performance of the controller is quite impressive: it seems to work really well, beyond the proposed theoretical explanations. Also, contrary to previous "one-mode" (or one-frequency) controllers, no stable mode is destabilized or excited by the control action on the unstable modes. On the negative side, no experimental result is shown, and no "noise" or any kind of disturbance was introduced in the simulations. It is likely that the dynamics of the controller (it tends to be chaotic) will be consistently affected once these are added, affecting the issues of robustness and stability. Another limitation of the controller lies in the fact that there must be as many terms in the analysis as modes expected in the observed signal. In any case, for simple systems it might be a very viable starting point for the design of a control system.

D.3.2.2 Active Control of Combustion Instabilities

The work directly involving control of combustion instability is mainly analytical and numerical.

A heuristic one-dimensional combustor model, based on the solution of a set of Euler equations modified by the addition of source terms to account for the effects of mixing and combustion processes, is used as a test-bench for control systems (Mohanraj and Zinn 1998).

A controller based on the observer described in the previous section is compared with an adaptive controller, based on a delayed least mean square (*LMS*) method.

The adaptive controller is based on a quite straightforward application of the *LMS* algorithm to adapt the weights of a digital filter, whose input is the signal from the pressure sensor, and the output is the fuel modulation. The parameters in both the applications are based on the knowledge of the combustor model (mainly time delays).

Figure D.15 shows the results of simulation for both controllers, which actually have extremely similar performance.

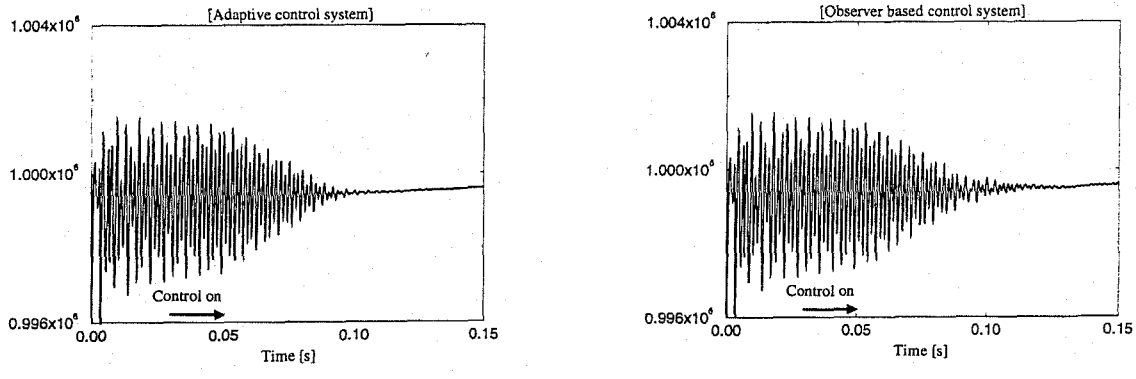

Figure D.15. Adaptive (left) and observer based (right) controller response (from Mohanraj and Zinn 1998).

The authors report that a correct choice of parameters and weights is necessary to avoid instability of the adaptive controller, encountered during their numerical study.

It is important to note that the model of the plant does not include any source of disturbance, and no robustness analysis is performed. The authors only present two controllers working (well) in their well-defined design conditions, and this poses a limit to the validity of the work for practical applications.

A more analytical framework is used for an application of robust feedback control design (Haddad et al. 1997). A state space model of a combustor is built by using conservation equations to obtain a wave equation for the oscillating component of the pressure, similar to equation (D.4). The general solution to the equation is written as a superposition of the classical acoustic modes of the chamber, and the pressure is expressed as a sum of these modes with time dependent amplitudes. This part of the analysis follows closely the one of Culick 1976.

After spatial averaging and considering terms up to linear acoustics, the system of equation reduces to a system of ordinary differential equations for the amplitudes, representing coupled oscillators:

(D.10) $$\ddot{\eta}_n + \omega_n^2 \eta_n + \sum_{i=1}^{k} \left(D_{ni}\dot{\eta}_i + E_{ni}\eta_i \right) + F_n^{NL}(\ldots) = w_n(t) + U_n(t) \qquad n = 1,\ldots,k$$

Where η_n is the time dependent amplitude of mode n, ω_n is the mode frequency, D_{ni}, E_{ni} are the linear acoustic coefficients, F_n^{NL} includes the non-linear contributions (from combustion, for example), w_n is noise entering the system and U_n is the control input.

The control action is performed by point actuators that introduce energy in the combustion system (mass and momentum are not controlled). The sensing is performed by point measurements of the unsteady pressure signal. Both the control input and the sensor output can be easily written as a combination of the classical acoustic modes, to fit in the previous analysis.

The *state-space* representation of the system follows immediately from (D.10). Defining the state as the vector:

(D.11) $$\mathrm{x} = \left[\eta_1 \quad \dot{\eta}_1 \quad \ldots \quad \dot{\eta}_n \right]^T$$

The system (D.10), written as a system of first order equations, becomes:

$$\dot{x} = Ax + Bu$$
$$y = Cx + Du \tag{D.12}$$

Where $\boldsymbol{A}$, $\boldsymbol{B}$, $\boldsymbol{C}$ and $\boldsymbol{D}$ can be easily derived from (D.10) and $\boldsymbol{u}$ includes control input and noise. The model output ($\boldsymbol{y}$) is a single pressure measurement at 1/3 of the combustor chamber.

A second order speaker dynamics and sensor noise are also included in the state space model by properly augmenting $\boldsymbol{A}$ and $\boldsymbol{D}$.

The control objective is to stabilize the system and to minimize the unsteady acoustic pressure due to a disturbance in the input at a specified location in the chamber. A schematic of the combustor used in the modeling is presented in Figure D.16. The noise input to the system is placed at the combustor head and on the microphone line (both are independent white noise sources of specified maximum amplitude).

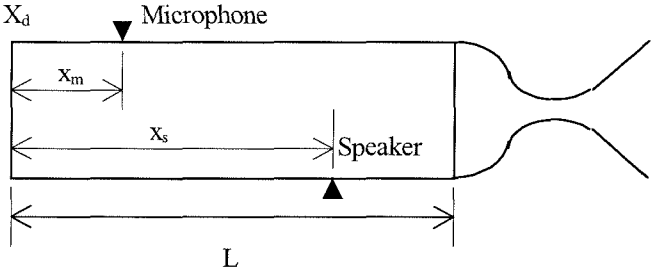

Figure D.16. Physical model.

The design of the controller is done for a system with constant real structured parameter uncertainty, i.e., the system matrix in the state space model is substituted by a perturbed matrix, where the perturbation is assumed to have a specific structure (in this case, symmetric) and be bounded.

A robust reduced-order controller is then designed by using a modification of the Lyapunov function method, and the resulting set of equations defining the controller matrices is solved numerically (see Haddad et al. 1997 for details).

As an example application of the method, the authors present a case with four modes, one microphone and one speaker (2x2+2=6 states) controlled by a second order controller.

A comparison between full-order *LQG* (Linear Quadratic Gaussian) and robust reduced order is presented in Figure D.17: the reduced order controller is more robust to perturbations, and also more stable without sacrifice in performance.

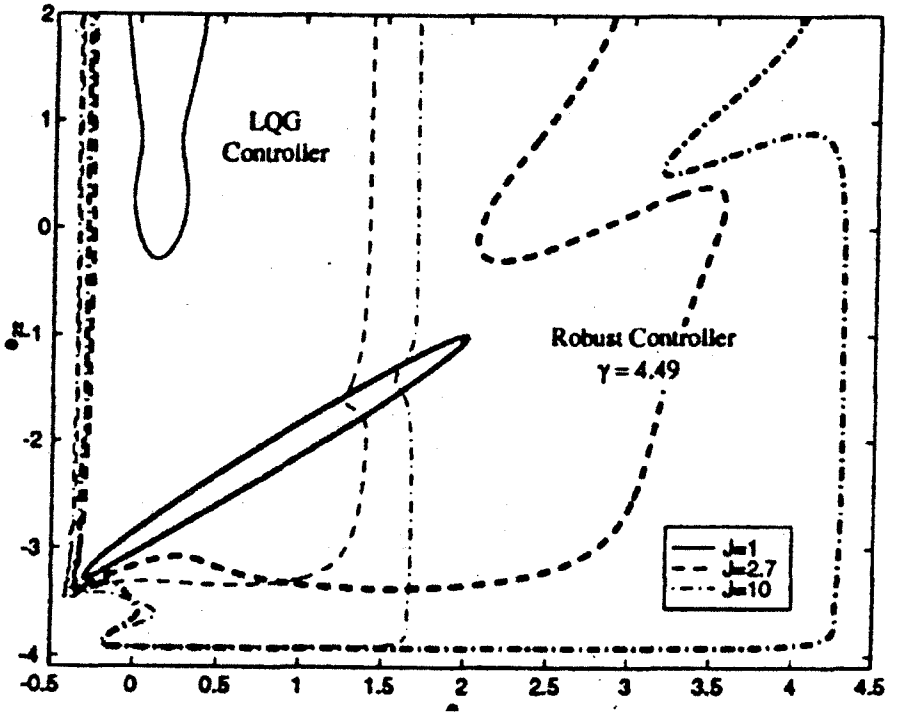

Figure D.17. Cost contours for *LQG* and robust-reduced order controllers (from Haddad et al. 1997).

While introduced in the analytical part of the work, it is not clear if the noise was actually considered in the numerical simulation. Figure D.18 shows the closed-loop response of the perturbed system with the reduced-order controller. The perturbation consists in the alteration of one of the acoustic coefficients: E_{11} in equation (D.1) is changed from –0.005 to 2 (non-dimensional units). The rationale of altering the acoustic coefficients comes from the fact that this is the most uncertain part of the system. The controller is turned on after 17 *ms*, and Figure D.18

shows that the controller easily handles the perturbation. Incidentally, the *LQG* controller is unstable in this same case.

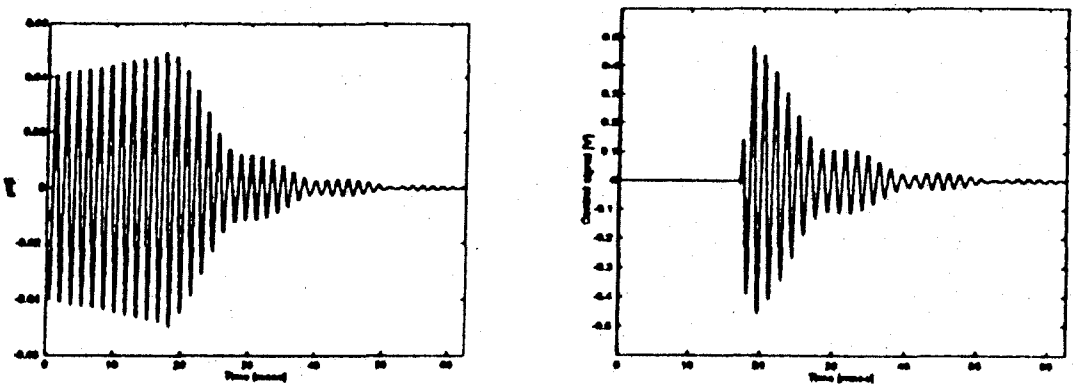

Figure D.18. Closed-loop response and control signal (from Haddad et al. 1997).

The problem is that the system appears completely free from noise, especially when compared to some test simulations we run: the system is substantially the same, and the noise levels introduced are the same as the ones claimed in Haddad et al. 1997. The following figure shows the results for a case similar to the one presented in Figure D.18: the general trend is very similar, but the noise has a much bigger influence.

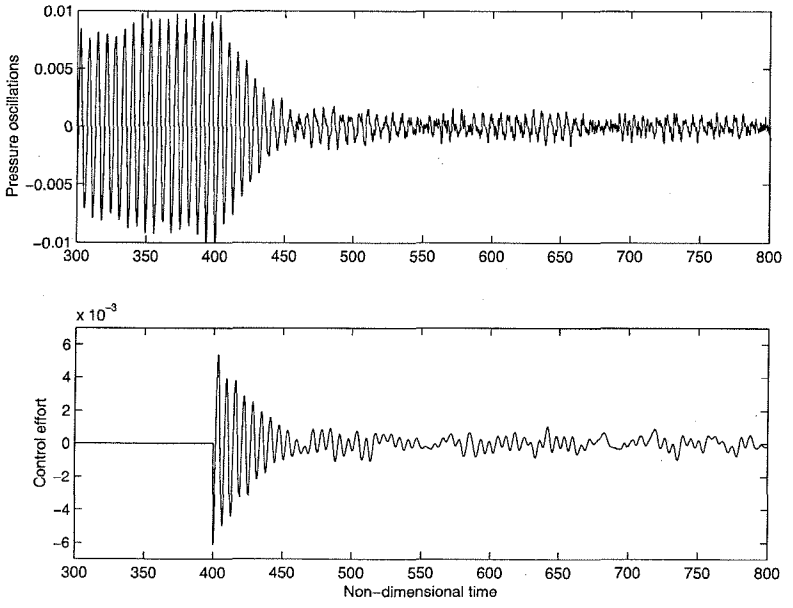

Figure D.19. Response of the system with noise.

In any case, this work is a good application of modern linear control, and shows the possibility of designing a low order, robust, linear controller for high order non-linear systems. A serious problem that might arise in real application to a combustion chamber is that time delays are completely ignored by the authors. But, as pointed out in many other works (Neumeier et al. 1997, Neumeier and Zinn 1997, Neumeier et al. 1997, Mohanraj and Zinn 1998, Lieuwen and Zinn 1998), time delays seem to be a very important characteristic of the dynamics of combustion systems (especially actively controlled systems), and can not be neglected for real applications.
The paper is a very good starting point for setting-up a state space control simulation of a combustor, even though some details regarding the actuator and the sensor are missing and there is some confusion between dimensional and non-dimensional quantities.

A different approach to control, not specifically of combustion, is presented in Shapiro and Zinn 1997. In this case, taking advantage of a complete knowledge of the dynamics of the system described by a differential equation (an inverse pendulum), nonlinear open loop control is performed to enlarge the stability limits of an unstable equilibrium of the system. This is just an academic exercise: an application of this idea to a real system is hardly imaginable.

D.4 Concluding Remarks

The work of the group at the Georgia Institute of Technology on the analysis and control of combustion instability has been analyzed through the published paper.
The main interest of the group lies in the modeling effort: different combustor types are experimentally tested and then a model is fitted to reproduce the experimental results. A shortcoming of this part of the work consists in the lack of a flame or combustion model: the flame zone is always treated as a discontinuity in the fluid field and the characteristics of the combustion zone have to be derived experimentally and then put into the model. This procedure

produces very good agreement between experiment and theory, but also seriously limits the utility of the study for a general or predictive application.

An important consideration is that over the years the papers do not show a continuous and planned study path: it is more like an exploration of different possibilities, without pursuing a defined general objective.

Specific considerations regarding the experimental activity are:

- Most of the experimental activity stopped between 1993 and 1997.
- An interesting experiment is the one conducted in 1997 to characterize a secondary fuel injector, producing results very useful for control simulations.
- Some experiments produced strange results, left unexplained by the authors (Hegde et al. 1990).

Regarding modeling:

- Most of the modeling refers to linear acoustics.
- No flame or combustion dynamics models are ever considered. Heat release is introduced as a point source with no internal dynamics.
- An interesting paper (Neumeier et al. 1993) presents the complete frequency domain model of a combustor, but the results are not used in further works.
- No consideration is given to scaling the models of laboratory combustors to industrial applications.

Regarding control:

- Control does not seem to be the main interest of the group. The control part is always introduced as a secondary item, and normally kept very simple (proportional, proportional-derivative or integral controllers are commonly used).

- The nonlinear observer, very promising in the simulation, seems abandoned after 1997: it is not clear if testing on a real system has ever been done. Also, important questions regarding robustness and stability of the controller can not be answered analytically, and this poses a serious limitation to possible applications.
- The work on modern control (done by a different group) is quite different from the rest. It is certainly helpful as a problem setting for future investigations or applications, in the sense that they introduce control system terminology in the description of combustion system. This allows them to use classical and modern methods to try some design on simple models, and identify some of the issues, like time delays, stability, and robustness.

Bibliography

Ananthkrishnan, N. 2001. Personal communications.

Baum, J. D., Daniel, B. R., Zinn, B. T. (1982). *Determination of Alluminized Solid Propellant Admittances by the Impedance Tube Method*, AIAA 81-01222R, 1982.

Beckstead, M. W., Mathes, H. B., Price, E. W., Culick F. E. C. (1969). *Combustion Instability of Solid Propellants*, 12th International Symposium on Combustion.

Blomshield, F. S. (2000). *Pulsed Motor Firings*, in Solid Propellant Chemistry, Combustion, and Motor Interior Ballistics, Progress in Astronautics and Aeronautics, Vol. 185.

Burnley, V. S. (1996). *Nonlinear Combustion Instabilities and Stochastic Sources*, PhD Thesis, California Institute of Technology.

Burnley, V. S., Culick, F. E. C. (2000). *Comment on "Triggering of Longitudinal Combustion Instabilities in Rocket Motors: Nonlinear Combustion Response,"* Journal of Propulsion and Power, Vol. 16, No. 1, pp. 164-166.

Chen, T. Y., Hegde, U. G., Daniel, B. R., Zinn, B. T. (1993). *Flame Radiation and Acoustic Intensity Measurements in Acoustically Excited Diffusion Flames*, Journal of Propulsion and Power, Vol. 9, No. 2.

Cheng, S.-I. (1962). *Unstable Combustion in Solid Propellant Rocket Motors*, Eight Symposium (International) on Combustion, Williams and Wilkins.

Chu, B. T., Kovásznay, L. S. G. (1958). *Nonlinear Interactions in a Viscous Heat-conducting Compressible Gas*, Journal of Fluid Mechanics, Vol. 3, No. 5, pp. 494-514.

Clavin, P., Lazmi, D. (1992). *Theoretical Analysis of Oscillatory Burning of Homogeneous Solid Propellant Including Non-Steady Gas Phase Effects*, Combustion Science and Technology, Vol. 83, pp 1-32.

Culick, F. E. C. (1967). *Calculation of the Admittance Function for a Burning Surface*, Astronautica Acta, Vol. 13.

Culick, F. E. C. (1968). *A Review of Calculations for Unsteady Burning of a Solid Propellant*, AIAA Journal, Vol. 6, No. 12.

Culick, F. E. C. (1976). *Nonlinear Behavior of Acoustic Waves in Combustion Chambers, Parts I and II*, Acta Astronautica, Vol. 3, pp. 714-757.

Culick, F. E. C. (1994). *Some Recent Results for Nonlinear Acoustics in Combustion Chambers*, AIAA Journal, Vol. 32, No.1, pp. 146-169.

Culick, F. E. C. (1999). A Short Course Lectures on *Combustion Dynamics: Fundamental, Acoustics and Control*, United Technologies Research Center.

Culick, F. E. C., Dehority, G. L. (1969). *An Elementary Calculation for the Burning Rate of Composite Solid Propellants*, Combustion Science and Technology, Vol. 1, pp. 193-204.

Culick, F. E. C., Isella, G., Seywert, C. (1998). *Influences of Combustion Dynamics on Linear and Nonlinear Unsteady Motions in Solid Propellant Rockets*, AIAA-98-3704.

Culick, F. E. C., Yang, V. (1992). *Prediction of the Stability of Unsteady Motions in Solid-Propellant Rocket Motors*, in "Nonsteady Burning and Combustion Stability of Solid Propellants," Progress in Aeronautics and Astronautics, Vol. 143.

Doedel, E. J., Champneys, A. R., Fairgrieve, T. F., Kuznetsov, Y. A., Sandstede, B., Wang, X. (1997). *AUTO 97: Continuation and Bifuraction Software for Ordinary Differential Equations*, Concordia University, Montreal, Canada.

Doedel, E. J., Keller, H. B., Kernevez, J. P. (1991). *Numerical Analysis and Control of Bifurcation Problems, (I) Bifurcation in Finite Dimensions*, International Journal of Bifurcation and Chaos, Vol. 1, No. 3, pp. 493-520.

Doedel, E. J., Keller, H. B., Kernevez, J. P. (1991b). *Numerical Analysis and Control of Bifurcation Problems, (II) Bifurcation in Infinite Dimensions*, International Journal of Bifurcation and Chaos, Vol. 1, No. 4, pp. 745-772.

Ermentrout, B. (1998). *XPPAUT3.91-The Differential Equations Tool*, University of Pittsburgh.

Franklin, G., Powell, J., Emami-Naeini, A. (1995). *Feedback Control of Dynamic Systems*, Addison Wesley.

Fung, Y.-T., Yang, V. (1992). *Active Control of Nonlinear Pressure Oscillation in Combustion Chambers*, Journal of Propulsion and Power, 8(6).

Furukawa, T., Shimemura, W. (1983). *Predictive Control for Systems with Time Delay*, International Journal of Control, vol. 37, No. 2, pp. 399-412.

Goldstein, R. J. (1983). *Fluid Mechanics Measurements*. Hemisphere Publication Corp.

Guckenheimer, J., Holmes, P. (1983). *Nonlinear Oscillations, Dynamical Systems and Bifurcations of Vector Fields*, Springer-Verlag, New York.

Grad, H. (1949). *Resonance Burning in Rocket Motors*, Communications in Pure and Applied Mathematics, Vol. 2, March 1949.

Gulati, A., Mani, R. (1992). *Active Control of Unsteady Combustion-Induced Oscillations*, Journal of Propulsion and Power 8(5): 1109-1115.

Haddad, W. M., Bernstein, D. S. (1995). *Parameter Dependent Lyapunov Functions and the Popov Criterion in Robust Analysis and Synthesis*, IEEE Trans. Autom. Contr., Vol. 40, pp. 536-543.

Haddad, W. M., Leonessa, A., Corrado, J. R., Kapila, V. (1997). *Robust Reduced-Order Control of Combustion Instabilities*, 1997 IEEE International Conference on Control Applications, Hartford, CT, October.

Hathout, J. P., Annaswamy, A. M., Ghoniem, A. F. 2000. *Modeling and Control of Combustion Instability Using Fuel Injection*, AVT Nato Symposium, Braunschweig, Germany, May 8-11, 2000.

Hegde, U. G., Reuter, D., Daniel, B. R., Zinn, B. T. (1987). *Flame Driving of Longitudinal Instabilities in Dump Type Ramjet Combustors*, Combustion Science and Technology, vol. 55; (4-6) pp. 125-138.

Hegde, U. G., Reuter, D., Zinn, B. T. (1988). *Sound Generation by Ducted Flames,* AIAA Journal, vol. 26, No. 5.

Hegde, U. G., Reuter, D., Zinn, B. T. (1990). *Frequency Control in Unstable and Pulse Combustors,* 23rd Symposium on Combustion.

Huang, I-Te, Micci, M. M. (1991). *Gas Phase Analysis of Homogeneous Solid Propellant Combustion*, Combustion Science and Technology, Vol. 75, pp. 73-88.

Isella, G., Culick, F. E. C. (2000). *Modeling the Combustion Response Function with Surface and Gas Phase Dynamics*, AIAA-2000-0310, AIAA 38th Aerospace Sciences Meeting, January 10-13, 2000/Reno, NV

Isella, G., Seywert, C., Culick, F. E. C., Zukoski, E. (1997). *A Further Note on Active Control of Combustion Instabilities based on Hysteresis*, Combustion Science and Technology, Vol. 126, (1-6) pp. 381-388.

Jahnke, C. C., Culick, F. E. C. (1993). *An Application of Dynamical Systems Theory to Nonlinear Combustion Instabilities*, AIAA-93-0114, AIAA 31st Aerospace Sciences Meeting.

Keller, H. B. (1977). *Numerical Solution of Bifurcation and Nonlinear Eigenvalue Problems*, in Applications of Bifurcation Theory, pp. 359-384, Academic Press.

Kim, S.-I. (1989). *Nonlinear Combustion Instabilities in Combustion Chambers*, PhD Thesis, Pennsylvania State University.

Knoop, P. (1995). *A Comparison of H_2, N_2, and CH_4 as Pilot Fuel for Suppression of Self-Sustained Pressure Oscillations in a Dump Combustor*, Diplomarbeit, Technische Universität München.

Knoop, P., Culick, F. E. C., Zukoski, E. E. (1996). *Extension of the Stability of Motions in a Combustion Chamber by Nonlinear Active Control Based on Hysteresis*, internal report, California Institute of Technology.

Kraeutle, K. J. (1978). *Particle Size Analysis in Solid Propellant Combustion Research*, AIAA.

Krylov, N. M., Bogoliubov, N. N. (1947). *Introduction to Nonlinear Mechanics*, Princeton University Press, Princeton.

Levine, J. N., Baum, J. D. (1983). *A numerical Study of Nonlinear Instability Phenomena In Solid Rocket Motors*, AIAA Journal, Vol. 21, No. 4, 1983, pp. 557-564.

Levinson, N., Coddington, E. (1955). *Theory of Ordinary Differential Equations*, Mc. Graw-Hill.

Lieuwen, T., Neumeier, Y., Zinn, B. T. (1998). *The Role of Unmixedness and Chemical Kinetics in Driving Combustion Instabilities in Lean Premixed Combustors*, Comb. Sci. & Technol. 135: (1-6) 193-211.

Lieuwen, T., Zinn, B. (1998). *The Role of Equivalence Ratio Oscillations in Driving Combustion Instabilities in Low NO_x Gas Turbines*, 27th International Symposium on Combustion, August 1998.

Lieuwen, T., Zinn, B. (2000). *Experimental Investigation of Limit Cycle Oscillations in an Unstable Gas Turbine Combustor*, 38th Aerospace Sciences Meeting and Exhibit, AIAA No. 2000-0707.

Manitius, A., Olbrot, A. (1979). IEEE Transactions Automatic Control 24:541.

McManus, K. R., Poinsot, T., Candel, S. M. (1992). *A Review of Active Control of Combustion Instabilities*, Progress in Energy and Combustion Science, vol. 19, pp. 1-29.

Menon, S., Yang, V. (1993). *Some Issues Concerning Active Control of Combustion Instabilitiy in a Ramjet*, 31st Aerospace Sciences Meeting & Exhibit, January 1993, Reno NV.

Mohanraj, R., Zinn, B. T. (1998). *Numerical Study of Active Control Systems for Combustion Instabilities*, AIAA 98-0356, 36th Aerospace Sciences Meeting & Exhibit, January 12-15, 1998, Reno NV.

Murray, R. M. (1995). *Sparrow Reference Manual*, California Institute of Technology.

Na, T. Y. (1979). *Computational Methods in Engineering Boundary Value Problems*, Academic Press.

Neumeier, Y., Lubarsky, E., Heising, R., Israeli, O., Neumaier, M., Zinn, B. T. (1998). *Liquid Injector Actuator for Control of Combustion Processes*, AIAA-98-3540, 34th AIAA/ASME/SAE/ASEE, Joint Propulsion Conference and Exhibit, July 13-15, 1998/Cleveland, OH.

Neumeier, Y., Markopoulos, N., Zinn, B. T. (1997). *A Procedure for Real-Time Mode Decomposition, Observation and Prediction for Active Control of Combustion Instabilities*, proceedings of the 1997 IEEE International conference on Control Applications, Hartford, CT.

Neumeier, Y., Nabi, A., Arbel, A., Vertzberger, M., Zinn, B.T. (1997). *Open-Loop Performance of a Fast-Response, Actively Controlled Fuel Injector Actuator,* Journal of Propulsion and Power, vol. 13, No. 6, November-December.

Neumeier, Y., Zinn, B. T. (1996). *Experimental Demonstration of Active Control of Combustion Instabilities Using Real Time Modes Observation and Secondary Fuel Injection*, 26th International Symposium on Combustion, Naples, Italy, July 1986.

Neumeier, Y., Zinn, B. T. (1996b). *Active Control of Combustion Instabilities With Real Time Observation of Unstable Combustor Modes*, 34th Aerospace Sciences Meeting & Exhibit, January 15-18, 1996, Reno NV.

Neumeier, Y., Zinn, B. T. (1997). *An Overview of Active Control of Combustion Instabilities*, AIAA-97-0461, AIAA 35th Aerospace Sciences Meeting, January 6-10, 1997/Reno, NV.

Neumeier, Y., Zinn, B. T., Jagoda, J. I. (1993). *Frequency Domain Analysis of the Performance of a Valved Helmholtz Pulse Combustor*, Combustion Science and Technology, vol. 94.

Paparizos, L., Culick, F. E. C. (1990). *The Two-Mode Approximation to Nonlinear Acoustic in Combustion Chambers. II. Influence of Third-Order Acoustics and Mean Flow in Triggering.* Unpublished.

Poinsot, T., Bourienne, F., Candel, S., Esposito, E. (1987). *Suppression of Combustion Instabilities by Active Control*, Journal of Propulsion 5: 14-20.

Poncia, G. (1998). *A Study on Thermoacoustic Instability Phenomena in Combustion Chambers for Active Control*, PhD Thesis, Politecnico di Milano, Milan, Italy.

Richards, G. A., Yip, M. J., Robey, E., Cowell, L., Rawlins, D. (1995). *Combustion Oscillation Control by Cyclic Fuel Injection*, ASME Turbo Expo, June 5-8, Houston, TX.

Seywert, C. (2001). *Combustion Instabilities: Issues in Modeling and Control*, PhD Thesis, California Institute of Technology.

Seywert, C., Isella G., Culick F. E. C. (2000). *Active Feedback Control of Combustor Dynamics with Time Delay and Noise*, AIAA 2000-3124, 36th AIAA/ASME/SAE/ASEE Joint Propulsion Conference and Exhibit.

Shapiro, B., Zinn, B. T. (1997). *High-Frequency Nonlinear Vibrational Control*, IEEE Transactions on automatic control, vol. 42, no. 1, January 1997.

Smith, D. A. (1985). *An Experimental Study of Acoustically Excited, Vortex Driven, Combustion Instability Within a Rearward Facing Step Combustor*, PhD Thesis, California Institute of Technology, 1985.

Sterling, J. T. (1987). *Longitudinal Mode Combustion Instabilities in Air Breathing Engines*, Ph.D. Thesis, California Institute of Technology.

Strogatz, S. H. (1994). *Nonlinear Dynamics and Chaos, With Applications to Physics, Biology, Chemistry and Engineering*, Addison-Wesley publishing company.

Torres, H., Lieuwen, T., Johnson, C., Daniel, B. R., Zinn, B. T. (1999). *Experimental Investigation of Combustion Instabilities in a Gas Turbine Combustor Simulator*, 37th AIAA Aerospace Sciences Meeting and Exhibit, January 11-14, 1999, Reno, NV.

T'ien, J. S. (1972). *Oscillatory Burning of Solid Propellants including Gas Phase Time Lag*, Combustion Science and Technology, Vol. 5, pp. 47-54.

Wang, Y. (2000). *Effects of Actuator Limits in Bifurcation Control with Applications to Active Control of Fluid Instabilities in Turbomachinery*, PhD thesis, California Institute of Technology.

Wicker, J. M., Greene, W. D., Kim, S.-I., Yang, V. (1996). *Triggering of Longitudinal Combustion Instabilities in Rocket Motors: Nonlinear Combustion Response*, Journal of Propulsion and Power, Vol. 12, No. 6, pp. 1148-1158.

Wiggins, S. (1996). *Introduction to Applied Nonlinear Dynamical Systems and Chaos*, Springer-Verlag, Inc.

Yang, V., Kim, S. I., Culick, F. E. C. (1987). Third Order Nonlinear Acoustic Waves and Triggering of Pressure Oscillations in Combustion Chambers, Part I: Longitudinal Modes, AIAA 25th Aerospace Sciences Meeting. AIAA-87-1973.

Yang, V., Kim, S. I., Culick, F. E. C. (1988). *Third Order Nonlinear Acoustic Waves and Triggering of Pressure Oscillations in Combustion Chambers, Part II: Transverse Modes*, AIAA 26th Aerospace Sciences Meeting.

Yang, V., Kim, S. I., Culick, F. E. C. (1990). *Triggering of Longitudinal Pressure Oscillations in Combustion Chambers, I: Nonlinear Gasdynamics*, Combustion Science and Technology, Vol. 72, No. 5, pp. 183-214

Yang, V., Sinha, A., Fung, Y.T. (1992). *State-Feedback Control of Longitudinal Combustion Instabilities*, Journal of Propulsion, Vol. 8, No.1.

Zinn, B. T., Daniel, B. R., Neumeier, Y. (1994). *Investigation of Active Control of Combustion Instabilities in Chemical Rockets*, AFOSR technical report, March 1993 - February 1994.

Zinn, B. T., Neumeier, Y., Daniel, B. R., Lieuwen, T., Torres, H., Johnson, C. (1999). *Active Control of Combustion Instabilities in Low NO_x Gas Turbines*, AGTSR Combustion Workshop VI, April 1999.

Lo duca e io per quel cammino ascoso
intrammo a ritornar nel chiaro mondo;
e sanza cura aver d'alcun riposo,

salimmo sù, el primo e io secondo,
tanto ch'i' vidi de le cose belle
che porta 'l ciel, per un pertugio tondo.

E quindi uscimmo a riveder le stelle.

Dante Alighieri 1310, *Inferno, Canto XXXIV*